BASAL FOREBRAIN CHOLINERGIC SYSTEM: STUDIES ON INTRINSIC PHYSIOLOGY AND CONNECTIVITY

By

ÇAĞRI TEMUÇİN ÜNAL

A Dissertation submitted to the Graduate School-Newark, Rutgers,
The State University of New Jersey

In partial fulfillment of the requirements for the degree of Doctor
of Philosophy Graduate Program in Behavioral and Neural Science

Written under the direction of

Professor Laszlo Zaborszky, M.D., Ph.D. and approved by

Jorge Golowasch, Ph.D. (Thesis Committee Chair)

Tibor Koos, Ph.D.

Zoltan Nusser, Ph.D. (Outside Member)

James M. Tepper, Ph.D.

Laszlo Zaborszky, M.D, Ph.D. (Supervisor)

Newark, New Jersey

January, 2013

ABSTRACT OF THE DISSERTATION

BASAL FOREBRAIN CHOLINERGIC SYSTEM: STUDIES ON INTRINSIC PHYSIOLOGY AND CONNECTIVITY

By ÇAĞRI TEMUÇİN ÜNAL

Dissertation director:

Laszlo Zaborszky, M.D., Ph.D.

The term basal forebrain (BF) refers to a collection of nuclei found in the ventromedial aspects of the mammalian forebrain. The cholinergic corticopetal neurons in these nuclei received particular attention due to the intricate involvement of acetylcholine in cardinal cognitive functions. These neurons are referred to as the basal forebrain cholinergic (BFc) neurons and constitute the BFc system.

This thesis asks three questions regarding the BFc system. The first question (Aim 1) pertains to the electrophysiological properties of its constituent neurons. Second question (Aim 2) deals with their interactions. The final question (Aim 3) is aimed at answering how these neurons modulate cellular properties in target neurons, considering the regular-spiking (RS) basolateral amygdala (BLA) neurons as a model system. To answer these questions, patch-clamp recordings in acute brain slices obtained from transgenic mice were done. The cholinergic effects on BFc neurons themselves and RS-BLA neurons were studied via optogenetically stimulating BFc neurons.

Aim 1 revealed that BFc neurons can be differentiated into two electrophysiologically identifiable subtypes: early and late firing neurons. Early firing neurons (70%) are more excitable, show prominent spike frequency adaptation and are more susceptible to depolarization blockade, a phenomenon characterized by complete silencing of the neuron following an initial discharge of action potentials. Late firing neurons (30%), albeit being less excitable, could maintain a tonic discharge at low frequencies.

In Aim 2, the inhibitory nature of BFc interactions were revealed using different approaches of slice electrophysiology that include the application of cholinergic agonists/antagonists, paired whole-cell recordings, and optogenetic activation of a subset of BFc neurons while recording the postsynaptic responses in others. The mechanisms and potential functional implications of these inhibitory actions are discussed in detail later.

Experiments in Aim 3 were concerned with the effects of endogeneously released acetylcholine on RS-BLA neurons. The results reveal that cholinergic action depends on the recent history of RS-BLA neurons: It is excitatory following high frequency prior spiking while muscarinic inhibition dominates during lower firing frequencies. These results might point out to a thresholding function of acetylcholine *in vivo*.

PREFACE

Neuromodulators affect a plethora of cellular processes which make the study of their actions a daunting task. When I joined Dr. Zaborszky's laboratory, I was familiar with the abovementioned difficulties. What I was not aware of was the fact that he was interested in the organizational principles of the basal forebrain cholinergic system, a neuromodulatory hub influencing the entire cortical mantle. So, the task was not only characterizing what its constituent neurons do in relatively well characterized target structures but also what they are like and how they influence each other.

Cholinergic fibers are extensively found in the cerebral cortices, the vast majority of which are issued by basal forebrain (BF) cholinergic neurons (BFc neurons). The activity of these neurons is higher during cortical activation and their involvement in higher cognitive functions has been illustrated by a multitude of studies using diverse approaches.

BF is composed of different sets of nuclei occupying the ventromedial aspects of the mammalian forebrain. Corticopetal (i.e. cortically projecting) BFc neurons account for ~20% of the total BF cell population and comprise the BFc system. One aspect that differentiates this system from other neuromodulatory systems is its anatomical organization: unlike other systems (e.g. noradrenergic system), single BFc neurons typically innervate a very limited region in the cerebral cortex suggesting a level of specificity in its functions. Moreover, these neurons are organized into tightly packed clusters that might represent organizational modules similar to the ones found in the striatum, superior colliculus, the pontine nucleus, and the brainstem auditory nuclei (for a discussion of this idea, refer to Zaborszky et al., 2002). In line with this thinking, emerging evidence indicates that BFc neurons within the same clusters innervate functionally related cortical areas (Zaborszky et al., unpublished observations). In a relatively more recent ultrastructural study utilizing serial section analysis, around 60% of cholinergic terminals were found to form conventional synapses with cortical pyramidal neurons while the remaining terminals were not associated with synaptic appositions (Turrini et al., 2001). These latter findings might signify another level of functional organization within the BFc system with some of its constituent neurons functioning through wired while others functioning through volume transmission.

In our initial discussions with Dr. Zaborszky, we came to the conclusion that the anatomical complexities of this system should be paralleled by electrophysiological heterogeneity in its constituent neurons. I pursued this question with systematic patch clamp experiments in acute BF slices obtained from transgenic mice where cholinergic neurons were tagged with a fluorescent protein (i.e. enhanced green fluorescent protein; eGFP). The results suggested that BFc neurons can be dissociated into two subcategories based on their membrane properties. In this thesis and the related publication (Unal et al., 2012), these neurons are referred to as early-firing (EF) and late-firing (LF) neurons based on their action potential delays in response to depolarizing current injections. Overall, EF neurons were more excitable compared to LF neurons. Conversely, LF

neurons were endowed with the capability of prolonged action potential discharge while the firing of EF neurons was limited by pronounced spike frequency adaptation. The potential significance of these findings is discussed in the upcoming sections.

While most of the noncholinergic BF neurons are possibly projection neurons, a significant portion of them also issue local collaterals. However, different neurochemical subpopulations (parvalbumin-; PV-, somatostatin-; SOM-, calretinin-; CR, calbindin-positive neurons) are restricted to limited anatomical loci within the BF. Although these neurons might influence the cholinergic cell excitability within restricted locations, a global role to these neurons in influencing cholinergic output is difficult to envision. Conversely, there is no scarcity of cholinergic neurons within the BF cholinergic space itself. Moreover, BFc neurons issue local axon collaterals within the BF. This thinking motivated me to pursue the second aim that involves the characterization of cholinergic interactions within the basal forebrain. Using conventional pharmacological, paired recordings, and optogenetics, inhibitory interactions between BFc neurons were revealed. The implications of these findings are not clear at this time point. However, it is plausible that the communication between BFc neurons is well suited for regulating global cortical interactions.

As mentioned in the beginning, neuromodulatory actions are difficult to study due to the inherent complexities in the receptors, downstream pathways, and membrane conductances even in relatively well characterized pyramidal neurons. Further complications in their investigation arose by an inability to stimulate neuromodulatory neurons in a selective manner in the whole brain or in acute slices. Hence, the physiological validity of previous studies needs to be tested. By using optogenetic strategies to selectively stimulate cholinergic afferents to the regular spiking (RS) neurons of the basolateral amygdala (BLA), I have shown that cholinergic influences can be either excitatory or inhibitory based on the recent firing history of the postsynaptic neuron.

In short, this thesis includes a detailed investigation of the intrinsic physiology of BFc neurons and their interconnections. Interactions among BFc neurons themselves and their influences on BLA RS neurons involve one of the first attempts to characterize postsynaptic neuromodulatory actions with selective stimulation of BFc neurons using optogenetics. Moreover, these studies provide the first compelling evidence that BFc neurons are connected to each other and acetylcholine actions on extra-BF target neurons not only depend on the cholinergic receptors stimulated but also on the state of the cholinoreceptive neurons.

All the data in the main results of the thesis were acquired and analyzed by me with the exception of the durcupan embedded slice in Figure 4.3 B. This was kindly provided to me by Ms Erzebet Rommer who worked as Dr. Zaborszky's EM technician for many years and taught me a lot. I included an appendix section that contains data regarding the morphology of some of the recorded BFc neurons. The processing of slices was done by Ms Anett Nagy, a graduate student in the department of Physiology at University of Szeged, during her summer stay, and by Ms Erzsebet Rommer. Ms Anett Nagy did all the reconstructions in this section and analyzed the data.

Data acquisition and analysis is only a small part of the thesis when considering the constant feedback and education I received from my thesis supervisor Dr. Laszlo Zaborszky. His anatomical insights and scientific stance shaped the thesis. Regarding the specific aspects of electrophysiological methods, I received constant support from the members of my thesis committee which includes Dr. Zoltan Nusser, Dr. Jorge Golowasch, Dr. James Tepper, and Dr. Tibor Koos. With respect to optogenetics, I received a huge support from Dr. Koos and Dr. Tepper who opened their lab doors to me. Dr. Eran Stark, Harry Xenias, and Matt Gielow gave valuable advice regarding stereotaxic surgeries for virus injections. Discussions with colleagues and friends were a daily exercise for me in developing new ideas. Although this thesis would not form without all this immense support, I, Cagri Temucin Unal, assume full responsibility about its contents by submitting it. My hope is to convince the reader about the significance of this small but original contribution to the field.

ACKNOWLEDGEMENTS

In my difficult times, I was never left alone. My thesis advisor, Dr. Laszlo Zaborszky, never hesitated to give me his direct support. I am grateful to him for devoting his precious time in teaching me the brain from an anatomical and functional perspective. Without his guidance, this thesis would not form. Thanks Laszlo, for always being an exemplary mentor and teacher.

I would like to thank my thesis committee members, Dr. Jorge Golowasch, Dr. Tibor Koos, Dr. Zoltan Nusser, and Dr. James Tepper for devoting a significant amount of their time and energies for my scientific development.

I learned slice electrophysiology during my rotation in Dr. Denis Pare's laboratory. Things I have learned in his laboratory opened new avenues to explore to me and I will always remember his deep understanding and appreciation of physiological phenomena. I should also thank all the rest of the CMBN faculty members for always being exemplary scientists and teachers.

I would like to express my thanks to the members of the research animal facility. Without their care, I would not be able to do my experiments with accuracy and efficiency. Apart from their professionalism, I will always remember them with their warm friendship.

During the graduate school time, faculty members are not the only sources of knowledge. In this respect, I am indebted to my colleagues for their stimulating scientific discussions.

My friends were always with me when I needed them. Their contribution to my life in general is very big as compared to my modest scientific achievements. In a similar manner, my family always showed complete trust in me even during my failures. Their help cannot be described with words. I hope I am in the path for becoming the man I should be for deserving their unconditional love and respect.

TABLE OF CONTENTS

TABLES

FIGURES

LIST OF ABBREVIATIONS

4-AP: 4-Aminopyridine

AAV: Adeno-associated virus

AChE: Acetylcholinesterase

ADP: Afterdepolarization

AHP: Afterhyperpolarization

AP: Action potential

AP-5: D(−)-2-Amino-5-phosphonopentanoic acid

BAC: Bacterial artificial chromosome

BF: Basal forebrain

BFc: Basal forebrain cholinergic

BL: Basolateral amygdala

BLA: Basolateral complex of the amygdala

BM: Basomedial amygdala

cAMP: Cyclic AMP

ChAT: Choline-acetyltransferase

ChR2: Channelrhodopsin-2

CNQX: 6-cyano-2,3-dihydroxy-7-nitro-quinoxaline

DAB: Diaminobenzidine

DAG: Diacylglycerol inositol triphosphate

DSEVC: Discontiuous single electrode voltage clamp

DPSP: Depolarizing postsynaptic potential

EEG: Electroencephalogram

GFP: Green fluorescent protein

eGFP: Enhanced green fluorescent protein

EPSP: Excitatory postsynaptic potential

HDB: Horizontal diagonal band

HVA: High voltage-activated

I_A: Transient potassium current

I_{CAN}: Calcium-activated nonselective cation conductances Transient receptor potential membrane channels (TRPCs)

IP_3: Inositol triphosphate

IPSP: Inhibitory postsynaptic potential

IRES: Internal ribosomal entry site

LA: Lateral amygdala

LDT: Laterodorsal tegmental nucleus

LFP: Local field potential

LTP: Long-term potentiation

LVA: Low voltage-activated

MS: Medial septum

MTA: Methoctramine hydrate

PB: Phosphate buffer

PKA: Protein kinase A

PKC: Protein kinase C

PIP_2: Phosphatidylinositol biphosphate

PLC: Phospholipase C

PPT: Pedunculopontine nucleus

PV: Parvalbumin

RS: Regular-spiking

SI: Substantia innominata

SOM: Somatostatin

TEA: Tetraethylammonium chloride

TRPC: Transient receptor potential membrane channel

TTX: Tetrodotoxin

vAChT: Vesicular acetylcholine transporter

VDB: Ventral diagonal band

VP: Ventral pallidum

YFP: Yellow fluorescent protein

CHAPTER I: INTRODUCTION

1.1 Overview

The experiments in this thesis deal with three interrelated questions about the basal forebrain cholinergic (BFc) system. The first two questions pertain to the intrinsic physiological properties of BFc neurons and their interconnectivity. The third question is concerned with the effects of BFc activation in target structures, considering the regular spiking (RS) neurons of the basolateral amygdala (BLA) as a model system. These experiments were done with the assumption that a true understanding of the BFc system entails the characterization of their fundamental elements (BFc neurons), their interactions, and their effects on target structures. Patch clamp slice electrophysiology was used as the primary tool for answering these questions. The cell type specificity in recordings (selective recordings of BFc neurons) and/or stimulation (selective stimulation of BFc neurons) was achieved through a combination of novel strategies, briefly described below.

The incorporation of green fluorescent protein (GFP) and its improved variant enhanced green fluorescent protein (eGFP) has revolutionized biology in multiple ways. In genetically engineered animals, cell-type dependent expression of GFP/eGFP proteins has allowed researchers to easily visualize cells with different neurochemical identities (see Yuste, 2005 for a review). This visualization is easily achieved in living tissue. The ease with which fluorescence microscopy can be coupled to patch clamp techniques in slices provided a major impetus for many researchers to characterize the electrophysiology of distinct cell populations in different brain regions. In my experiments, I have used bacterial artificial chromosome (BAC) transgenic mice where eGFP expression is driven by the choline acetyl transferase (ChAT) promoter. As will be

described in some detail later, ChAT is a definitive marker of cholinergic neurons. During slice experiments, eGFP expressing ChAT neurons were easily identified with fluorescent microscopy. Subsequent to this initial identification, the neurons could be targeted for patch clamp recordings.

Modern slice electrophysiology experiments are not only about visualization. Stimulation of specific neuronal populations with optogenetics (see Zhang et al., 2007) is equally important. This methodology is slowly replacing electrical stimulation which indiscriminately stimulates different neurons/fiber systems. In the case of the experiments in this thesis, an adeno-associated virus (AAV) infusion into the basal forebrain (BF) was made in internal ribosomal entry site (IRES) transgenic mice that express cre recombinase under the promoter of ChAT. The AAV contained the inverse coding sequences of two critical proteins: a yellow fluorescent protein or mCherry which serve as reporters (similar to eGFP) and channelrhodopsin-2 (ChR2) bordered by two pairs of incompatible loxP sides. Channelrhodopsin is a light activated cation channel that normally serves as a photoreceptor to control phototaxis in green algae (Nagel et al., 2002). When expressed in the relevant cell populations in the brain (BFc neurons in the current case) through the inversion of the coding sequences only in cholinergic neurons that express cre recombinase, their activation with blue light opens a nonselective cation conductance that can generate firing specifically in these neurons. This strategy was used both for investigating interactions between BFc neurons (using double transgenic mice, see Chapter IV) and BFc system's influences on RS BLA neurons.

Before further describing the organization and function of the BF in general and BFc in particular, I will provide a short summary of cholinergic transmission. This will

involve the basic description of cholinergic neurotransmission and acetylcholine receptors.

1.2 Acetylcholine: From synthesis to removal

Acetyl-coenzyme A, choline, and ChAT are the necessary components of acetylcholine synthesis. ChAT transfers the acetyl group of acetyl-coenzyme A to choline for the synthesis of acetylcholine, an event that predominantly take place in terminals. Hence, the presence of the ChAT enzyme signifies the cholinergic identity of a cell. Synthesized acetylcholine is loaded into the synaptic vesicles via the vesicular acetylcholine transporter (vAChT) (Ferguson et al. 2003; Brandon et al. 2004).

The enzyme acetylcholinesterase (AChE) hydrolyzes acetylcholine through an extremely efficient mechanism (1000 Acetylcholine molecules hydrolyzed/second/molecule of AChE). This enzyme exists both in membrane bound and releasable forms (Soreq and Seidman, 2001). AChE can be found in cholinoreceptive neurons and therefore is not a specific marker of cholinergic neurons in general. The extracellular choline arising from the hydrolysis of acetylcholine is transported back into the cholinergic cells by sodium-dependent transporters. Apart from being involved in re-filling neurotransmitter stores, endogenous choline serves as an agonist for some nicotinic acetylcholine receptors (Mike et al. 2000) described below.

1.3 Acetylcholine receptors

Cholinergic transmission is mediated by ionotropic and metabotropic receptors which are named nicotinic and muscarinic respectively after the substances serving as their agonists.

Nicotinic receptors are ionotropic receptors and mediate fast acetylcholine actions in the order of milliseconds. These receptors are composed of five subunits being in various combinations of twelve subunits ranging from α2 to α10 and β2 to β4. They are found in the brain both at pre- and post-synaptic sites (Wada et al. 1989; Sahin et al. 1992) and can produce currents with different kinetics (Alkondon and Albuquerque, 1993; Castro and Albuquerque, 1995). Homomeric nicotinic receptors are composed of α7 subunits ($(\alpha7)_5$). Unlike other nicotinic receptors [$(\alpha4)_2(\beta2)_3$ and $(\alpha3)_2(\beta4)_3$ in the brain] which are mainly permeable to Na^+ and K^+, this homomeric receptor is also Ca^{2+} permeable. These receptors are rapidly desensitized [see Albuquerque et al. (2009) for a detailed review].

Muscarinic acetylcholine receptors are G-protein coupled metabotropic receptors with canonical seven transmembrane spanning domains, a characteristic of many different metabotropic receptors. Metabotropic receptors exert their physiological effects via activating GTP-binding proteins (G-proteins) which serve as an intermediary transducing molecule. Heterotrimeric G-proteins are composed of α, β, and γ subunits. The α subunit binds to guanine nucleotides, either GTP or GDP. When bound to GDP, α, β, and γ form an inactive trimer. Binding of a signaling molecule to the receptor causes the replacement of GTP for GDP, dissociation of the α subunit, which interacts with effector proteins. The hydrolysis of GTP, as determined by the activity of GTPase-activating-proteins, terminates the signaling event by forming the inactive α, β, γ trimer again. Five types of muscarinic receptors exist: M1, M3, and M5 receptors (i.e. odd numbered ones) are classified as M1 type while M2 and M4 receptors (i.e. even numbered ones) are classified as M2 type.

M1-type receptors are coupled to the G_q type G-proteins. The activation of the α subunit of these G-proteins by acetylcholine binding leads to the activation of phospolipase C (PLC) which cleaves the lipid component of the phosphatidylinositol biphosphate (PIP_2). As a result, PIP_2 becomes divided into two second-messengers: the membrane associated diacylglycerol (DAG) and diffusible inositol triphosphate (IP_3). DAG activates protein kinase C (PKC) which in turn phosphorylates various proteins implicated in the activaton of calcium binding proteins such as calmodulin. IP_3 activates their receptors found on the endoplasmic reticulum (IP_3 receptors), leading to calcium release from this organelle into the cytosol. These events lead to a rise in cytosolic calcium concentration from the nanomolar (50-100 nanomolar) to a milimolar range in a transient manner which in turn leads to the activation of kinases and calcium binding proteins (Hille, 2001; Brown, 2010).

The G_i type G-proteins are coupled to M2-type receptors. The activation of the α subunit of these G-proteins by acetylcholine binding leads to the inhibition of adenyl cyclase, an enzyme that normally converts ATP to cAMP. Hence, the activation of cyclic AMP activated protein kinase A (PKA) is reduced. This leads to a reduced phosphorylation of proteins that are targets of the adenylyl cyclase pathway. On the other hand, the βγ dimer, which constitutes the membrane delimited pathway, can lead to PLC activation and cleavage of PIP_2 and directly target some ion channels, leading to uncharacteristic fast metabotropic responses in the range of 10s of milliseconds (Hille, 2001; Brown, 2010).

Thus the amount and kinds of proteins phosphorylated heavily depend on the muscarinic receptors stimulated, altering the function of ion channels that shape the

electrophysiological properties of neurons (described later). See figure 1.1 for a summary of muscarinic receptor signaling. This scheme is prepared based on the information presented by a review (Brown, 2010).

Orly and Schramm (1976 as cited in Brown 2010) proposed “collision coupling” as a mechanism for metabotropic actions. This notion suggests that enzymes and effectors are “freely floating” in the cell and receptor activation engages these mechanisms randomly. A new notion described by Delmas et al. (2004) suggests that a particular neuromodulator action not only depends on the voltage, the receptor type, and the channels expressed by the target cells. In their view, the receptors, their signaling pathways, and the effectors can be clustered within signaling microdomains found on restricted anatomical sites. Therefore, two neuromodulators sharing the same pathways can lead to distinct changes in a particular cell while the opposite is also true (Delmas et al., 2004). The optogenetic studies described in this thesis are expected to respect these rules more than conventional pharmacological approaches for a variety of reasons discussed later.

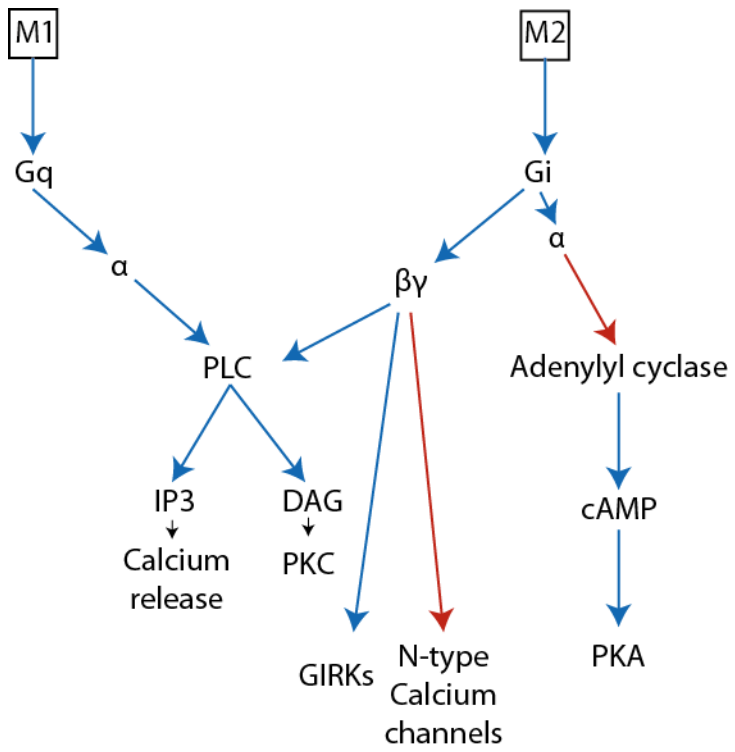

Figure 1.1 Signaling through M1 and M2 type metabotropic acetylcholine receptors. Blue and red arrows correspond to activation and inactivation respectively. Note that βγ dimer of the Gi has direct actions on voltage dependent channels. Adapted from Brown, 2010.

So far, I reviewed basics about the methodologies used in this thesis and cholinergic transmission. Having done that, I will now review briefly what is known about the BFc system and its effects in target structures. This is by no means an extensive review and the reader is referred to the original references cited for further information.

1.4 Historical notes about the structure and function of the BFc system

The term BFc system does not only correspond to an anatomical entity. It is also described on the basis of its functions. Hence, the union of "basal forebrain" and "cholinergic" is the result of decades of research in different fields of neuroscience. The history of this union defines the motives behind the experiments in this thesis.

The anatomical descriptions of the BF date back to the 19th century starting with the description of the subcomissural area as the unnamed substance by Reil (1809 as cited in Zaborszky et al., 2011). It is followed by the treatment of BF as a separate anatomical entity in a human brain atlas [Bogislaus (1861 as cited in Zaborszky et al., 2011)] followed by the description of the large BF hyperchromatic cells [Meynert (1872 as cited in Zaborszky et al., 2011)]. von Kolliker (1896 as cited in Zaborszky et al. (2011) made the full topographical description of the BF, named it as the nucleus basalis of Meynert. This description passed the test of time and includes the areas known to harbor the cortically projecting cholinergic neurons we know of today. Zaborszky et al. (2011) describe these advancements in more detail.

This anatomical research was going on along with seemingly unrelated findings in other fields. In the beginning of 20th century, the physiological actions of acetylcholine (and the discovery of it) in ganglionic transmission were described by pioneering experiments of Dale and Loewi [for a historical discussion see Rubin (2007)]. The leading work of Katz and his colleagues in 1950s and 1960s not only described the basic rules of synaptic transmission but included the first description of acetylcholine as a neurotransmitter in the neuromuscular junction (Katz and Miledi, 1966). At around the same time, the role of acetylcholine in neurotransmission in the central nervous system was discovered by Eccles et al. (1954) who found the nicotinic activation of Renshaw inhibitory neurons by intraspinal branches of motorneurons in the spinal cord.

The discoveries by Moruzzi and Magoun (1949) revealed the positive effects of brainstem stimulation on cortical arousal. The consideration of BF as a continuation of the brainstem reticular formation based on the similar morphological makeup of its

constituent neurons (Ramon-Moliner and Nauta, 1966) helped to conceptualize the BF as an “activating system” and motivated research on the relationship between cortical activation and the BF.

Shute and Lewis (1967 as cited in Semba, 2004) for the first time tentatively described the cholinergic pathways within the brain using acetylcholinesterase (AChE) staining. With the development of antibodies for ChAT and later tracing studies, it became certain that the BF contains cholinergic neurons (BFc neurons) that project to the entire cortical mantle [see (Semba, 2004)]. The demonstration that acetylcholine is released during cortical arousal by Kanai and Szerb (1965) along with the first pharmacological/electrophysiological demonstrations of excitatory actions of acetylcholine in the cortex (Krnjevic and Phillis, 1963) provided strong support for the notion that BFc system is closely related to cortical arousal.

The appreciation that EEG involves more than the sole measurement of drowsiness-arousal, the enhancing effect of acetylcholine on higher cognitive function related cortical rhythms (Metherate et al., 1992) lead to the thinking that acetylcholine is not only involved in regulating general cortical arousal but also in processes such as attention, learning and memory. Accumulating evidence from selective cholinergic lesions, selective receptor knockout studies, and electrophysiology provided strong support for this notion.

1.5 General anatomical and physiological features of the basal forebrain (BF)

The BF encompasses cytoarchitectonically diverse areas located in the ventromedial aspects of the mammalian forebrain. These areas include the medial

septum/ventral diagonal band complex (MS/VDB), the horizontal diagonal band (HDB), the substantia innominata (SI), the magnocellular preoptic area (MCPO), the ventral pallidum (VP), the extended amygdala (EA), the internal capsule (IC), and the ansa lenticularis. A number of fiber tracts including the diagonal band of Broca, medial forebrain bundle, ventral amygdalofugal pathway, and inferior thalamic peduncle traverse through connecting the BF neurons with afferent targets [see Heimer and Alheid (1991) for a detailed description of the BF anatomy). A unifying anatomical description of BF in this thesis entails nuclei that harbor cholinergic projection (i.e. BFc) neurons (Zaborszky and Duque, 2003). Figure 1.2 illustrates different BF subnuclei and the distribution of cholinergic projection neurons within this space.

While BF neurons in general innervate all cortical areas, cortical feedback to the BF arises exclusively from prefrontal, insular, and piriform cortices (Mesulam and Mufson, 1984; Zaborszky et al., 1997). Correlated light and electron microscopic investigations suggest that prefrontal cortical inputs terminate preferentially on noncholinergic neurons that include PV+ neurons (Zaborszky et al., 1997) (see the next section for the cellular composition of the BF). Cholinergic and noncholinergic BF neurons receive input from ascending neuromodulatory hubs including noradrenergic (Zaborszky et al., 1993), adrenergic (Hajszan and Zaborszky, 2002), and dopaminergic (Gaykema and Zaborszky, 1996; 1997) systems in addition to inputs arising from different amygdalar (Grove, 1988; McDonald, 1991; Petrovich et al., 1996) and hypothalamic (Cullinan and Zaborszky, 1991) nuclei. Serotonergic input exists but no specific synapses between serotonergic terminals and BFc neurons have been described so far (Gasbarri et al., 1999; Leranth and Vertes, 1999; Hajszan and Zaborszky, 2000).

The array of inputs coming from these regions is likely to endow the BF with a significant integration capability, a notion that has extensive experimental support [see Zaborszky and Duque (2003) for a review].

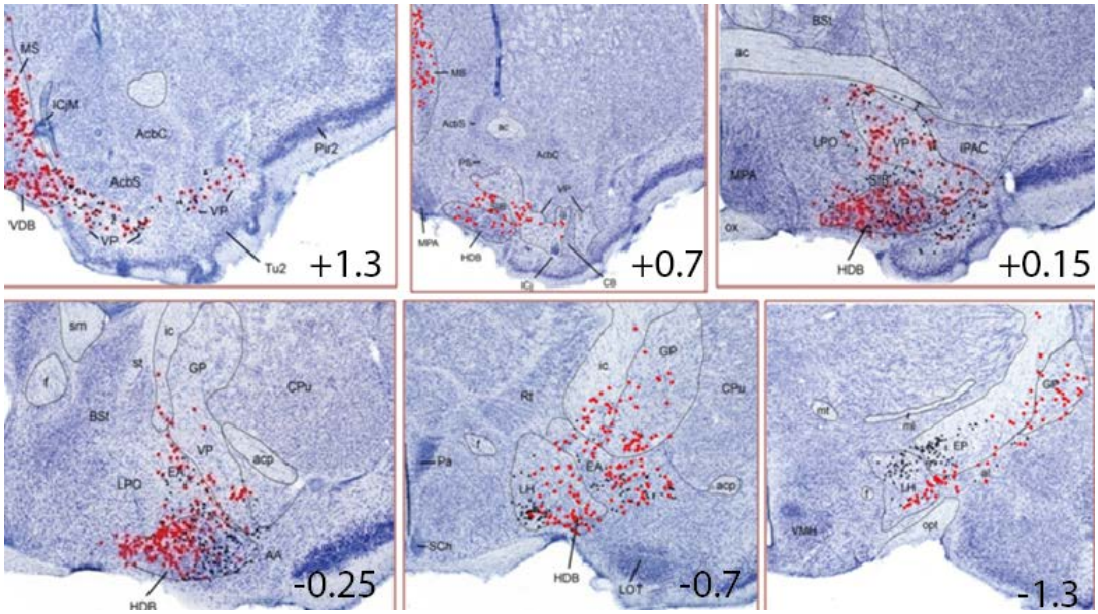

Figure 1.2 Layout of the basal forebrain cholinergic (BFc) system. Coronal slices are obtained from an NPY-GFP mouse and were processed for ChAT fluorescent immunocytochemistry. Both populations were mapped (black markers for NPY; red markers for ChAT) Values on the images indicate the approaximate position (in mm) from the Bregma [see. Franklin and Paxinos (2008)]. Note the continuity of cholinergic neurons beginning from the dorsal pole of medial septum to caudal areas . Additional abbreviations: ac, anterior commissure; AcbC, accumbens nucleus, core; AcbS, accumbens nucleus, shell; CB, cell bridge connecting the nucleus accumbens with the layer of the olfactory tubercle; HDB, horizontal diagonal band ICj, island of Calleja; ICjM, island of Calleja, major island; MPA, medial preoptic area; MS, medial septal nucleus; Pir2, piriform cortex, layer 2; PS, parastrial nucleus; SIB, substantia innominata, basal part; Tu2, olfactory tubercle, dense-cell layer; VDB, ventral diagonal band. Modified from Zaborszky et al. (2011)

1.5.1 Cellular composition of the BF

BFc neurons are intermingled with noncholinergic BF projection neurons and/or interneurons (Parent et al., 1988; Asanuma and Porter, 1990; Freund and Meskeinate, 1992; Zaborszky and Cullinan, 1992; Gritti et al., 1997; Zaborszky and Duque, 2000) expressing different markers (Zaborszky et al., 1999). In fact, BFc neurons make up only

~20% of the total BF cell population. It is estimated that BF contains about 20,000 BFc neurons in addition to around 35,000 CB+, 26,000 CR+, and 24,000 PV+ neurons per hemisphere in the rat brain (Zaborszky et al., 1999). Other neurons expressing neuropeptide Y (NPY) and/or somatostatin (SOM) are also found in the BF (Zaborszky et al., 2011) while no data are available pertaining to the co-localization of these two markers within single BF neurons. While BFc neurons target both glutamatergic projection and GABAergic interneurons in target structures, noncholinergic BF neurons selectively target GABAergic interneurons (Freund and Meskenaite, 1992).

1.5.2 Basic electrophysiological properties of BF neurons

In vitro electrophysiological studies described a variety of physiological phenotypes, possibly reflecting the heterogeneity in neural markers. BF neurons were initially characterized into three categories in slice experiments. Neurons in one category were silent at rest and responded to depolarizing current injections with low frequency discharge, the discharge rate being limited by long afterhyperpolarizations (AHPs) following single action potentials. The action potentials of these neurons were relatively wider and characterized by a shoulder during decay. These neurons were named S-AHP neurons after their slow AHPs following single spikes. A fast inward rectification, sensitive to external barium and cesium was another characteristic of these neurons. The second group of neurons exhibits a bursting discharge profile when depolarized from hyperpolarized membrane potentials and are therefore referred to as bursting neurons. The third group fired repetitive action potentials (100-200 Hz), partially owing to their short action potential durations and exhibited profoundly fast AHPs. Therefore these neurons were referred to as F-AHP neurons after their fast AHPs. F-AHP neurons

exhibited prominent voltage sag and could be further subdivided into two categories based on the presence or absence of spike frequency adaptation (Griffith and Matthews, 1986; Griffith, 1988).

While burst firing neurons lose the ability to burst at depolarized membrane potentials, the qualitative aspects of discharge mode was insensitive to membrane voltage in S-AHP and F-AHP neurons (Griffith and Matthews, 1986; Griffith, 1988). The S-AHP neurons can fire single spikes rhythmically when positive bias current is injected, a phenomenon that most likely reflects the interplay of depolarizing and hyperpolarizing conductances expressed by these neurons. Later studies found that S-AHP neurons correspond to BFc neurons (Sotty et al., 2003) while some proportion of F-AHP neurons are found to be PV+ (Morris et al., 1999). Unlike their cortical counterparts, these PV expressing neurons exhibit prominent voltage sag mediated by h-currents. Additional cell types were found; including the vesicular glutamate transporter positive (VGluT+) neurons which displayed a clustered firing pattern but overall did not fire at higher frequencies than BFc neurons (Sotty et al., 2003).

Although the descriptions of firing patterns match the patterns observed *in vivo*, the percentages of encountered neurons displaying different firing patterns are strikingly different. For instance, bursting neurons in MS in acute slices constitute around 10% of all the neurons recorded (Griffith and Matthews, 1986) while the percentage was around 50% in the same region *in vivo* (Lamour et al., 1984 as cited in Griffith et al., 1991). These inconsistencies might be due to a combination of experimental (e.g. sampling bias) and physiological factors (e.g. synaptic input).

Recording the neurons and filling them with biocytin in acute BF slices, Henderson et al. (2001) further distinguished burst firing neurons in the MS into two classes based on the activation/inactivation kinetics of low-threshold spikes. According to this scheme, type I bursting neurons exhibited faster low-threshold spike kinetics and it was found to be the only neuron type whose main axon never coursed toward the fornix. On the other hand, all neurons possessed axonal varicosities and innervated other neurochemically unidentified neuronal profiles *en passant* while fast-spiking neurons issued basket like axonal endings (Henderson et al., 2001). These results suggest that BF neurons overall might have dual functions that involve the innervation of target structures in addition to participating in local interactions.

1.6 BF cholinergic (BFc) neurons

The entire cortical mantle, with the exception of the prefrontal cortex, receives cholinergic inputs exclusively from BFc neurons. As described previously, BFc neurons make up to ~20% of the entire cell population in the BF. These neurons are tightly packed in MS, vDB, and hDB whereas more scattered distribution patterns emerge in other BF areas (Zaborszky et al. 2005; Nadasdy et al. 2010; Zaborszky et al. 2011). It is important to note that cholinergic cell groups in higher primates are more compact and far exceed the number in rats [220,000 per hemisphere in humans (Arendt e al., 1985) as opposed to ~18,000 in the rat]. Although increased brain size might account for increments in cell numbers, it is also plausible that increased cell numbers indicate further functional specialization across the phylogenetic scale as is seen in other regions such as the thalamus [see Buzsaki (2006), p.179)].

1.6.1 Inputs to BFc neurons

Ultrastructural studies indicate that BFc neurons receive dopaminergic (Gaykema and Zaborszky, 1996), noradrenergic (Zaborszky and Cullinan, 1996), adrenergic (Hajszan and Zaborszky, 2002), and possibly glutamatergic inputs from brainstem nuclei (as reviewed in Detari, 2000). The BFc neurons also receive inputs from different hypothalamic nuclei that include orexin neurons (Zaborszky and Cullinan, 1989; Cullinan and Zaborszky, 1991; Wu et al., 2004). These neurons are surrounded by histaminergic axons from the tuberomammilary nucleus but ultrastructural evidence for synapses between histaminergic fibers and BFc neurons is still lacking (Turi et al., 2004). Paralimbic cortical areas are likely to be the only cortical areas forming synapses in the BF but they seem to avoid contacting BFc neurons (Zaborszky et al. 1997). The latter projections are likely to influence BFc neurons through indirect mechanisms involving noncholinergic BF neurons that target BFc neurons locally. There are direct glutamatergic and GABAergic synapses arising from amygdalar nuclei (Zaborszky et al. 1984) and nucleus accumbens respectively (Zaborszky et al. 1984; Zaborszky and Cullinan, 1992). Local inputs arising from PV+ and NPY+ neurons have been described at the ultrastructural level (Zaborszky and Duque, 2000; Zaborszky et al., 2009). While potential polysynaptic inputs from the prefrontal cortical areas might mediate BFc output to different cortical areas [see Golmayo et al., 2003; Rasmusson et al., 2007], inputs from orexinergic/histaminergic fibers and their excitatory actions on BFc neurons (Khateb et al., 1995; Eggermann et al., 2001; Wu et al., 2004) might shape BFc system's involvement in general arousal.

1.6.2 General organization of BFc projections to target structures

The BFc outputs to target structures are roughly as follows: MCPO and hDB provide the major acetylcholine input to the olfactory bulb, piriform cortex, and entorhinal cortex (Luskin and Price, 1982). The basolateral amygdala (BLA) (Carlsen et al., 1985) and the entire neocortex (Mesulam and Van Hoesen, 1976) receive inputs from VP, SI, EA, GP, IC, and ansa lenticularis in a rough medio-lateral and anterior-posterior topography. Light microscopic data suggest that MS vDB complex, hDB, and MCPO all contribute cholinergic inputs to the hypocretin neurons in the LH (Henny and Jones, 2006). Hippocampus receives most of its cholinergic input from the MS/vDB complex (Amaral and Kurz, 1985).

A primary method of choice for inferring the extent of BFc axonal collateralization in target structures entails the combined application of different retrograde tracers into two cortical areas along with immunocytochemistry for ChAT (Price and Stern, 1983; Koliatsos et al., 1988). These studies rarely identified double-labeled BFc neurons suggesting that the area innervated by individual neurons is limited. Detailed single cell reconstructions by Duque et al. (2007) provide direct support for this notion. In this respect, the specificity of the BFc system as compared to other neuromodulatory systems has been acknowledged by Woolf (1996) who advocates that neuromodulatory systems are diffuse in nature in his commentary.

While BFc axons seem to innervate limited cortical areas, neighborhood relations within the BF do not “match up” with their cortical targets. Baskerville et al. (1993) have found a high spatial overlap among BFc neurons projecting to different cortical regions. Zaborszky et al. (2002), revisited this issue by using isodensity surface rendering for BFc

neurons projecting to different cortical areas. In this analysis, an algorithm delivers a plane around voxels of comparable cell densities. This allows the 3-dimensional visualization of multiple cell groups projecting to different cortical targets. This rendering reveals that BFc projections are ordered as evidenced by the rostromedial to caudolateral distribution of cells projecting to mediolaterally located cortical areas (see figure 1.3).

1.6.3 Morphological features of BFc neurons

BFc neurons have relatively big somata (>15 µm) that display fusiform, triangular, or round forms (Dinopoulos et al. 1986). They have an isodendritic morphology with one to five primary dendrites branching out in all directions. These primary dendrites typically bifurcate in a repetitious manner with the total length of daughter branches exceeding the length of the primary branches. The entire dendritic length is approximately 4 mm, occupying a volume around 0.1 mm^3 (Duque et al., 2007). BFc neurons have abundant axon collaterals ranging ~3-27 mm length and bearing *en passant* varicosities in a volume encompassing 0.2-0.3 mm^3 within the BF itself (Duque et al., 2007). On the basis of these morphological data, it has been suggested that BFc neurons might also play roles in local BF interactions (Zaborszky and Duque, 2000; Duque et al., 2007). The potential functional significance of these anatomical features will be discussed further in the following sections.

1.6.4 Similarity of dendritic orientations between neighboring BFc neurons

Estimates suggest that 50-80 other BFc neurons are found within the area occupied by the dendritic arborizations of a single BFc neuron. Rendering of 3D vectors of the dendrites of hundreds of neighboring BFc neurons in different BF regions suggest that BFc neurons' dendrites are collectively organized in an iso-orientated fashion

(Zaborszky et al., 2002). Considering the isodendritic organization of BFc neuron populations occupying the same space (Zaborszky et al. 2002), it can be speculated that certain cortical regions found on similar mediolateral coordinates receive input from different BFc neurons sharing their inputs. This notion is supported by recent quantitative descriptions of dense BFc neuron aggregates, whose density cannot be accounted by chance factor (Nadasdy et al., 2010). These cell aggregates are referred to as BFc cell clusters and unpublished work from Dr. Zaborszky's laboratory revealed that BFc neurons in each cell cluster project to functionally-related cortical areas.

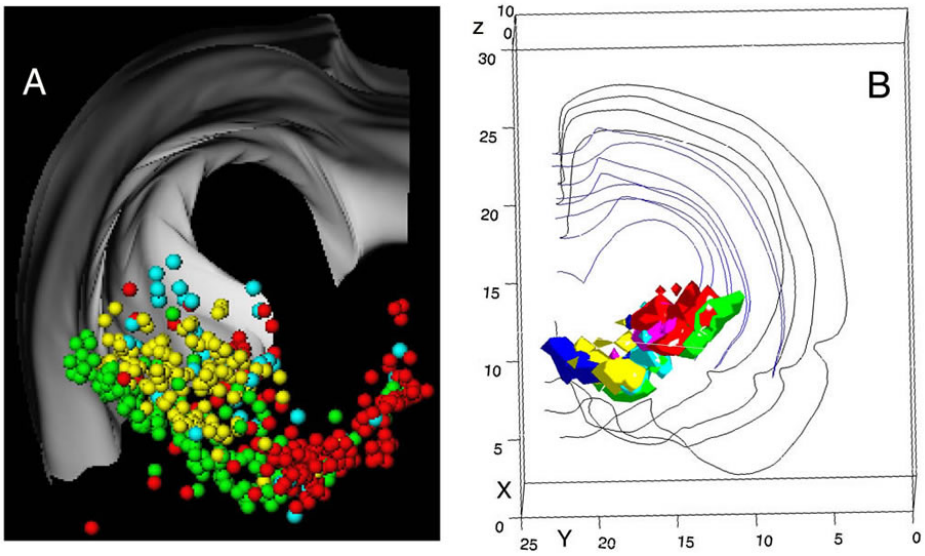

Figure 1.3 Topographical organization of the BFc system. A Composite map illustrating the 3D distribution of BFc neurons projecting to 4 different mediolateral sectors of the neocortex. **Red:** medial; **blue and yellow**: intermediary; **green:** lateral. **B** Isodensity surface rendering to illustrate the major organizational features of the BFc system. Voxel size: 400 X 400 X 50 µm; density threshold: ≥2 neurons/voxel. **Dark blue:** posteromedial cortex (M1/M2); **yellow:** mPFC; **red:** barrel cortex; **green:** posterior insular-perirhinal; **light blue:** agranular insular-lateral orbital; **magenta:** lateral frontal cortex. Panel B is the mirror image of Panel B. Adapted from Zaborszky et al., 2002.

1.6.5 Neurochemical heterogeneity of BFc neurons

BFc neurons exhibit some level of heterogeneity with respect to the expression of different neurochemical markers. They have been shown to be variously colocalized with galanin (Melander and Staines, 1986), GABA (Brashear et al., 1986; Kosaka et al., 1988), N-acetyl-aspartyl-glutamate (Forloni et al., 1987), tyrosine hydroxylase (Henderson, 1987), CB+ (Chang and Kuo, 1991) and secretagogin (Gyengesi et al., 2010), among others. The functional implications of these different colocalization patterns are not known at present.

Later in the background section, the physiology of BFc neurons will be briefly described. A more extensive description along with some problematic aspects is presented in Chapter 3.

1.7 Functions of the BF in general

Since the majority of previous work did not directly identify the neurochemical identity of recorded BF neurons, their cholinergic/noncholinergic identity could not be ascertained. However, these experiments provided a major framework for describing the cholinergic contributions to cortical activation in later studies [e.g. Duque et al. (2000)] and need to be considered for understanding BFc function.

A principal method of choice for probing BF function entails concomitant electroencephalogram (EEG) and single unit recordings from the BF (Detari, 2000). Recording of electrical activity from the scalp or cortical surface with EEG reveals that different conscious states are characterized by different EEG signatures. During an alert state, the EEG is characterized by low voltage, fast activity. This state is referred to as the desynchronized (or “activated”) state, a term criticized by some researchers as different regions can exhibit coherence in their activity during these states [see Harris and Thiele (2011) for a review]. During more drowsy states, the amplitude of the EEG increases with an accompanying reduction of frequency. These rhythmic oscillations can range between ~1-15 Hz. During these states, the membrane potential of pyramidal neurons fluctuates in synchrony leading to the summation of electrical fields [see Buzsaki et al. (2012) for a review], giving the name “synchronized” to this EEG state. These up and down fluctuations in membrane voltage make pyramidal neurons unreceptive to incoming information, a phenomenon that most likely underlies “drowsy” states when the animal

becomes less responsive to environmental stimuli. The different cortical states are largely determined by the thalamocortical synapses and the neuromodulatory influences impinging on cortical and thalamic neurons. The reader is referred to Steriade (2004) for a detailed review on cortical oscillations and their intracortical, thalamic, and neuromodulatory origins. It is important to note that cortical activation is not a uniform state and information processing ability can vary within these states as well within a single region recorded or among different regions (Harris and Thiele, 2011). Caution also needs to be exerted when comparing behavioral states and EEG patterns. For instance, rapid-eye movement (REM) sleep is characterized by EEG desynchronization similar to that occurs during wake states (Detari, 2000).

Studies combining *in vivo* single unit recordings from BF neurons with cortical EEG monitoring suggest a critical role for BF neurons in cortical activation. According to these studies, the BF neurons can be categorized into three broad categories in anesthetized (Nunez, 1996; Zaborszky and Duque, 2003) and unanesthetized (Buzsaki et al., 1988; Detari et al., 1987) animals with F-cells (F referring to “fast cortical activity”) firing at higher rates during fast cortical EEG, S-cells (S referring to “slow cortical activity”) exhibiting the opposite pattern, and cells indifferent (i.e. firing at similar frequencies across sleep/wake cycle) to different cortical states. F- and S- cells can be further distinguished into “tonic” and “phasic” neurons depending on the temporal resolution requirements for detecting their correlations with cortical EEG (Detari, 2000). For instance, the activity of F-cells can precede cortical activation by as much as 26 seconds (i.e. tonic influence of BF neurons on cortical EEG) (Detari et al., 1987), or as little as 400 msec when cortical activity alternates between high and low frequency

events around 0.2 Hz (i.e. phasic influence of BF neurons on cortical EEG) (Detari et al., 1997).

BF neurons have also been studied in relation to different behavioral contexts. A majority increase their firing rates to stimuli that predict appetitive stimuli in monkeys (Wilson, 1991) and rats (Rigdon and Pirch, 1986). Another study in monkeys performing go/nogo tasks has shown that BF neurons were recruited specifically during the choice phase (Richardson and DeLong, 1990). Similar changes in the discharge rates of BF neurons were also seen for noxious stimuli (Richardson and DeLong, 1991). The responses reported in these studies were of short latency (30-500 msec) and duration (~500 msec) and might be correlated with phasic changes in cortical arousal [as discussed by Richardson and DeLong (1991)]. In agreement with these findings, learning-related beta-frequency oscillations with a duration of 500-1000 msec have been reported within the BF during learning tasks (Quinn et al., 2010).

The abovementioned studies are entirely correlational. Studies utilizing BF lesions and pharmacological inhibition give hints about the causal role the BF plays in cortical activation. Pharmacological inhibition (Cape and Jones, 2000) and lesioning of BF neurons (Buzsaki et al., 1988) slow down the EEG. In an elegant study, Stewart et al. (1984) performed unilateral BF lesions with kainic acid. During voluntary movements, fast cortical activity was observed in both parietal cortices while the EEG on the lesioned side was dominated by slow waves when the animal was motionless. These results reveal the critical, behavior dependent influence of BF in cortical activation. Rigdon and Pirch (1984 as cited in Pirch et al., 1991) reported that silencing BF neurons via GABA or procaine microinjections into the BF abolished frontal cortical unit responses to a

conditioned stimulus (tone) predicting an appetitive conditioned stimulus supporting a causal role between BF and higher cognitive faculties that extend beyond sleep/wake regulation.

1.8 Recent *in vivo* studies utilizing immunocytochemical identification of recorded neurons

More recent *in vivo* studies combining cortical EEG monitoring, juxtacellular labeling, and *post hoc* immunocytochemistry identified the transmitter content of recorded neurons and provided critical insights about the functions of different BF neuron types. Manns et al. (2000a; 2000b) found BFc neurons to exhibit increased discharge during cortical activation while GABAergic (GAD+) BF neurons were heterogeneous with respect to their EEG relationship. Duque et al. (2000) also reported the heightened activity of BFc neurons during cortical activation. In addition, this study found that PV+ neurons also exhibited increased firing rates during active cortical states. On the other hand, NPY+ neurons exhibited the opposite EEG relationship and discharged more during inactive cortical states. In other words, these studies for the first time identified the neurochemical identity of some of the previously described S (i.e. those that fire during slow cortical activity) and F cells (i.e. those that fire during fast cortical activity). These results are described in more detail in Chapter III.

1.9 Where does the BFc stand with respect to cortical activation?

It is clear that the BF contains neurochemically and electrophysiologically distinct neuronal populations. Although the studies discussed so far revealed valuable information regarding the overall BF function, they fall short in deciphering the contribution of different neuronal populations in different behavioral states. There is now

compelling anatomical evidence that BF contains a population of interneurons that express the neuromodulators somatostatin and NPY (Zaborszky and Duque, 2000). It is postulated that these interneurons release GABA and locally regulate the activity of cortically projecting BF GABAergic and BFc neurons (Detari, 2000; Zaborszky and Duque, 2000). On the other hand, GABAergic projections arising from the BF, through their exclusive fast actions on GABA interneurons in target structures (Freund and Meskeinate, 1992; Detari, 2000) are proposed to regulate cortical rhythms through rhythmic disinhibition. BFc neurons, on the other hand, through their relatively slower actions, modulate almost every possible ionic conductance in target principal neurons and interneurons in addition to providing fast excitation to interneurons (discussed in detail later). Through this immense conundrum of actions, BFc neurons are thought to play a critical permissive role in cortical activation.

1.9.1 Cortical acetylcholine release and general arousal

Kanai and Szerb (1965) for the first time measured cortical acetylcholine release along with EEG measurements in anesthetized cats using the cortical cup method. The authors have demonstrated that stimulation of the mesencephalic reticular formation led to a desynchronized EEG along with a 5-fold increase in released acetylcholine in frontal, parietal, and occipital cortices. The EEG desynchronization was sensitive to muscarinic receptor blockade in the cortex (which receives its major input from BFc neurons), illustrating a causal link between postsynaptic muscarinic receptor activation and EEG desynchronization. Later studies in freely moving animals confirmed these findings (Collier and Mitchell, 1967; Jasper and Tessier, 1971).

Interventions targeting cholinergic components provide further support for the abovementioned findings. Atropine or scopolamine induces slow waves in EEG, a pattern similar to sleep [e.g. Metherate et al., (1992)]. Conversely, electrical or chemical stimulation of BF *in vivo* increases cortical acetylcholine levels and desynchronizes EEG [(e.g. Metherate and Ashe, 1991; Metherate et al., 1992; Fournier et al., 2004b) in an atropine sensitive manner.

Livingstone and Hubel (1981) found that sleep to wake transition was characterized by reduced spontaneous discharge and an increased responsiveness of visual cortical neurons to visual stimuli with a concomitant sharpening of receptive fields. A similar effect was seen in visual cortical neurons when visual stimuli were paired with an appetitive stimulus (Haenny and Schiller, 1988). Although these authors were not interested in acetylcholine involvement in these processes, heightened activity of BFc neurons during wake states and possibly during the presence of appetitive, arousing stimuli entail (Richardson and DeLong, 1991) contributing factors. In line with this thinking, cortical acetylcholine release does not only change during robust alterations of cortical EEG and across sleep/wake cycles. Cortically released acetylcholine appears to play a significant role in learning related enhancement of sensory processing and cortical plasticity (Juliano et al., 1990; Metherate and Ashe, 1991; Baskerville et al., 1997; Dykes 1997; Kilgard and Merzenich, 1998; Rasmusson, 2000; Conner et al., 2003). BFc system also appears to be critical in cortical receptive field reorganization subsequent to peripheral deafferentiation (Juliano et al., 1990; Baskerville et al., 1997). Besides, performance deterioration in tasks that gauge attention is closely related to the degree of selective cholinergic deafferentiation (McGaughy et al., 1996). During delayed

matching tasks that require a “working memory” process, muscarinic antagonists impair behavioral performance (Penetar and McDonough, 1983) and reduce spiking in prefrontal cortical units (Pirch et al., 1991).

Recent research utilizing optogenetic strategies for selectively stimulating cholinergic BF elements provide direct support for the notion that BFc neurons are involved in cortical activation (Kalmbach et al., 2012) and improved sensory processing by sharpening receptive fields that possibly underly increased sensory discrimination capacities (Ma and Luo, 2012).

In summary, BFc neurons are critically involved in cortical activation and sensory processing. The ability to do so bestows this system with a significant capacity in regulating a plethora of different cognitive processes that include attention, learning, and memory. See Sarter et al. (2005) and Hasselmo and Sarter (2011) for detailed reviews about the cognitive tasks influenced by the BFc system.

BFc system achieves its functional powers through its dense cortical projections and the intricate nature of acetylcholine effects. Next, I will shortly review these aspects to shed some light on some of the mechanisms of cholinergic action.

1.9.2 Anatomical features of cholinergic fibers in target structures

In the neocortex, cholinergic axons (as revealed by immunocytochemistry for ChAT) are found at all layers with layers I and V receiving the densest innervation in general. Eckenstein et al. (1987 as cited in Descarries et al., 2004) reported a similar level of cholinergic innervation of all cortical areas with entorhinal and olfactory cortices constituting exceptions with higher density of ChAT-immunoreactive fibers. The authors found terminal densities to be lower in layer IV of motor/sensory cortices with the exception of visual cortex which exhibited a dense band of ChAT-immunoreactive terminals in this layer. Estimates regarding the total length of cholinergic fibers in the rat neocortex reach up to 7.6 km (Descarries et al. 2004). Mechawar et al. (2000) reports a varicosity/length ratio of 4/10 µm suggesting that ~30 billion cholinergic axonal varicosities are found in neocortical regions in rats. Based on the abovementioned ratio, the authors report that frontal cortex received the densest innervation (5.4 X 10^6 varicosities/mm^3) followed by occipital (4.6 X 10^6 varicosities/mm^3) and parietal (3.8 X 10^6 varicosities/mm^3) cortices. Among these three areas, layers I and V received the highest innervation. Layers IV and VI were the least innervated areas in the primary sensory cortices. Aznavour et al. (2002) did the same quantitative analysis in rat hippocampus and revealed higher figures for hippocampal innervation: 4.1 X 10^6 varicosities/mm^3 in CA1 and 6.2 X 10^6 varicosities/mm^3 in CA3. The dense innervation of layers I and V are particularly relevant considering the importance of layer I in integrating information from multiple sources mainly through the apical dendritic tufts of pyramidal neurons and horizontally oriented axons from layers II/III and layer V constituting the main neocortical output (Douglas et al., 2004).

Ultrastructurally, most cholinergic terminals were initially observed to be asynaptic with ~15-50% of profiles associated with classical synapses (Umbriaco et al., 1994; Mrzljak et al. 1995; Smiley et al. 1997). However, a recent study by Turrini et al. (2001) using the more sensitive serial section analysis (Zaborszky et al., 2011) revealed a higher synapse probability (66%) for each varicosity in the layer V of the rat parietal cortex. Cholinergic synapses targeted mainly dendritic shafts while a lower proportion of synapses were observed on dendritic spines. Synapses on somata were rare. Moreover, most synapses observed were symmetric in nature (Turrini et al., 2001). Although not much is known with respect to the innervation pattern of different kinds of interneurons, anatomical work suggests that BFc axons largely avoid synapsing on PV+ interneurons (Dougherty and Milner, 1999; Henny and Jones, 2008).

1.9.3 Cholinergic receptors in target structures

Abovementioned data show that cortex is heavily innervated by the BFc system. The density of this innervation is far more than the innervation of other neuromodulatory systems [as discussed in Mechawar et al. (2000)]. This massive innervation is reciprocated by widespread acetylcholine receptors. Immunoprecitation (Levey et al., 1991) and *in situ* hybridization (Buckley et al., 1988) experiments revealed that M1, M2, and M4 muscarinic receptors are extensively expressed in the rat brain while M3 and M5 expression is lower and mostly limited to the thalamus and brainstem nuclei. Immunocytochemistry revealed that M1 receptors are found on pyramidal neurons in all layers and were qualitatively more enriched in layers II/III and VI while M2 receptors were found rarely on putative interneuron cell bodies (Levey et al., 1991). Studies in rats (Yamasaki et al., 2010) and monkeys (Mrzljak et al., 1993) have conclusively shown that

the M1 receptors are found on pyramidal cell dendrites and spines. Two different studies, employing immunocytochemistry with affinity purified antibodies (Levey et al., 1991) and *in situ* hybridization (Buckley et al., 1988) converge on the interesting finding that M4 receptors are localized in cell bodies on layer IV. A recent electrophysiological study illustrated the possible functional implications of these findings (Eggermann and Feldmeyer, 2009) and will be discussed in detail later. A study in monkeys demonstrated the presence of M2 receptors on layer III and V pyramidal neurons and interneurons in all layers (Mrzljak et al., 1998). It is important to note that basal forebrain lesions spared the majority of M2 receptors found in target regions (Mrzljak et al., 1998) supporting the idea that this receptor protein can function as a heteroreceptor. Similar observations for M2 receptors were obtained in rat hippocampus with selective cholinergic lesions using the selective cholinergic neuron lesion using 192-IgG immunotoxin (Levey et al., 1995b). Some of these M2 heteroreceptors are found in the terminals of basket cells in the hippocampus (Hajos et al., 1998) and neocortex (Salgado et al., 2007) and they are likely to be expressed the same way in other cortical areas (Chaudhuri et al., 2005; Freund and Katona, 2007). The main message of these studies is that M2 is not only responsible for modulating acetylcholine release but also the release of other neurotransmitters while autoreceptor role of M2 receptors should not be underestimated. Indeed, Dudar and Szerb (1969) demonstrated ~3-fold increase in cerebral cortical acetylcholine release as a result of atropine application. This notion was later supported by studies utilizing sniff patch methodologies to detect acetylcholine release in cultures (Allen and Brown, 1996), anatomical studies in hippocampus (Rouse et al., 2000), and studies combining selective

knock-out strategies and monitoring of radioactive acetylcholine in acute slices (Zhang et al., 2002).

Nicotinic receptor expression is more modest as compared to its muscarinic counterpart. However, the critical sites of action endow these receptors with functional powers. Nicotinic receptor expression is relatively high on thalamocortical terminals in layer IV as revealed by radioligand binding studies (Sahin et al., 1992; Bina et al., 1995; Lavine et al., 1997). The presence of α3-5,α7, and β2 subunit mRNAs has been illustrated in *in situ* hybridization studies cortex-wide (Wada et al., 1989; 1990). While nicotinic responses were uncommonly observed in pyramidal cells [but see. Roerig et al. (1997); Kassam et al. (2008)], these responses are observed in general in cortical interneurons with the exception of parvalbumin positive basket cells [e.g. Porter et al. (1999)]. A single cell PCR electrophysiological study recording from layer II, III, and V interneurons of motor cortex revealed the expression of α4, α5, and β2 nicotinic receptor subunits in cholecystokinin+ (CCK+) and vasoactive intestinal peptide+ (VIP+) interneurons while the presence of α7 was unique to a subpopulation of VIP+ interneurons (Porter et al., 1999).

Having reviewed function/structure with regards to the BFc innervation of cortical structures and acetylcholine receptors, I will try to fill in the gap by shortly reviewing the mechanisms of acetylcholine actions.

1.10 Electrophysiology of cholinergic actions in target structures

The electrophysiological actions of acetylcholine are complex: the overall effect depends on a multitude of factors that include the type of cholinorecipient neurons

affected and how these alterations change circuit dynamics. In general, acetylcholine is regarded as “excitatory”, increasing the activity of target projection neurons.

1.10.1 Postsynaptic mechanisms of acetylcholine actions

Destexhe and Pare in 1999 conclusively demonstrated the impact of synaptic activity on the input resistance of cortical pyramidal neurons *in vivo* in anesthetized cats: during heightened synaptic activity, the pyramidal neurons experience a significant drop in their input resistances due to the increased synaptic conductances (Destexhe and Pare, 1999). Steriade et al. (2001) replicated these findings in chronically implanted cats: Pyramidal neurons experienced a similar drop in their input resistance when they were depolarized during slow wave sleep. Paradoxically, the drop in input resistance was not apparent when the neurons were depolarized during REM sleep and waking, states characterized by increased acetylcholine efflux in the cortex (Collier and Mitchell, 1967; Jasper and Tessier, 1971). Thus, acetylcholine seems to preserve the electrical compactness of the neurons despite the opposing influences of other synaptic conductances. These findings can be better appreciated in the light of overwhelming evidence regarding the potency of acetylcholine in blocking various potassium conductances in pyramidal neurons in slices [e.g. (Halliwell and Adams, 1982; McCormick and Prince, 1985; Nakajima et al., 1986 Madison et al., 1987)].

The potassium conductances do not only contribute to the overall input resistance at rest but also have profound effects on how the neurons transform incoming stimuli to output. For instance, M-current blockade by acetylcholine removes the brake to repetitive firing (Constanti and Sim, 1987) and makes neurons more receptive to incoming inputs (Weight and Votava, 1970). The blockade of slow afterhyperpolarizations reduces spike

frequency adaptation (Madison et al., 1987). After all, reduction of afterhyperpolarizations following spikes is necessary for M-current removal to exert its meaningful actions. On the other hand, an acetylcholine mediated reduction in transient potassium currents (Nakajima et al., 1986) would determine the temporal precision of action potential discharge in response to incoming inputs by reducing the action potential delay (Storm, 1988). The “slow EPSP” is the other common phenomenon observed when acetylcholine is present and is mediated by the inhibition of leak potassium conductances. It increases the overall responsiveness of neurons (Cole and Nicoll, 1984; Benson, 1988).

The suppression of potassium conductances in pyramidal neurons largely entails M1 receptor activation (Krnjevic, 2004). However, there are broadly two kinds of exceptions to this rule. M1 receptor activation does not always produce an increased excitability through actions on potassium channels. For instance, M1 receptor activation can lead to an enhancement of delayed rectifier potassium currents in CA1 pyramidal neurons, mediated by PKC activation through intracellular calcium signaling (Zhang et al., 1992). Moreover, M1 receptor signaling engages apamin sensitive, calcium dependent potassium currents and genarate muscarinic IPSPs in cortical (Gulledge et al., 2007), hippocampal (Dasari et al., 2011), and amygdala (Power and Sah, 2008) pyramidal neurons. At this point in time, it is important to note that the latter phenomenon is activity dependent and possibly requires priming of intracellular calcium stores through action potential-dependent calcium entry. Morever, the muscarinic IPSP becomes replaced by an afterdepolarization once the neurons fire action potentials phasically above certain frequencies [e.g. Dasari et al. (2011)]. Thus, even the regulation of potassium conductances seem to be related to the state of the neurons which are

receiving the cholinergic inputs. On the other hand, bath application of carbachol increased the excitability of CA3 and dentate granule cells via the inhibition of slow afterhyperpolarizations mediated through M2 receptors (Muller and Misgeld, 1986). Another exception entails the M current blockade that occurs through M2 receptor activation in olfactory cortical neurons (Constanti and Sim, 1987). Thus, acetylcholine actions can be complex and the sole presence of M1 or M2 receptors does not guarantee an increased or reduced excitability. In fact, muscarinic activation of cortical interneurons likely entail M2 receptors and in contrast to the effects on pyramidal cells, the effects on these neurons entail a drop in input resistance in these cells associated with increased cationic conductances (McCormick and Prince, 1985). Exceptions regarding the M2 receptors possibly involve cytosolic calcium rises through PIP2 breakdown [see (Noda et al., 1993; Wang et al., 1997, 1999; Callaghan et al., 2004)].

Voltage or calcium gated potassium channels are not the only ones affected by acetylcholine. Low-voltage activated Ca^{2+} channels are enhanced (Toselli and Lux, 1989; Fraser and MacVicar, 1991) by acetylcholine while the reverse seems to be the case for their high voltage activated counterparts (Toselli and Lux, 1989). Although these actions are not as well studied, the suppression of high voltage activated calcium currents in presynaptic terminals has clear implications for synaptic depression.

Multiple aspects of hyperpolarization activated cationic- (H-currents) currents in principal cortical neurons are subject to cholinergic modulation through muscarinic mechanisms (Colino and Halliwell, 1993; Dembrow et al., 2010; Heys and Hasselmo, 2012). Recent evidence also indicates that acetylcholine alters fast voltage-dependent sodium channel function, primarily reducing its amplitude and slowing down its

inactivation kinetics, through PKC-dependent phosphorylation of these channels (Cantrell et al., 1996; Chen et al., 2005). Mittman and Alzheimer (1998), in sensory-motor cortex principal neurons, have shown a selective reduction in slow, persistent sodium channel current without alterations in other kinetic properties. Currently, our knowledge on modulation of sodium channels is relatively poor and inconsistencies, due in part to differences in cell types investigated and differences in pharmacological and electrophysiological approaches taken, exist [e.g. Chen et al. (2005); Franceschetti et al., 2000; Carrillo-Reid et al. (2009)].

Another interesting point entails the cholinergic modulation of calcium-activated nonselective cation conductances (I_{CAN}), which are mediated through the transient receptor potential membrane channels (TRPCs) [for a review see Fleig and Penner (2004)]. Although different cortical regions are likely to have differences in their activation mechanisms, acetylcholine has been shown to activate/uncover these channels in pyramidal neurons of different structures that include the entorhinal cortex [e.g. (Klink and Alonso, 1997], hippocampus [e.g. (Fraser and MacVicar, 1996)], primary sensory and motor areas [e.g. (Rahman and Berger, 2011)]. The depolarizing influences of these channels exceed the duration of synaptic inputs (or intracellular current injections) and are typically associated with further action potential discharge.

Acetylcholine actions should not only be seen as simple depolarization/hyperpolarization. Slow oscillations occurring at hyperpolarized membrane potentials are largely governed by voltage dependent channels normally suppressed by acetylcholine. Therefore, cholinergic activation reduces these oscillations (Pape and Driesang, 1998). Membrane depolarization alone recruits different voltage

dependent membrane currents which have pronounced actions on firing patterns and intrinsic oscillations occurring at depolarized potentials. Acetylcholine has been found to increase the amplitude of 20-40 Hz oscillations occurring slightly before firing threshold is reached in a TTX sensitive manner suggesting the involvement of voltage dependent sodium channels (synaptic blockers were present before TTX) (Metherate et al., 1992). This was accompanied by a shift in firing pattern from a bursting to a tonic mode (Metherate et al., 1992). As discussed by Metherate et al. (1992), this has evident implications for cortical EEG as rhythmic bursting (~2-5 Hz which is in the range of slow EEG) layer V neurons are thought to synchronize the cortical EEG through their intralaminar connections (Silva et al., 1991) and acetylcholine is likely to veto this mechanism by depolarizing layer V neurons, changing their oscillatory properties along with accompanying changes in firing pattern from bursting to tonic. On the other hand, I_{CAN} activation through depolarization of cholinoreceptive cortical principal cells might specifically be involved in endowing these neurons with the ability to extend their firing beyond the presence of relevant sensory stimuli, which is thought to be a potential underpinning of working memory (Durstewitz et al., 2000).

In short, acetylcholine influences a diverse array of voltage and/or calcium gated ion channels. In general, this translates into increased responsiveness to incoming inputs in principal cortical neurons. This is coupled to changes in firing mode from bursting to tonic. The subthreshold oscillations occurring in response to acetylcholine will in turn determine the temporal properties of this increased responsiveness. Lastly, the recruitment of I_{CAN} by acetylcholine can lead to spiking activity that extends beyond the inputs triggering the initial spikes. However, cortical principal neurons do not exist in

isolation but receive inputs from other principal neurons, thalamic neurons, and interneurons.

1.10.2 Acetylcholine effects on thalamo- and cortico-cortical information processing

Cholinergic modulation is notorious for favoring thalamocortical inputs over corticocortical inputs on pyramidal cells and many computational models are based upon these principles (Giocomo and Hasselmo, 2007). The importance of this can be best appreciated by considering receptive fields in sensory systems. For instance, neurons in the auditory cortex have two kinds of receptive fields: one defined on the basis of spikes and the other on the basis of EPSPs/IPSPs a particular tone elicits. When defined on the basis of the latter, the receptive fields are wider. In line with this, optical imaging studies *in vivo* reveal a tonotopic organization with respect to peak tone-evoked activity while weak responses to the same tones engage the entire auditory cortex (Horikawa et al., 1996). The spiking responses are thought to reflect the efficacy of thalamic inputs while EPSPs/IPSPs reflect recurrent cortical interactions (Wallace et al., 1991; Miller et al., 2001).

In a sense, recurrent excitation which is useful for generating distributed networks, can also introduce noise into the system when out of control (Giocomo and Hasselmo, 2007). Acetylcholine makes use of these principles when exerting its actions: it is likely to exploit presynaptic nicotinic receptors in thalamocortical terminals, excite them, and lead to an increase in glutamate release from thalamic terminals while decreasing the efficacy of corticocortical connections through presynaptic muscarinic receptors (Metherate and Ashe, 1993; Hsieh et al., 2000; Metherate et al., 2012 but see

Goard and Dan, 2009). These mechanisms, along with increased intrinsic excitability of principal neurons mentioned before, are thought to increase signal/noise ratio and improve signal processing in other sensory [visual cortex: Kimura et al., 1999;Brocher et al., 1992, somatosensory cortex: Hasselmo and Cekic (1996)] and associative cortices [e.g. frontal cortex: Vidal and Changeux (1993), Gioanni et al. (1999)]. These physiological phenomena are thought to account for acetylcholine's involvement in improved sensory processing, attention, and memory (Giocomo and Hasselmo, 2007).

Eggermann and Feldmeyer (2009) introduced a new dimension to these effects. Recording in sensory cortices (both somatosensory and visual cortex) of the rat, they found that spiny stellate neurons of layer IV, the major thalamic recipients, were inhibited by acetylcholine through M4 receptor activation of inwardly rectifying potassium conductances. Using paired recordings, they also revealed a suppression of EPSPs between layer IV – layer IV and layer IV – layer II/III excitatory synapses. Hence, the authors speculate that acetylcholine exerts a filtering role in layer IV microcircuit, which in turn allows only the strongest inputs to excite them. In later steps, the "selected" responses are amplified through the increased responsiveness of other layers (Eggermann and Feldmeyer, 1999). Indeed, the notion that layer IV has a dampening function is in line with findings pertaining to the necessity of synchronous thalamic inputs for exciting layer IV neurons (Bruno and Sakmann, 2006) and acetylcholine seems to have the potential to reduce signal/noise ratio through exploiting this mechanism (Eggermann and Feldmeyer, 1999).

1.10.3 Acetylcholine effects on interneurons

When researchers puff acetylcholine in neocortical or hippocampal slices, the postsynaptic cholinergic response is typically preceded by a hyperpolarization accounting for ~5% of the total response [e.g. McCormick and Prince (1986a)]. This hyperpolarization is achieved through the activation of cortical interneurons, key players in cortical information processing. Fast nicotinic responses in hippocampal GABA neurons were first reported by Jones and Yakel (1997) and Alkondon et al. (1997) followed by the important findings by Frazier et al. (1998) demonstrating the effect of endogeneously released acetylcholine (achieved through electrical afferent stimulation coupled to the blockade of GABA, glutamate, serotonin-5HT1-A, and ATP receptors) in eliciting nicotinic EPSCs.

The important question is whether acetylcholine actions depend on the interneuron type. If it does, what does it mean? The answer to the first question is a “yes”. Not all interneurons respond to acetylcholine. The answer to the second question is not as clear.

PV+ fast-spiking interneurons do not seem to be affected by acetylcholine and possibly lack functional somatodendritic muscarinic/nicotinic receptors [for a review, see Lawrence, (2008)] while a study reported a slight depolarizing influence through the inhibition of M-curents (Cea-del Rio et al., 2010). PV+ neurons express functional M2 receptors in their presynaptic terminals which reduce GABA release onto pyramidal neurons (Hajos et al., 1998; Szabo et al., 2010; but see. Tang et al., 2011). These neurons constitute the fast-spiking interneurons and innervate soma/proximal dendrites or axon

initial segments and receive strong thalamocortical inputs [(Glickfeld and Scanziani, 2006; Bartos et al., 2007; Freund and Katona, 2007; Cruikshank et al., 2010)].

The participation of PV+ neurons in γ oscillations and the inability of cholinergic stimulation to exert readily observable effects in these neurons remains an enigma. Lawrence (2008) puts forth the possibility that cholinergic depression of GABA release in PV+ neurons might help to sustain GABA release during γ oscillations.

However, in light of other experimental evidence (Palhalmi et al., 2004; Nagode et al., 2011), it seems likely that CCK+ neurons, some of which provide somatic inhibition, partially fulfill the role of entraining pyramidal cells during the presence of acetylcholine. It is also worthwhile to remember that acetylcholine does also not inhibit PV+ neurons. While acetylcholine also depresses GABA release from CCK neurons, the effect seems to be mediated through an indirect mechanism involving the release of endocannabinoids from postsynaptic pyramidal neurons (Freund and Katona, 2007; Szabo et al., 2010). Porter et al. (1999) employing whole cell recordings coupled to RT-PCR have revealed profound nicotinic receptor mediated EPSPs of CCK+ colocalizing interneurons through non-α7 containing receptors in different layers (II, III, V) of primary motor cortex. CCK+ neurons are also shown to be excited by muscarinic receptors (Kawaguchi, 1997; Cea-del Rio et al., 2010).

Kawaguchi (1997) implementing whole cell recordings along with *post hoc* immunocytochemistry reported robust muscarinic depolarization of SOM+ neurons. SOM+ neurons compose the dendrite targeting Martinotti cells and innervate distal dendrites, playing crucial roles in attenuating EPSPs pyramidal neurons receive (Wang et

al., 2004; Silberberg and Markram, 2007; Lovvett-Barron et al., 2012). Based on their weak responses to thalamic stimulation (Cruikshank et al., 2010) and strong excitatory inputs from pyramidal neurons (Silberberg and Markram, 2007; Fanselow et al., 2008), these cells possibly exert consequential feedback inhibition.

In short, acetylcholine seems to change the contribution of different perisomatic neurons by favoring non-fast spiking CCK+ interneurons over PV+ interneurons. On the other hand, the contribution of dendrite targeting interneurons which receive prominent cortical feedback excitation becomes prominent. The increased recruitment of dendrite targeting neurons might be involved in attenuating a subgroup of excitatory inputs while allowing the summation of others. The availability of novel transgenic tools started delineating some aspects of cholinergic modulation of interneurons in more detail (Arroyo et al., 2012).

Taken as a whole, acetylcholine influences a variety of mechanisms that involve the intrinsic properties of neurons and the excitatory/inhibitory connections between them. These mechanisms, by interacting at various levels during information processing [e.g. Stiefel et al. (2009)], seem to mediate cholinergic effects in cortical structures in concert.

1.11 Thesis statements

Having provided basic information about the BFc system and its effects in target structures, I can now return to the problems addressed in this thesis.

From an anatomical and functional perspective, it becomes evident that the BFc system is more than a mere diffuse activating system. In this respect, understanding its

cellular organization both at a single-cell and network level is cardinal for grasping certain functional implications. Conversely, understanding cholinergic function in target structures were either limited to correlations and/or manipulations that have uncertain physiological relevance. These problems are listed below. Introductory sections in corresponding chapters (Chapters III, IV, and V) provide a more elaborate summary of these aspects.

1- BFc neurons are neurochemically diverse. A similar level of diversity has been shown just recently even in historically well-described pyramidal neurons which were most of the time regarded as members of a homogeneous population (Krook-Magnuson et al., 2012). Inconsistencies regarding the intrinsic membrane properties of BFc neurons between different studies might partially reflect this neurochemical diversity. However, the different studies also differed in their methodologies: there is an immense variability pertaining to the regions studied in slices, differences in neurochemical identification strategies and recording conditions being some of them. Only recent studies focused on the potential diversity of BFc neurons with a particular emphasis. However, these studies did not entail definitive neurochemical verification of BFc neurons (Garrido-Sanabria et al., 2007; 2011).

2- Acetylcholine release does not necessarily occur globally in the neocortex: specific sensory and other functional areas experience selective enhancement in detected acetylcholine levels depending on the sensory system and brain regions stimulated (Zmarowski et al., 2005; 2007; Fournier et al., 2004a; Rasmusson et al., 2007). This notion is further supported by

electrophysiological studies (Metherate et al., 1992; Golmayo et al., 2003). This argues against the previously proposed diffuse nature of the BFc system. There seem to be organizing principles within the BF that have the capacity to endow the BFc system with its specific functions. These principles include a restricted target innervation by single BFc neurons, the proximity of BFc neurons projecting to possible functionally related cortical areas, and the iso-oriented dendrites of BFc neurons potentially belonging to a single functionally related cluster. An additional important detail involves the presence of local collaterals of BFc neurons. While all these aspects are anatomically well-defined, no study has directly addressed whether these have a meaningful functional correlate.

3- Interest in the BFc system does not only concern how it is organized. Its actions on single regions/columns and neurons is equally interesting. Efforts to do so were partly hampered by the complex organization of the brain. Pathways in the brain contain a diversity of axons that release different kinds of neurotransmitters. This complexity made it impossible for past investigators to selectively stimulate cholinergic afferents. On the other hand, pharmacological studies do not seem to be optimal for three reasons. First, the concentration of agonists in those studies is largely referenced to neurochemical studies. While neurochemical studies provide perfect measures for functional neurotransmitter interactions, they do not measure the synaptic concentration of neurotransmitters. Second, acetylcholine actions on different membrane conductances are concentration dependent [e.g. Madison et al.

(1987)]. Third, pharmacological approaches might not have enough resolution to capture subtleties in G-protein signaling pathways which proved to have important physiological consequences (Brown, 2010). For these reasons, the true physiological meaning of acetylcholine can only be approximated by using recent approaches that will allow the selective stimulation of BFc afferents to their targets. As it will become evident soon, these problems also apply to the second problem discussed above.

In the light of the abovementioned problems, this thesis involves three different sets of experiments.

AIM 1 involves the detailed electrophysiological characterization of BFc neurons in transgenic mice that exhibit eGFP expression under the ChAT promoter. These experiments were designed to give insights about the heterogeneity of the electrophysiological properties of BFc neurons which might reflect the neurochemical and input/output heterogeneity of these neurons and translate into differences in cholinergic signaling in target structures.

AIM 2 involves the functional characterization of local BFc collaterals. The experiments entail pharmacological approaches and paired recordings. In addition, crossbreds of transgenic mice (see Methods, AIM 2) were used in order to selectively stimulate a subpopulation of BFc neurons via optogenetics while recording others in the absence of direct optogenetic depolarization/spiking. These experiments entail the first direct electrophysiological tests about the functional relevance of certain anatomical characteristics (i.e. does the presence of local BFc collaterals mean something?) in BFc

system's functional organization and were designed to investigate whether BFc interactions exist. This is a prerequisite question to be answered for an initial understanding of this system's functional organization.

AIM 3 involves the characterization of cholinergic actions in RS BLA neurons. The complexities in BFc function do not only arise from its intrinsic anatomical organization but includes the complex actions of acetylcholine which is expected to involve state dependence in target neurons. To my knowledge, this study is also the first to investigate a pure postsynaptic neuromodulatory action (i.e. a long-lasting and metabotropic receptor signaling mediated postsynaptic effect) using optogenetics.

CHAPTER II: GENERAL MATERIALS AND METHODS

2.1 Humane treatment of experimental animals

All experiments in this thesis were performed in accordance with the U.S. Public Health Service Policy on Humane Care and Use of Laboratory Animals, the National Institutes of Health *Guidelines for the Care and Use of Animals in Research*, and approved by the Rutgers University institutional animal care and use committee (IACUC).

2.2 Animals

Female and male adult transgenic mice (1-15 months), with or without prior delivery of adeno-associated viral vectors (AAVs), were used in all the experiments. Refer to table 2.1 for the strains used in different aims. More information about the specific strains is available in specific methods sections.

AIM	Experimental question	Experimental approach	Animals	Virus used / amount (µl)	Injection site
AIM 1	Physiology of BFc neurons	Whole cell recordings	ChAT-eGFP	N/A	N/A
AIM 2	Connectivity of BFc neurons	Paired whole cell recordings/Pharmacology	ChAT-eGFP	N/A	N/A
AIM 2	Connectivity of BFc neurons	Whole cell recordings and optogenetics	ChAT-cre x ChAT-eGFP	AAV2/5-EF1a-ChR2-mCherry/1	hDB and vDB[#]
AIM 3	Cholinergic modulation of BLA pyramidal neurons	Whole cell and perforated patch clamp recordings and optogenetics	ChAT-cre	AAV5-EF1a-DIO-ChR2-EYFP / 1.5	Caudal BF[#]

Table 2.1 A summary of the animals and techniques used in the thesis. [#] See specific methods in corresponding sections for injection coordinates. N/A: not available.

2.3 Electrophysiology: Data acquisition and analysis for electrophysiology

In vitro whole-cell recordings were performed from adult mice. Animals were first anesthetized with an i.p. injection of a ketamine/xylazine mixture (150 and 30 mg/kg, respectively) and transcardially perfused with 10 ml of an ice cold perfusion solution. Contents of the perfusion solution per aim are summarized in table 2.2.

	Sucrose	KCl	$MgCl_2$	$NaHCO_3$	$NaHPO_4$	$CaCl_2$	Glucose	Choline
AIM1	248	2.5	7	23	1.2	0	7	N/A
AIM2	0	2.5	1.3	26	1.2	2	10	242
AIM3	0	2.5	2.3	26	1.2	0	10	242

Table 2.2 A summary of the perfusion solutions used in different aims. Values indicate mM.

Subsequently, the brains were removed and 250 µm (for Aim 1) and 300 µm (for Aims 2 and 3) thick sections containing the regions of interest (BF for Aims 1 and 2, BLA for Aim 3) were obtained with a vibrotome. The abovementioned perfusion solutions were used during the slicing procedure and the slices were transferred to an oxygenated (with 95% O_2, 5% CO_2) artificial cerebrospinal fluid (ACSF) containing incubation chamber. The ACSF contained (in mM): 124 NaCl, 2.5 KCl, 1.2 $NaHPO_4$, 26 $NaHCO_3$, 1.3 $MgCl_2$, 2 $CaCl_2$, 10 glucose unless otherwise indicated.

Whole-cell recordings were performed after a >1 hour incubation period. The slices were visualized with an Olympus BX51WI (Center Valley, PA) microscope, equipped with infrared differential contrast optics and epifluorescence, and superfused with oxygenated ACSF (3-5 ml/minute) at room temperature. These experiments were

conducted with 3-6 MΩ pipettes pulled with a a horizontal puller (P-97, Sutter Instrument, Novato. CA). The following intracellular solutions were used (contents in mM):

1- Potassium based intracellular: 130 $KMeSO_4$, 10 NaCl, 2 $MgCl_2$, 10 HEPES, 3 Na_2ATP, 0.3 GTP, 1 EGTA. This solution was used in **Aim 1 (Chapter III), Aim 2 (Chapter IV),** and **Aim 3 (Chapter V)** for characterizing the membrane properties of BFc neurons, investigating the influences of cholinergic synapses on BFc and RS BLA neurons respectively. See specific methods in **Aim 3 (Chapter V)** for perforated patch clamp recordings.
2- Cesium based intracellular: 125 $CsMeSO_4$, 16 K-gluconate, 2 $MgCl_2$, 10 HEPES, 3 Na_2ATP, 0.3 Na_3GTP, 1 EGTA, and 0.1 $CaCl_2$. This solution was used in **Aim 1 (Chapter III)** for recording Ba^{2+} currents to investigate low voltage activated calcium channel function.
3- Cesium based intracellular for aim 2: 125 $CsCl^-$, 0.1 EGTA, 10 HEPES, 2 $MgCl_2$, 4 Na_2-ATP, 0.4 Na_2-GTP. This solution was used to evoke spikes in potential presynaptic cholinergic neurons in **Aim 2 (Chapter IV)**.

All whole recordings used had stable access resistances (<10% change throughout recording) of less than 20 MΩ and were obtained only if a GΩ seal formed before whole cell access. Access resistances of 25-35 MΩ were accepted for perforated patch clamp recordings (see specific methods in Chapter 5). An Axoclamp 900A amplifier and Digidata 1440A data acquisition device (Molecular Devices, Palo Alto, CA) were used for recordings. Discontinuous single electrode voltage clamp (DSEVC) experiments were done with a sampling frequency of 10 kHz and filtered at 2 kHz.

The junction potential was experimentally determined to be 10 ±2 mV for all solution combinations used to characterize the passive/active properties of neurons and was not corrected for. Data acquisition started 10 minutes after access for AIM 1 which characterizes the intrinsic physiological properties of BFc neurons.

Data were mainly analyzed using Clampfit and Origin. Statistical analysis was performed using IBM SPSS v20 (Chicago, IL). Means are represented as ± standard deviation (SD). The Kolmogorov-Smirnov test was used to determine the normality of distributions. To compare means, t-tests were used. Specifically, independent and paired t-tests were used for analysing between- and within-cell effects respectively. When the same parameter was tested multiple times using different intensity of an independent variable, a repeated measures analysis of variance (RM-ANOVA) was performed. The specific t-test results were determined based on the equality of variances determined with Levene's test for equality of variances.

2.4 Optogenetic experiments

2.4.1 Stereotaxic virus delivery for optogenetic experiments

For AAV injections, the animals were anesthetized with isoflurane. Subsequently, their skull was exposed via incising the adjacent skin which was locally anesthetized with subcutaneaus bupivacaine before. A small hole was drilled at the appropriate coordinates for both hemispheres (see specific methods sections for coordinates). Following this, an injection pipette (~50 μ outer tip diameter) containing the concentrated virus stock solution was lowered to the brain using a Nanoject-2 pressure injection apparatus. Subsequent to surgeries, the animals were placed in an air ventilated hood located in a

safe quarantine room for ≥7 days. Slice experiments were carried out after 3-7 weeks post-injection.

2.4.2 Activation of ChR2

Slice illumination was carried out using a blue LED bulb (470 nm) placed directly between the condenser and the recording chamber (~.5 cm distant from the bottom of the chamber). The maximum intensity of illumination reached to ~2 mW/mm^2. The digitizer used in data acquisition was also used for controlling the duration and intensity of illumination via a Mightex SLA LED driver.

2.5 Anatomy

2.5.1 ChAT immunocytochemistry

Animals were perfused with saline followed by 4% paraformaldehyde in 0.1 M PB. The brain was removed and placed into the same solution for overnight fixation. The next day, the brains were placed into sucrose solution (30%). Three days later, 50 µm thick BF sections were cut using a freezing microtome. Sections were placed into 0.1 M phosphate buffer (PB) for ~24 hours. Every third section was taken for immunohistochemistry in order to obtain 150 µm series. Sections were washed 3X in 0.1 M PB and incubated with Goat-anti-ChAT (1:500; Millipore, Temecula, CA) antibody with 1% normal donkey serum and 0.5% Triton-X in 0.1 M PB for overnight incubation at room temperature under dark. The next day, sections were washed 3X in 0.1 M PB and transferred into Donkey-anti-Goat Cy3 IgG (1:100) with 1% normal donkey serum and 0.5% Triton-X in 0.1 M PB for ~3 hours at incubation at room temperature under dark. Following incubation, sections were washed 3X in 0.1 M PB and mounted using Vectashield wet mounting medium. The eGFP+ and ChAT immunopositive somata in BF

areas were mapped using the Neurolucida software (MicroBrightField, Inc, Williston, VT) from six 50 µm thick serial sections containing the BF separated by 150 µm apart.

2.5.2 Cytochemistry for biocytin

Following the recordings with biocytin in the pipette (.2%), slices were transferred to 4% paraformaldehyde for at least 24 hours for fixation. For biocytin visualization, slices were incubated in 1:200 Cy3-conjugated streptavidin or Texas Red conjugated streptavidin (Invitrogen, Carlsbad, CA; Jackson ImmunoResearch Laboratories, West Grove PA) for 20-24 hours. Slices were then transferred to a slide and mounted with Vectashield wet mounting medium (Vector Labs Inc., Burlingame CA). For the acquisition of digital images Adobe Photoshop was used with an AxioCam camera attached to a Zeiss microscope.

Some neurons were developed using nickel-3,4 diaminobenzidine (Ni-DAB) as follows: the slices were washed first in 0.01 M PBS 4 times, 10 minutes each wash. Subsequently, the slices were left for overnight incubation in avidin-biotinylated horseradish peroxidase (ABC 1:100 on PB-0.3% Triton X-100) at room temperature. Next day, the slices were washed in 0.1 M PBS 2 times, 10 minutes each. Then, the slices were incubated in Ni^{2+}DAB for 3-10 minutes, air dried overnight, and coverslipped using DEPEX.

For AIM 2, recorded pairs were developed for Ni-DAB as follows: Following physiological experiments, slices were fixed overnight in the recording solution with 4% paraformaldehde and 0.1 % glutaraldehyde. Next day, slices were washed with 0.1 M PBS, 4 times, 10 minutes each wash. Slices were then incubated first in 10% (20 minutes)

followed by 20% (30 minutes) sucrose (in PBS, pH=7.4) for cytoprotection. Subsequently, slices were freeze thawed with liquid nitrogen and then washed with 0.1 M PBS for 2 times (10 minutes each wash). Subsequently, slices were incubated in 1% sodium borohydrate for 20 minutes followed by a wash in 0.1 M PBS for 2 times (5 minutes each wash). The slices were then transferred into a 1% H_20_2 solution for 20 minutes followed by a wash in 0.1 M PBS for 3 times (10 minutes each wash). Next, the slices were left for overnight incubation in avidin-biotinylated horseradish peroxidase (ABC 1:100 on PB-0.3% Triton X-100) at room temperature. Next day, slices were first washed in PBS followed by a final TBS wash. Following this, the slices were incubated in Ni-DAB for 3-10 minutes followed by initial visualization in 0.1 M PBS. Postfixation was done in 0.1 OsO_4 with sucrose (6.46 %) in 0.1 M PBS for 25 minutes. Dehydration was done with increasing ethanol concentrations (30, 50, 70, 90, and 100%). The slices were then flat embedded in durcupan and left in the oven at 59ºC overnight for polymerization.

CHAPTER III (AIM 1): PHYSIOLOGICAL PROPERTIES OF BFC NEURONS

3.1 Introduction

Most *in vivo* studies did not identify the neurochemical profile of the recorded neurons until juxtacellular labeling (Pinault, 1996) and *post hoc* immunocytochemistry was incorporated into BF studies. In rats under urethane anesthesia, the tail pinch induced cortical activation (i.e. shift from slow-irregular activity at delta range to theta-like activity) was found to be associated with an increase in BFc neuron firing rate along with a transition from an irregular firing to rhythmic burst firing. In this study, spike triggered averages revealed a robust cross-correlation between the unit burst firing and cortical theta activity (Manns et al., 2000a). The authors suggested that the firing rates and patterns of BFc neurons could be relayed to cortical neurons in a "uni-directional" manner (Manns et al., 2000). While this thinking accounts for the possible "bottom up" mechanisms whereby brainstem inputs are relayed to the cortical structures via BFc neurons, it falls short in identifying the potential role of "top down" processes whereby an interaction in the opposite direction occurs [see. Golmayo et al. (2003); Rasmusson et al. (2007)]. Conversely, Duque et al. (2000) did not observe bursting activity in BFc neurons under any circumstances including spontaneous and tail pinch induced changes in cortical activation. By analyzing different EEG epochs in detail and correlating single unit activity and EEG zero-crossings at different time windows, Duque et al. (2000) reported a two-way interaction between BFc neurons and cortical activation. During peaks at beta and delta frequencies, increased BFc neural activity preceded cortical activation while an opposite relationship was observed when the peak frequency band was constricted around 1 Hz. Finally, in a study recording from head fixed rats, Hassani

et al. (2009) confirmed that BFc neurons are active during naturally occurring REM sleep.

Studies investigating the membrane properties of BFc neurons employed different strategies to confirm their neurochemical identity. Initial studies recording from the MS/vDB complex relied on *post hoc* immunocytochemistry for AChE following biocytin labeling of cells in slices [e.g. Griffith and Matthews (1986)]. Later studies employed the same approach using ChAT instead of AChE as a marker [e.g. Markram and Segal (1990); Hedrick and Waters, (2010)]. Following the recognition that BFc neurons are large sized "slow-firing" neurons with prominent AHPs (S-AHP cells), a number of studies solely relied on these two characteristics for characterizing further attributes of BFc neurons in cultures [e.g. Allen et al. (1993)] and slices [e.g. Garrido-Sanabria et al. (2011)]. A fruitful approach has been *in vivo* prelabeling of BFc neurons with a cy3 conjugated p75 antibody based on findings that BFc neurons express this marker [e.g. (Wu et al., 2000)]. Experiments involving BF cultures heavily relied on single cell RT-PCR for detecting ChAT mRNA in recorded neurons [e.g. Han et al. (2002)] while one study adopted this approach in acute BF slices (Sotty et al., 2003).

The different methods employed by different laboratories certainly introduced a level of "noise" into the literature. For instance, p75 is not expressed by all BFc neurons (Hecker et al., 1994). Reliance on soma size alone is amenable to false positives. For instance, NPY+ BF neurons and BFc neurons cannot be distinguished based on soma size (Duque et al., 2007). Immunocytochemistry on recorded neurons on the other hand is likely to produce false negatives due to washout of proteins during recordings. In line with this thinking, Henderson et al. (2001) reports inconsistencies between the ratio of

slow firing neurons and other neuron types recorded in BF slices and immunocytochemical estimates from anatomical studies. So, it is possible that some neurons not exhibiting the slow firing (or non S-AHP as referred in Griffith et al., 1991) are cholinergic. Finally, the absence of reports documenting inconsistencies between neurons positive for ChAT and AChE is a source of concern as AChE is also found in noncholinergic neurons (Eckenstein and Sofroniew, 1983). This complicated scenario becomes even more intricate considering possible species and regional differences which are going to be described shortly.

Ignoring the inconsistencies for now, several unifying principles about the membrane physiology of BFc neurons can be described. In line with the initial suggestions, BFc neurons likely constitute slowest firing neuronal population in the BF (Griffith et al., 1991). Although reports about their spontaneous firing is mixed, intracellular current evoked spikes do not exceed 8-10 Hz. As initially proposed, the firing is delimited by the prominent afterhyperpolarizations following action potentials (Griffith, 1988; Alonso et al., 1996; Gorelova and Reiner, 1996). When these neurons are depolarized from a hyperpolarized potential, they typically exhibit a conspicuous delay in firing along with a voltage hump (Eggermann et al., 2001) indicative of the presence of a transient potassium current. This thinking has been supported by pharmacological and voltage clamp studies (Griffith and Sim., 1990; Tkatch et al., 2000). Finally, BFc neurons exhibit prominent time independent inward rectification and absence of voltage sag, indicating their membrane properties are minimally governed by h currents (Bengtson and Osborne, 2000).

However, apparent inconsistencies taint this unifying picture. In an initial study, Khateb et al. (1992) reported the presence of a prominent voltage sag in BFc neurons identified in guinea pig substantia innominata. This was not replicated by the same group recording in the same region and species (Khateb et al., 1995; 1997). A number of reports by other groups reporting lack of a voltage sag in BFc neurons seem to settle down the issue that there is no big contribution by h-currents to BFc neuron physiology [e.g. Bengtson and Osborne (2000)]. Perhaps the biggest inconsistency pertains to the proposition that 2 modes of operation exist in BFc neurons, a finding consistently reported by Jones and colleagues [e.g. Khateb et al., (1992; 1995; 1997); Alonso et al. (1996); Eggermann et al. (2001)] primarily in the guinea pig substantia innominata. According to these studies, when depolarized from hyperpolarized potentials, BFc neurons fire in rhythmic bursts with an intraburst frequency ~100-200 Hz while tonic discharge mode dominates these neurons when they are depolarized. These bursts happened spontaneously during NMDA application and were prolonged by the negative influence of carbachol on afterhyperpolarizations (Khateb et al., 1997). Although these results are exciting and fit with the *in vivo* data coming from the same group (Manns et al., 2000a), they contradict the reports by other groups using other species and recording from other regions [e.g. Griffith et al., (1991); Gorelova and Reiner (1996)]. Momiyama and Zaborszky (2006) recording from the SI in rats did not report bursting either, partially ruling out the possibility of regional differences. So far, the sources of these inconsistencies are not clear. Bengtson and Osborne (2000) recording in VP in rats reported a very prominent spike frequency adaptation in BFc neurons, again raising the possibility that there are subtle regional differences giving rise to different

electrophysiological properties. Conversely, Garrido-Sanabria et al. (2007) reported a considerable heterogeneity in slow-firing neurons (a proportion of which were confirmed to be BFc neurons with p75 labeling) within MS/vDB based on their firing patterns (i.e. firing delay and spike frequency adaptation). In cultures, a considerable heterogeneity is reported in the calcium current density of cholinergic neurons (Han et al., 2005). In short, the sources for the heterogeneity of the intrinsic membrane properties of BFc neurons are far from clear. Unfortunately, not a single study focused on multiple BF subregions using both current and voltage clamp recordings. Such a study would definitely help in unraveling the origins of the heterogeneity: Is it an experimental artifact, a regional specialization, or are different BFc neurons intermingled together? If there are differences, what are the mechanisms? Until these questions are answered clearly and more *in vivo* BFc neuron recordings are done, correlating the physiological properties of BFc neurons in the intact animal versus slices seems to be impossible.

3.2 Specific Methods

3.2.1 Animals

BAC transgenic mice expressing eGFP under the promoter of ChAT (B6.Cg-Tg(RP23-268L19-EGFP)2Mik/J) were used in these experiments.

3.2.2 Protocols for electrophysiological data acquisition and analysis

These experiments were done using potassium based intracellular solutions. Voltage-current (V-I) relationships were generated for each neuron using 500 msec current pulses ranging from -100 to +120 pA in 20 pA increments at 0.33 Hz in current clamp mode mode unless otherwise indicated. These pulses were delivered from -70 mV and from the resting membrane potential. In some recordings, higher current amplitudes

were used if necessary (see electrophysiological parameters tested in Table 1). Analysis of current clamp recordings was done for data obtained from -70 mV unless otherwise stated.

Current densities were calculated by dividing the current amplitude by whole cell capacitance. Whole cell capacitance was measured by applying 5 mV pulses from -70 mV and integrating the resulting capacitative transient. The half-maximal activation of currents were studied by applying a sigmoidal fit to the current-voltage (I-V) curves where current responses were normalized to the maximum recorded current.

For the measurement of I_A type currents, cells were kept both at -90 and -40 mV and voltage steps of 500 msec duration were applied in 10 mV steps up to +10 mV at 0.33 Hz for activation of transient outward currents. The current responses obtained with a V_{hold} of -40 mV were subtracted from those acquired with a V_{hold} of -90 mV. During these recordings, TTX (1 µM) and $CdCl^-$ (350 µM) were present in the bath to block voltage gated sodium and calcium conductances respectively.

In order to directly compare the firing properties and low voltage activated calcium channel function, the neurons were first examined and identified in current clamp experiments carried out using the potassium based intracellular solution. Following the identification of the firing properties, the patch pipette was withdrawn and cells were re-patched using the cesium based intracellular solution. Initial re-patching was done while the slice was still being perfused with the regular ACSF. Subsequently, the ACSF was switched to the modified ACSF containing Ba^{2+} containing (in mM): 79.5 NaCl, 2.5 KCl, 1.2 $NaHPO_4$, 26 $NaHCO_3$, 1.3 $MgCl_2$, 2 $CaCl_2$, 10 glucose, 40 TEA, and

5 $BaCl_2$. In these experiments, the neuron was kept at -80 mV and presented with 2 second-long prepulses ranging from -110 to -50 mV in 10 mV increments followed by a 500 msec step to -40 mV. TTX (1 µM) and TEA (40 mM) were present for blocking voltage gated sodium and potassium conductances. In addition, voltage steps from -70 to -40 mV were used to measure the total inward current under identical conditions.

3.3 Results

3.3.1 Co-localization of GFP signal and ChAT immunohistochemistry in BF

In sections processed for ChAT immunohistochemistry, a total number of 739 eGFP+ neurons in BF areas were counted, 640 (86%) of which were also immunopositive for the ChAT antibody. ChAT-immunopositive neurons negative for GFP were not observed (see Figure 3.1 for representative eGFP/ChAT+ neurons in hDB).

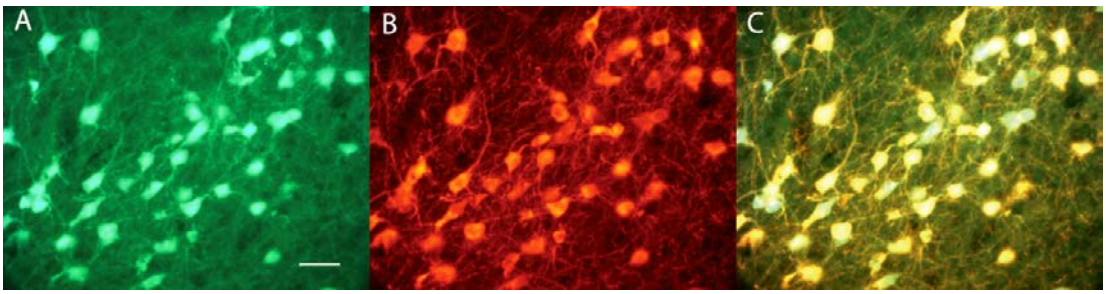

Figure 3.1 Colocalization of ChAT-eGFP and ChAT immuno-signal. A. eGFP expression. **B** ChAT immunostaining, **C.** Overlay of (A) and (B) shows that all eGFP expressing cells are stained with an antibody against ChAT. Scale bar: 50 µm.

3.3.2 Distribution of recorded neurons

The distribution of biocytin filled neurons was analyzed using fluorescent microscopy. See figure 3.2 for a demonstration of the variety of regions targeted. Nineteen neurons were located in the hDB. The rest of the neurons were localized in different areas including the lateral hypothalamus (n=1), VP (n=1), MS (n=1), vDB

(n=1), lateral preoptic area (n=2), SI (n=3), and anterior amygdaloid area (n=1); areas containing the bulk of cholinergic corticopetal neurons. One neuron was localized in the bed nucleus of the stria terminalis (BNST) and two neurons were found in the interstitial nucleus of the anterior commissure, posterior component (IPAC). These latter three neurons shared similar physiological properties with neurons in the aforementioned BF regions. A subset of neurons was found at the border of BNST/VP/LPO (n=1), hDB/VP border (n=1), VDB/hDB border (n=1) hDB/SI border and IPAC/VP border (n=1). I analyzed whether the physiological differences observed had an anatomical correlate in these cells. Due to the small number of samples from individual areas, hDB vs. non-hDB comparisons were made and none of the physiological parameters (described below) tested revealed any differences (data not shown) suggesting that BFc neurons with putatively different functions are intermingled in different areas of the BF. Finally, no region seemed to contain BFc neurons with unusual properties (i.e. no bursting cell was seen in SI; n=3).

3.3.3 Physiology of BFc neurons

BF neurons were characterized according to several physiological attributes (definitions for each in Table 3.1). Because no physiological parameter exhibited a significant alteration due to filling with biocytin (not shown) all data were pooled together. An additional number of neurons (n = 24) were recorded in further experiments (see below). Most BFc neurons exhibited a time independent anomalous rectification and a prominent after-hyperpolarization (AHP), outward rectification, and wide spikes (~1.8 msec half-width) (Figure 3.3).

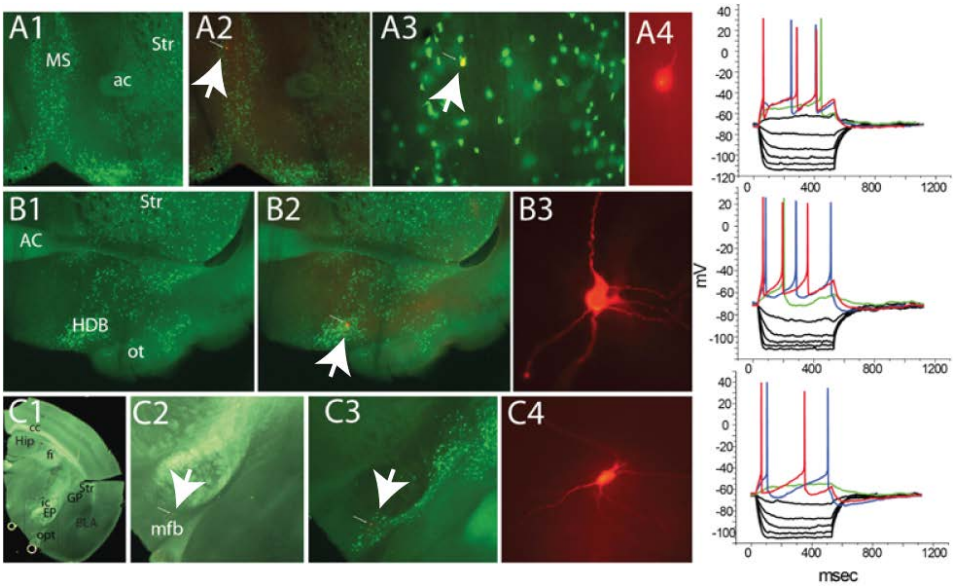

Figure 3.2 Diverse BF subregions were targeted during whole cell recordings. A. A neuron recorded from the medial septum (MS). (A1) Distribution of eGFP+ cells taken at 4X magnification. (A2) Overlay of eGFP and Texas Red signal. (A3) Image taken at 20X where eGFP and Texas Red signals are overlaid. Arrows here and in (A2) point to the recorded neuron that was filled with biocytin. (A4) Image of the cell taken at 40X. **B.** A neuron recorded from horizontal limb of diagonal band (HDB). (B1) Distribution of eGFP+ cells at 4X. (B2) Overlay of eGFP and Texas Red signals. Arrow points to the recorded neuron. (B3) 40X image of the same cell. **C**. A Neuron recorded in the vicinity of medial forebrain bundle (mfb) in the most caudal extent of BF. (C1) 1.25X image. (C2) Texas Red signal under dark field illumination taken at 4X. The field corresponds to the box in C1. (C3) Texas red image is overlaid with the intrinsic eGFP signal. Arrows here and in C2 point to the recorded neuron, (C4) Recorded cell at 40X. Abbreviations: BLA: basolateral amygdala, cc: corpus callosum, EP: entopeduncular nucleus, fi: fimbria hippocampus, GP: globus pallidus, Hip: hippocampus, ic: internal capsule, opt: optic tract, Str: striatum. Voltage responses to current injections in these neurons are shown on the right side.

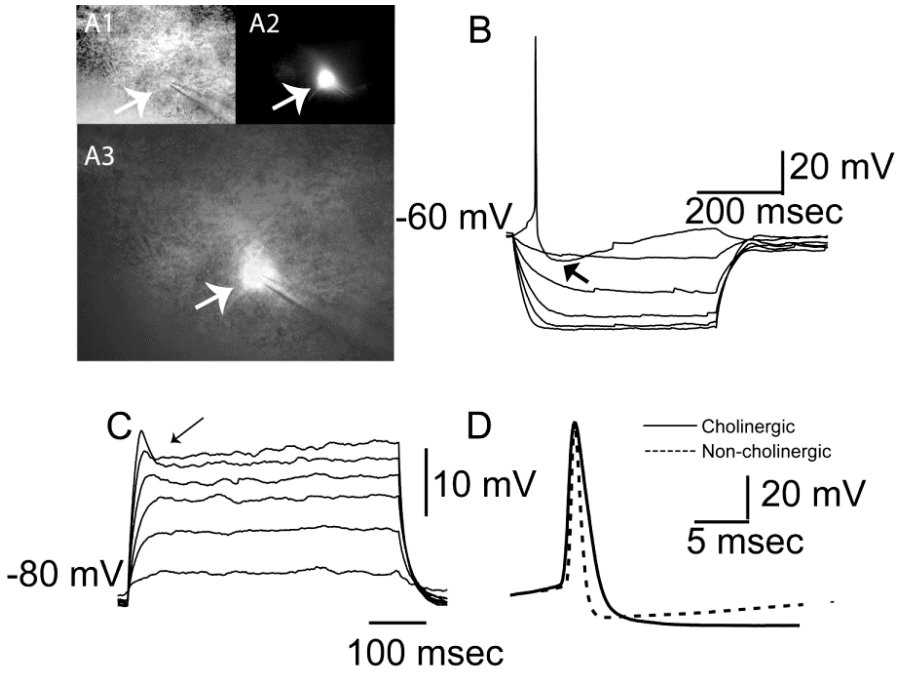

Figure 3.3 Morphological and physiological identification of eGFP expressing neurons in the BF. A. Morphology of a typical eGFP+ neuron. (**A1**) Image of the neuron taken with DIC. (A2) Same neuron imaged with epifluorescence illumination showing eGFP fluorescence. (A3) Overlay of images in A1 and A2. **B.** A cholinergic neuron at rest responding to negative and positive square pulses ranging between -100 to 20 pA in 20 pA increments. Note the prominent AHP following the single spike, and anomalous inward rectification at negative voltages. **C**. The same neuron recorded in the presence of 1 µM TTX from a membrane potential of -80 mV in response to positive square current pulses from 20 to 120 pA in 20 pA increments. Note the voltage hump (indicated by arrow) and the outward rectification in the positive direction. **D**. A representative cholinergic neuron spike (thick continuous line) and a spike from a non-cholinergic neuron (dashed line). Note the wide spike of the cholinergic neuron.

Two groups of BFc neurons could clearly be distinguished based on differences in firing delay at rheobase current injections: late-firing neurons (LF, Fig. 3.4A, *blue trace*) and early-firing neurons (EF, Fig. 3.4A, *red trace*). LF neurons had a mean firing latency of 343 ± 76 msec (n = 33, range: 240 to 499 msec) whereas EF neurons had a mean firing latency of 107 ± 53 msec (n = 70, range: 18 to 206 msec (Table 3.2). The AP delay distributions are shown in figure 3.4B in the form of cumulative probability plots. Each

of the distributions was normally distributed within itself (Kolmogorov-Smirnov, LF: $p = 0.200$, $n = 32$; EF: $p = 0.183$, $n = 69$) while the entire data set deviated significantly from a normal distribution (Kolmogorov-Smirnov, (102) .155 $p=0.00$), and no cells were observed that had delays between 206 and 240 msec (Fig. 3.2B). Further attributes differentiating these neurons are (see Table 3.2 for a summary): the linear slope of the current-frequency relationship of EF cells is steeper than LF neurons. This is also reflected by significantly higher firing rates elicited with current injections with 60 pA or higher from -70 mV (ANOVA, $F(5,96) = 2.762$, $p<0.05$, Fig. 4C). Moreover, EF neurons had lower AHP amplitudes (Fig. 3.4D).

The spike frequency adaptation in LF neurons was increased when their AHP amplitude was reduced following application of 100 nM apamin, a selective SK channel inhibitor (n=3; Fig. 3.5A1 *inset*) suggesting the participation of SK channels in determining the firing properties of LF neurons. In addition, EF cells exhibited significantly more spike frequency adaptation as compared to LF neurons (Table 3.2). The solid traces in Figure 3.5A1 and 3.5B1 illustrate the difference in spike frequency adaptation among LF and EF cells when stimulated with a strong depolarizing current pulse, while the dashed traces illustrate the basic delayed onset that characterizes the two cell types at rheobase. In line with the differences in spike frequency adaptation in these neurons, LF neurons could maintain a precise firing pattern when constant current was applied (Fig. 3.5A2), while most EF neurons fired irregularly under similar conditions or became completely silent (4 out of 21) following a train of spikes (Fig. 3.5B2). Such EF neurons could, however, fire regularly when hyperpolarizing pulses at a fixed frequency were superimposed on a constant depolarizing current (Fig. 3.5B2).

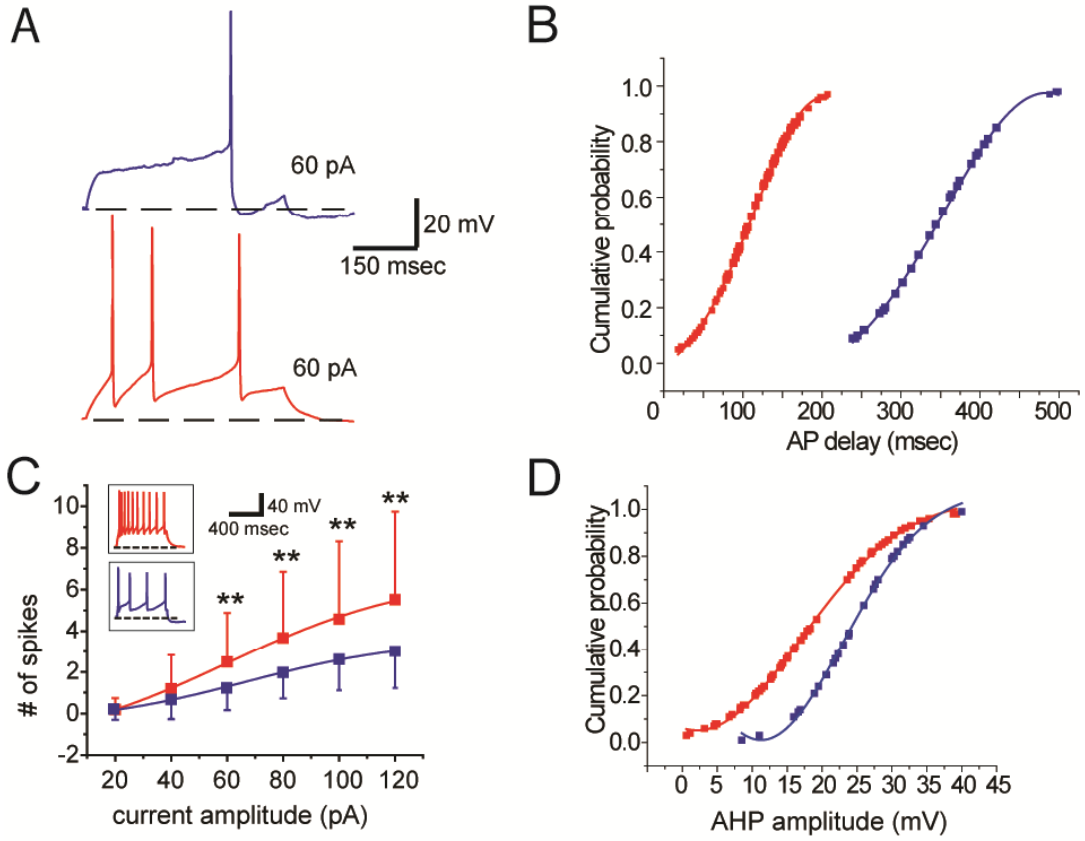

Figure 3.4 BFc neurons can be electrophysiologically classified into two groups. A A late-firing (LF) (top, blue trace) and an early-firing (EF) (bottom, red trace) neuron responding to rheobase current injections from -70 mV. **B** Cumulative probability plots for action potential delays in LF and EF neurons. X-axis: action potential delay with rheobase current injections. **C** Number of action potentials elicited as a function of the injected current. X-axis: injected current amplitude; y-axis: number of action potentials. **D** Cumulative probability plots for afterhyperpolarization (AHP) amplitudes in LF and EF neurons. X-axis: AHP amplitude following the first action potential. Error bars indicate S.D. ** $P < 0.01$

When measured with a 500 msec, 120 pA square pulse from -70 mV (see Table 3.1), varying degrees of depolarization block were apparent in many of the EF neurons within 500 msec, accompanied by significant statistical differences between the two populations along this dimension (Table 3.2). Conversely, 18 % LF neurons displayed spike frequency acceleration (Fig. 3.5C1 and 2).

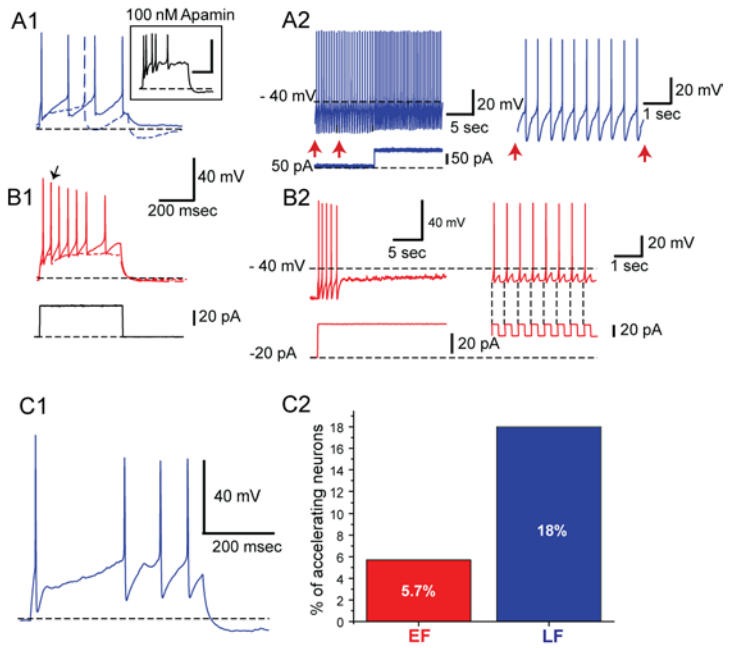

Figure 3.5 EF neurons show higher spike frequency adaptation than LF neurons. A An LF neuron without spike frequency adaptation (A1). Apamin application increased the spike frequency adaptation (A1 Inset). The dashed trace indicates response to a rheobase current injection. A2 shows the same neuron firing regularly in the presence of prolonged background pulses. On the right is an expansion of the time indicated with arrows. **B1** and **B2** The same arrangement as in **A1** and **A2**. The EF neuron fires transiently in response to a sudden positive shift in the injected current. This is followed by irregular low frequency firing and complete silencing. Superimposed hyperpolarizing pulses (B2**,** right side) on the background current, recovers firing. **C** An LF neuron exhibiting spike frequency acceleration (C1) and the percentage of neurons with spike frequency acceleration in both groups (C2).

In order to determine the possible mechanisms underlying the firing delay differences between EF and LF neurons, the membrane time constants of these neurons were compared. EF neurons displayed a significantly shorter time constant than LF neurons (Table 3.2). However, the difference is much smaller than the observed firing delay differences. On the other hand, action potential threshold for EF neurons is slightly, but statistically significantly, lower than for LF neurons (Table 3.2), which can also only partially explain the shorter delays.

3.3.4 Voltage clamp analysis

In an attempt to find the mechanism underlying different firing delays, I measured the transient K^+ current expressed in these neurons, an A-type current, I_A. Figure 3.6A shows the protocol and raw currents used to determine I_A like currents (Fig. 3.6A1) and the net I_A like current obtained after subtraction of non-inactivating currents from those obtained from a low, de-inactivating, voltage (-90 mV, Fig. 3.6A2). Both cell types expressed I_A to varying degrees, with LF neurons exhibiting slightly higher current densities than EF neurons, but this did not reach significance (ANOVA, $F(7,24) = 0.426$, $p = 0.43$). At a voltage of -40 mV, the voltage closest to the spike threshold in these neurons, current densities were 8.9 ± 3.6 pA/pF for LF neurons and 8.3 ± 5.1 pA/pF for EF, which also did not reach significance ($t(31) = -0.3452$, $p = 0.73$, Fig. 3.6B1). I_A like current decay time constants measured at -40 mV (which was the only potential where decay time constants could reliably be fitted with a single exponential) were 133.9 ± 116 msec for EF and 137.1 ± 65 msec for LF neurons. This was also not significantly different between these two populations ($t(31) = 0.0796$, $p = 0.93$, Fig.3.6B2). Finally, the

half-maximal activation voltages for I_A by fitting a sigmoidal function to the conductance vs voltage relationships of the two cell types were determined. Here again, there was no statistically significant difference (-31 ± 7 mV for EF and -28 ± 5 mV for LF neurons; t(31) = -1.109, p =0.85). Although no differences between mean values of any of these parameters of I_A were found, the delay in action potential firing in individual LF neurons appears to relate to decay time of the I_A they express. A clear linear relationship between I_A decay time constant (measured as single exponential fits to the decaying portion of I_A measured at -40 mV) and action potential firing delays was observed only in LF neurons (after subtracting the membrane time constant to remove its small contribution, see Table 3.2, Fig. 3.6C1, r (9) = 0.77, p = 0.007) but not in EF neurons (Fig. 3.6C2, r (21) = 0.0.34, p= 0.090). The general picture emerging from these correlations did not change when the absolute spike delay was considered instead of membrane time constant-subtracted spike delay (not shown). Figure 3.6D illustrates two LF neurons with different current densities and kinetics and the spiking delay differences in the expected direction.

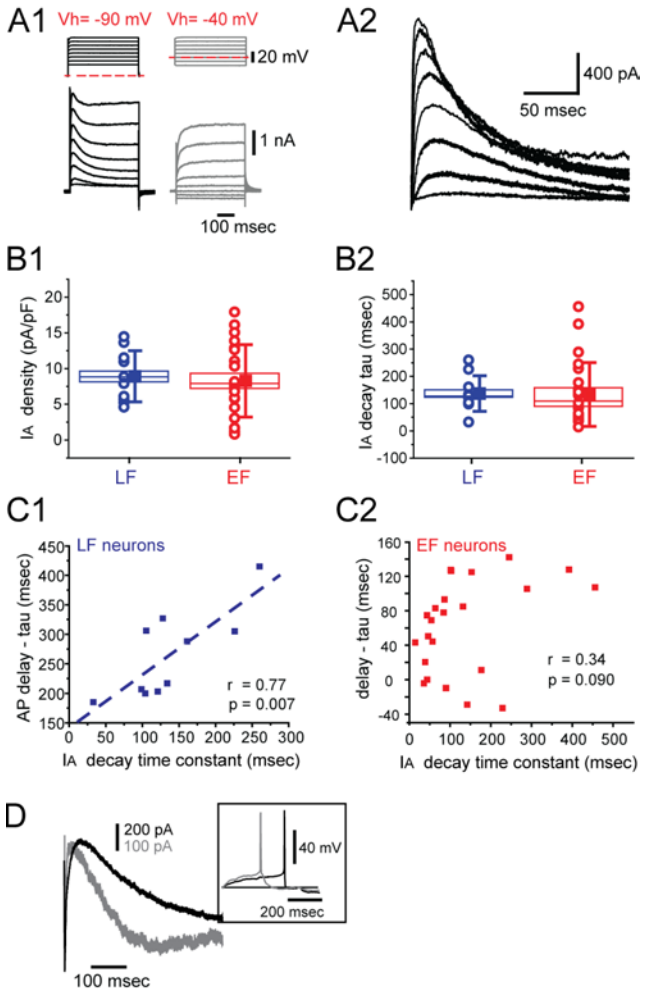

Figure 3.6 IA properties in BFc neurons do not differ. A. Measurement of I_A. (A1) Voltage clamp protocols (top left) used to isolate I_A. Currents were measured in the presence of 1 µM TTX and 350 µM $CdCl_2$. Examples of current responses to these two protocols are shown below. The currents shown on the right (V_{hold}= -40 mV, dashed red line, steps: -60 to +10 mV) were subtracted from the currents shown on the left (V_{hold}= -90 mV, dashed red line). (**A2**) The net I_A obtained after the subtraction described in A1. **B**. Box plots for I_A density (B1) and I_A decay at -40 mV (B2). LF and EF neurons are shown in blue and in red respectively. In B1 and B2, the box sizes indicate the standard error of the mean (S.E.M.) while whiskers indicate standard deviation (S.D.). Circles indicate individual data points while the filled square shows the group means. **C.** Membrane time constant corrected action potential onset (y-axis) correlations with I_A decay time constants (x-axis) in LF (C1) and EF (C2) neurons. **D**. Representative I_A recordings from two LF neurons along with their current clamp recording of spiking activity (inset). The cell indicated with darker trace has a slower inactivating I_A along with a more pronounced spike delay.

Given the absence of significant differences in I_A-type currents but a significant relationship between I_A decay time constant with spike delay only in LF neurons, the possibility of calcium currents contributing to the earlier spiking in EF neurons in separate experiments was considered. For these purposes, LVA mediated Ba^{2+} currents (I_{LVA}) in EF and LF neurons were compared (see Methods for details). In line with these results, I_{LVA} density was significantly higher in EF neurons when tested with pulses from -70 mV to -40 mV (6.4 ± 3.8 pA/pF for EF and 2.3 ± 2.4 pA/pF for LF neurons; t (13)=2.467, p =0.03, Fig. 3.7A). In order to confirm that these effects are due to I_{LVA}, I also measured the inward current at -40 mV obtained with different prepulse voltages (Fig. 3.7B1) and confirmed a statistically significant difference in I_{LVA} between EF and LF neurons for all values except -50 mV (ANOVA, $F(6,8) = 2.110$, $p < 0.05$; Fig. 3.7B2). No statistically significant difference was observed for either the half-maximal activation (-71 ± 12 mV for LF, -63 ± 10 mV for EF; t(13) = -1.327, p = 0.207) and decay time constant (16.7± 10.0 msec for LF, 20.9 ± 10.0 msec for EF; t(13) = 0.247, p = 0.808) between the two populations. HVA Ca^{2+} currents were measured with ramp protocols (Murchison et al. 2009) and yielded no significant differences in EF and LF neurons (data not shown).

To confirm these results independently in pharmacological experiments (n=4 for each group), I investigated potential spike onset changes under control conditions and in the presence of 5 μM Ni^{2+}, a concentration that is close to IC_{50} values for inhibition of Ca(v) 3.2 channels (Kang et al. 2006), which is the dominant channel isoform in cholinergic BF neurons (Han et al. 2005). In EF neurons, Ni^{2+} significantly delayed the spike onset (72.8 ± 12.1 msec without $Ni^{2+}$and 139.3 ± 31.8 with Ni^{2+}; t (3) = 3.6584, p <

0.0001, paired t-test) suggesting an important contribution of I_{LVA} to AP delay. Contrary to this, Ni^{2+} application did not produce a change in action potential delay in LF neurons (315.5 ± 89.3 msec without $Ni^{2+}$and 315.0 ± 81.9 with Ni^{2+}; t(3) = 0.092, p = 0.932, paired t-test; Fig. 3.7C1). A representative effect of Ni^{2+} application on AP delay is shown in figure 3.7C2.

Rheobase current	The current pulse that first elicits an action potential from a holding potential of -70 mV	**First AP delay**	The time between the onset of rheobase current and the threshold of the first action potential
RMP	Voltage value in the absence of DC injections 10 minutes after patching	**AHP amplitude**	The voltage difference between the first action potential threshold and the most negative voltage associated with the following AHP
R_{in}	Calculated from -70 mV in response to a -20 pA current injection	**AHP time to peak**	The time it takes from the action potential threshold to the most negative potential of the AHP
Membrane time constant	Obtained by a single exponential fit to the voltage response from -70 mV to a -20 pA current injection	**Adaptation ratio**	1/(First.ISI/Last ISI) in a recording that contains the first trace with 4 action potentials from -70 mV
First AP threshold	The point where the rising slope first exceeds 10mV/msec at rheobase current	**I-F slope**	The slope of the increase/decrease in action potential frequency as a function of current injection
First AP amplitude	The voltage difference between threshold and peak	**Sag ratio**	Minimum membrane response (around -100 mV for each neuron) / steady state potential.
First AP half-width	The time gap at half-maximal amplitudes of the first action potential	**Depolarization block**	Time between the end of the last AHP to the end of a 500 msec, 120 pA current pulse without an action potential.

Table 3.1. Physiological properties examined and their operational definitions.

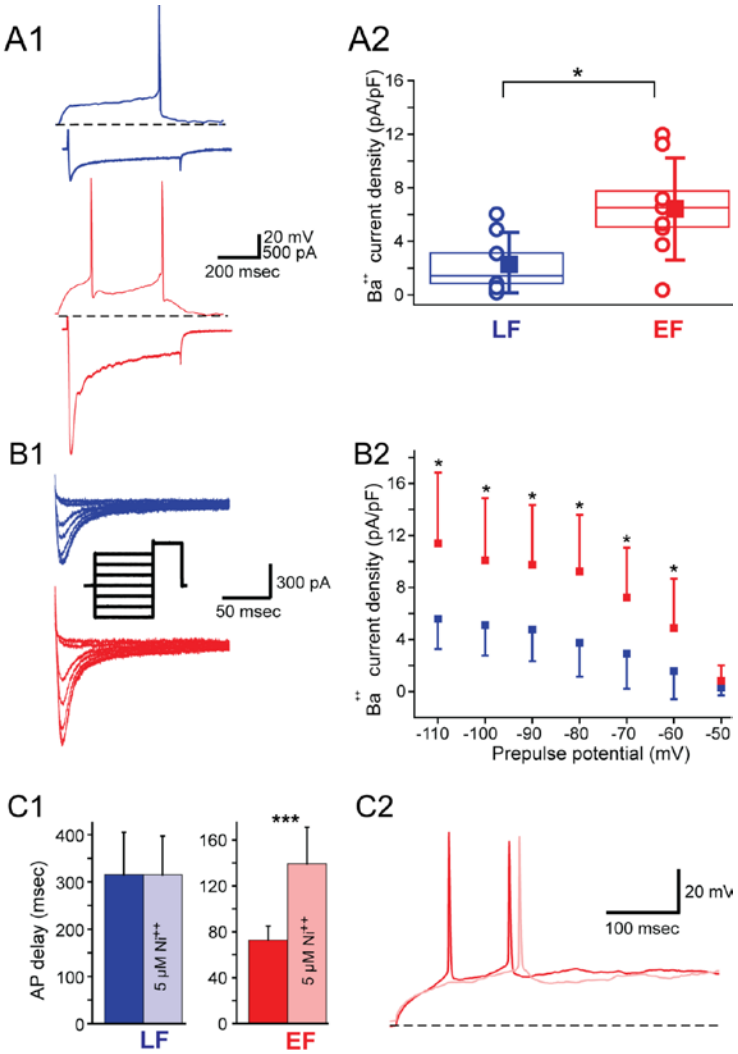

Figure 3.7 EF neurons have a higher density of ILVA calcium channels as evidenced by inward Ba2+ mediated currents. (**A1**) LF neuron (top blue traces) and EF neuron (bottom red traces) in current clamp (top trace in each case) showing the characteristic AP delay in response to a rheobase current injection (60 pA in this case). Bottom trace in each case shows I_{LVA} in response to a voltage clamp step from -70 mV to -40 mV upon re-patching the same cells with Cs-Meth intracellular solution and in Ba^{2+}-containing ACSF (see methods). Scale bars apply to both neurons. (**A2**) Box plot for I_{LVA} densities measured as described in A1. Box size indicates standard error of the mean (S.E.M.). Square and whiskers have been displaced for clarity and indicate mean and standard deviation (S.D.), respectively. Empty circles indicate individual data points (n = 7 LF; n = 8 EF). (**B1**) I_{LVA} measured at -40mV with a de-inactivation protocol (see inset) for an LF (blue) and EF (red) neuron. Inset shows the protocol used to elicit the currents (2000 msec long prepulses from –110 to -50 mV, and 500 msec long test voltage at -40 mV). (**B2**) I-V curve for the protocol in B1. (**C1**) Bar graph illustrating the selective effect of 5 μM nickel on firing delay in EF but not in LF neurons (n=4 for each group). (**C2**) demonstrates the effect of Ni^{++} application (light red trace) on firing delay in an EF neuron.

	Early-firing Mean ± SD	Late-firing Mean ± SD	t	p	df
First AP delay (msec)	107 ± 53 (n=70)	343 ± 76 (n=33)	-16.094	<0.001	101
I-F slope (Hz/pA)	0.06 ± 0.04	0.03 ± 0.02	4.287	<0.001	101
Adaptation ratio	2.74 ± 2.57	1.33 ± 0.57	4.126	<0.001	93
Depolarization block (msec)	136 ± 163	34 ± 79	4.234	<0.001	101
AHP (mV)	18 ± 10	24 ± 7	-3.576	<0.001	101
First AP threshold (mV)	42 ± 4	40 ± 3	2.839	0.006	101
Membrane tau (msec)	44 ± 18	52 ± 16	-2.268	0.025	101
RMP (mV)	58.9 ± 9.3	60.6 ± 7.0	-0.929	>0.05	101
R_{in} (MΩ)	610 ± 301	641 ± 247	-0.512	>0.05	101
First AP amplitude (mV)	71 ± 9	72 ± 7	-0.395	>0.05	101
First AP half-width (msec)	1.8 ± 0.5	1.8 ± 0.4	0.160	>0.05	101

Table 3.2. Early- (EF) and Late-firing (LF) cell's physiological properties. Ranked in order of highest-to-lowest significant difference. Differences tested using the t-Student test for independent measures.

3.4 Summary of the main findings

a) The regional variations within the BF were not associated with obvious physiological differences between BFc neurons.

b) BFc neurons could be divided into two populations based on their action potential delay in response to rheobase current injections. These neurons were named as early firing (EF) and late firing (LF) neurons after the most obvious property that dissociates them.

c) Overall, EF neurons were more excitable. LF neurons could maintain a more sustained firing albeit at lower frequencies.

d) The firing delay differences in the two populations are possibly underlined by the interplay between outward potassium and inward calcium conductances. These diffences along with others might contribute also to other properties such as the different spike frequency adaptation observed in these two populations.

CHAPTER IV (AIM 2): INTERACTIONS AMONG BFC NEURONS

4.1 Introduction

In addition to similar dendritic orientations among neighboring BFc neurons which might signify shared inputs/functions, there are also mechanisms that might support partitioning, possibly among BFc neurons with different projection patterns. This thinking is based upon certain anatomical and pharmacological studies. BFc neurons issue local axon collaterals (Duque et al., 2007), are immunopositive for M2 receptors (Levey et al., 1995a), and pharmacological studies unraveled inhibitory actions of acetylcholine/muscarine on these neurons (Harata et al., 1991; Wu et al., 2000). Second, activity dependent acetylcholine release has been reported in BF slices containing MS and the diagonal bands (Metcalf et al., 1988; Metcalf and Boegman, 1989; Nishimura and Boegman, 1990) suggesting that local BFc collaterals have functional release sites. Ultrastructurally, BFc neurons are shown to be innervated by ChAT positive terminals (Martinez-Murillo et al. 1990; Smiley and Mesulam, 1999). In addition, axons might not be the only release sites of acetylcholine. Nicotinic acetylcholine receptor rich membrane patches prepared from rat myotubes could “detect” acetylcholine release even when they were placed in the proximity of BFc neurites resembling dendrites in cultures (Allen and Brown, 1996). Furthermore, Allen and Brown (1996) reported acetylcholine release occuring from the somata of BFc neurons under hyper-physiological (i.e. recordings with higher potassium and calcium ions in the bath solution) conditions.

The BF also receives inputs from pedunculopontine (PPT) and laterodorsal tegmental nuclei (LDT), two brainstem nuclei that contain cholinergic and noncholinergic neural populations (Semba, 2004). However, direct cholinergic inputs from these brainstem nuclei do not seem to impinge on BFc neurons. Retrograde labeling

studies coupled with immunocytochemistry revealed that the majority of BF projecting PPT/LDT cells was negative for ChAT (Hallanger and Wainer, 1988). Moreover, PPT/LDT stimulation lead to cortical acetylcholine release and EEG activation (Rasmusson et al., 1994), while as previously mentioned, acetylcholine has inhibitory actions on BFc neurons (Wu et al., 2000). In keeping with this, PPT/LDT induced desynchronization of cortical EEG and increased acetylcholine release in cortex was blocked by the delivery of kynurenic acid, a blocker of fast glutamatergic transmission, into the BF but not by muscarinic/nicotinic antagonists. Accordingly, the PPT/LDT and BFc neuron interactions are not mediated by cholinergic synapses on BFc neurons but entail glutamatergic signaling within the BF.

In short, these studies raise the possibility that local acetylcholine release does occur under physiological conditions and this release has inhibitory actions on BFc neurons. Concluding whether these interactions exist with more elaborate functional approaches, as is the case in the current thesis, is cardinal for more realistic hypothesis about the organization of the BFc system.

4.2 Specific methods

4.2.1 Animals

BAC transgenic mice expressing eGFP under the promoter of ChAT (B6.Cg-Tg(RP23-268L19-EGFP)2Mik/J) were used in conventional electrophysiological experiments. For optogenetic experiments, double transgenic mice obtained by crossing ChAT-eGFP mice (the strain mentioned above) and ChAT-IRES-cre (B6;129S6-ChAT$^{tm1(cre)Lowl}$/J) were used. This double transgenic strategy allowed for recording BFc

neurons not expressing ChR2 (eGFP only cells) while stimulating BFc neurons that express it (eGFP/mCherry+ cells).

4.2.2 Injection sites, and viruses

The injections were done in a bilateral fashion. The injection coordinates for each hemisphere were: 1.4 mm anterior and 1.1 mm lateral to bregma with a depth (with respect to dura) of 5.6 mm (for hDB) and 0.74 mm anterior and 0.25 lateral mm to bregma with a depth of 4.25 mm (for vDB). A single injection of 0.5 µL of AAV5-EF1a-ChR2-mCherry was done on each side and the injection pipette was left in its place for 15 minutes before removal.

4.3 Protocols for electrophysiological data acquisition and analysis

4.3.1 Pharmacological experiments

Carbachol (CCh) (10 µM) was bath applied in the presence of AP5 (100 µM), CNQX (20 µM), and picrotoxin (100 µM). During these pharmacological experiments, the ACSF flow rate to the chamber was increased to ~10 ml/minute. To monitor changes in the membrane potential and input resistance, the neurons were brought to around -70 mV with constant current injections and were presented with 10-30 pA square current pulses of 200 msec duration, every 2.5 seconds. A baseline activity before CCh activation was recorded for 30 to 60 seconds. Subsequently, CCh was applied for at least 3 minutes. Finally, atropine (1.5 µM) was added for at least another 2 minutes. The baseline, CCh and atropine periods were carefully observed for assuring the stability of recordings. For analysis, 12 traces at each condition were averaged that corresponded to the last 12 sweeps during baseline period, 12 sweeps during CCh application that corresponded to a

time between 2 and 2.5 minutes after CCh application, and 12 sweeps during atropine corresponding to 1.5 to 2 minutes following its application.

In another set of experiments, the ACSF flow rate was kept the same as in CCh experiments. Subsequent to whole cell access, the ACSF was replaced with a modified ACSF containing (in mM): 124 NaCl, 3.5 KCl, 1.2 $NaHPO_4$, 26 $NaHCO_3$, 1 $MgCl_2$, 1.2 $CaCl_2$, 10 glucose in addition to 100 AP-5, 20 CNQX, and 100 picrotoxin. After 5-10 minutes in this solution, data acquisition started. The baseline was recorded for 100 to 400 seconds. This was followed by atropine (1 µM) application and data were acquired for an additional duration of 100 to 500 seconds.

4.3.2 Paired recordings

The putative presynaptic cell was patched with a $CsCl^-$ intracellular solution to increase release probability. The spikes were elicited in voltage clamp mode through 5 msec, 40 mV voltage commands from a holding potential of -70 mV. Four spikes separated by 50 msec intervals were generated in this manner every 10 seconds (0.1 Hz). In all instances, the postsynaptic cell was recorded in current clamp mode throughout the recording. The potential postsynaptic cell was kept at a voltage range where the cell's input resistance was from 500-600 MΩ. The top peak to peak membrane potential fluctuations were in the range of 3-5 mV in potential postsynaptic neurons. Decisions about the presence/absence of connectivity were based on the difference between the SD of membrane fluctuations and the peak of the putative response, a methodology adopted from Feldmeyer et al. (2006). See results for details. In all these experiments, CNQX (20 µM) and AP-5 (100 µM) were present in the ACSF and the distances between BFc

neurons recorded were ~10-60 µm. Atropine (1 µM) was added in instances where a connection was suspected on-line.

4.3.3 Optogenetic experiments

In these experiments, mCherry/eGFP+ neurons were patched in order to confirm the ability of blue light to cause action potentials in infected BFc neurons. BFc neurons, positive only for eGFP were patched to record possible nicotinic/muscarinic synaptic influences. See figure 4.4 for the appearance of a representative slice. In all cases, the entire slice was illuminated with an LED bulb (see general methods for details) between 3 to 5 msec every 10-30 seconds. General muscarinic antagonist atropine (1 µM) or the specific M2 receptor antagonist methocramine (MTA; 1 µM) were used for the pharmacological identification of the receptors involved. In some instances, apamin (100 nM), an SK channel blocker, was added to the solution either before (for between cell analysis) or after (for within cell analysis) patching.

4.4 Results

Following biocytin cytochemistry for Ni-DAB, putative axonal arborizations confined to the BF were readily observed in most BFc neurons. Since the processing did not entail plastic embedding and tissue shrinkage may interfere with an accurate quantification of neuronal morphology, no quantitative analysis was done in these sections. However, a representative case is used for illustrating the putative local axonal arbor of a BFc neuron (Figure 4.1). The preservation of axonal collaterals was commonly observed in filled BFc neurons and validates the analysis of synaptic connections between BFc neurons in acute slices.

4.4.1 Carbachol experiments

To investigate whether BFc neurons express somatodendritic muscarinic receptors, the membrane potential and input resistance changes were monitored in the absence/presence of 10 µM CCh and 10 µM CCh+1 µM atropine in these neurons while slices were continuously superfused with blockers for fast GABAergic and glutamatergic neurotransmission. From -70 mV, CCh hyperpolarized the BFc neurons (-4.20 ± 3.57 mV; $t = -2.879$, $p < 0.05$, paired t-test). This hyperpolarization was accompanied by a reduction in input resistance (109.83 ± 47.02 MΩ drop in input resistance). This drop corresponds to around 20 % reduction in total input resistance (23.36 ± 10.29 % reduction). However, this did not reach significance ($p = 0.07$). I did not do a dose/response profiling of CCh effects. As an alternative route for ascertaining the accuracy of possible interpretations, muscarinic receptor antagonist, atropine (1 µM) was added to the ACSF following the monitoring of CCh effects. Student's t-tests did not reveal significant differences between membrane potential and input resistance values during CCh free and CCh+atropine periods ($p > 0.05$) (Figure 4.2) suggesting that BFc neurons are hyperpolarized through muscarinic acetylcholine receptors.

Figure 4.1 Local axonal arborization of a BFc neuron. This neuron was filled with biocytin and processed with Ni-DAB. The image is taken at a single z-depth. Putative axons did not exhibit tapering and varicosities were apparent (indicated with black arrows) were apparent. Bar scale: 15 µm.

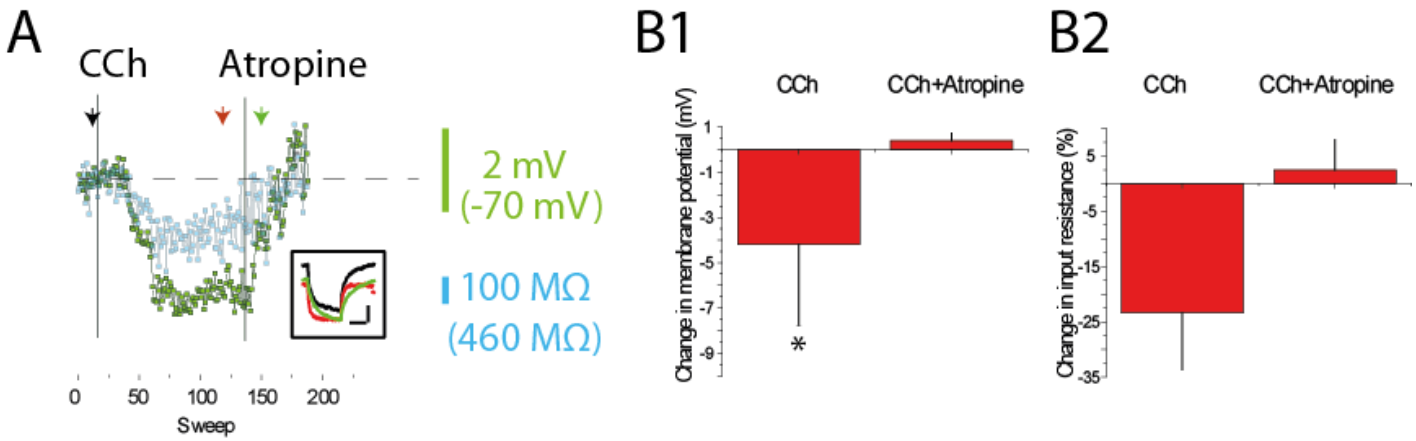

Figure 4.2 Carbachol inhibits BFc neurons. A Illustration of a single neuron responding to carbachol (10 µM) application. Green data points: Membrane potentials recorded just before the onset of negative square pulses. Blue data points: Input resistance values as measured from the response to a 10 pA square pulse of 200 msec duration. In scale bars, numbers in paranthesis correspond to the value at the dashed line. Inset shows the average of 12 traces taken from the area indicated by arrows (see methods). Traces and arrows are color-matched. Horizontal scale bar: 100 msec; vertical scale bar:2 mV **B** Change in membrane potential (B1) and percentage change in input resistance (B2). * $p < 0.05$

4.4.2 Paired recordings between BFc neurons

Twenty BFc pairs were tested for connectivity. The connection tests could be carried only in one direction as the potential presynaptic neuron was patched using a cesium-based intracellular solution to increase neurotransmitter release through blockade of potassium channels. In 3 pairs tested (15%), firing of the presynaptic neuron resulted in a hyperpolarizing response whose amplitude was >8 times bigger than the standard deviation of voltage fluctuations prior to the response in the postsynaptic neuron. Thus, the amplitude of this hyperpolarizing event was much higher than what would be expected from random noise. The peak average amplitude of these hyperpolarizations ranged from -0.37 to -1.13 mV (mean: -0.68 ± 0.39 mV) from membrane potentials in the range of -58 to -71 (-64.66 ± 6.50 mV). For the three postsynaptic neurons, the averaged onset latencies ranged from 14.6 to 73 msec (35.5 ± 32.54 msec; Table 4.1) while the variability along this dimension within individual neurons was not discernible. The high variability in onset latencies relates to one case where the hyperpolarization was observed after the second action current in the presynaptic neuron (Table 4.1).

	Membrane potential of postsynaptic cell (mV)	Onset latency (msec)	Peak amplitude (mV)	Time to peak (msec)	10-90% rise time (msec)	Return to baseline from peak (msec)	Total response duration
Connected pair 1	-71	73.0	-0.37	40	33.2	177	217
Connected pair 2	-58	14.6	-1.13	48	33.2	219	267
Connected pair 3	-65	18.9	-0.54	55	36.8	229	284

Table 4.1 The properties of muscarinic connections among BFc neurons.

One of the connected pairs (Figure 4.3A) could be successfully recovered with biocytin cytochemistry and embedded in durcupan, which preserved z-depth of the slice and helped with the judgement of potential contact sites. In this pair, a putative axonal element of the presynaptic neuron and the primary dendrite of the postsynaptic neuron were strikingly close (Figure 4.3B) when viewed at 100X magnification at light microscopic level. Unfortunately, the putative contact side was lost during attempts for ultrastructural investigations.

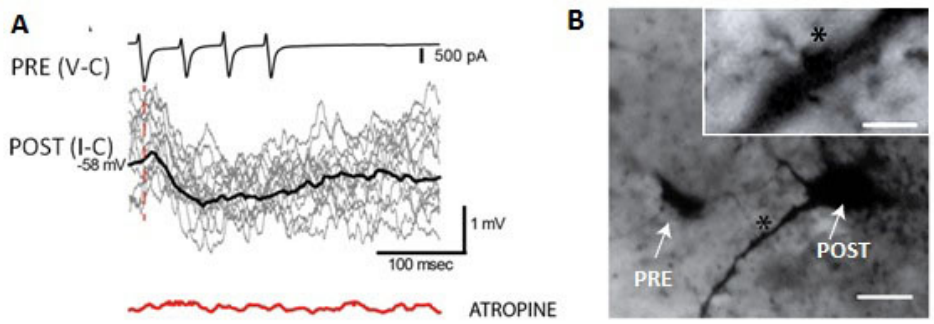

Figure 4.3 Direct muscarinic connections between BFc neurons. A Top: Action currents elicited in the presynaptic BFc neuron in voltage clamp mode. Middle: Black trace is the average of 50 traces and gray traces are representative single traces. Bottom: Average of postsynaptic responses in the presence of muscarinic receptor blockade with atropine. **B** Nickel-DAB processing of the same pair. The section is durcupan embedded and the photomicrograph is taken at a single z-level. Inset is a magnified view of the area indicated with asterisk. Note the close apposition of pre- and post-synaptic neurites and the terminal-like structure (near the asterisk on the magnified image). Scale bars are 15 µm for the low magnified image and 2 µ for the inset.

4.4.3 Optogenetic experiments

Most of the time, mCherry/eGFP+ neurons could be easily discriminated from eGFP only BFc neurons through fluorescent imaging based on the punctated appearance of the mCherry reporter on somata and dendrites (Figure 4.4). The recordings were always taken from an area occupied by multiple mCherry/eGFP+ neurons. mCherry signal was completely absent ~1.5 mm anterior and posterior from the injection sites and in brainstem slices (not shown). In addition, striatal cholinergic neurons on the same coronal slices were not infected either.

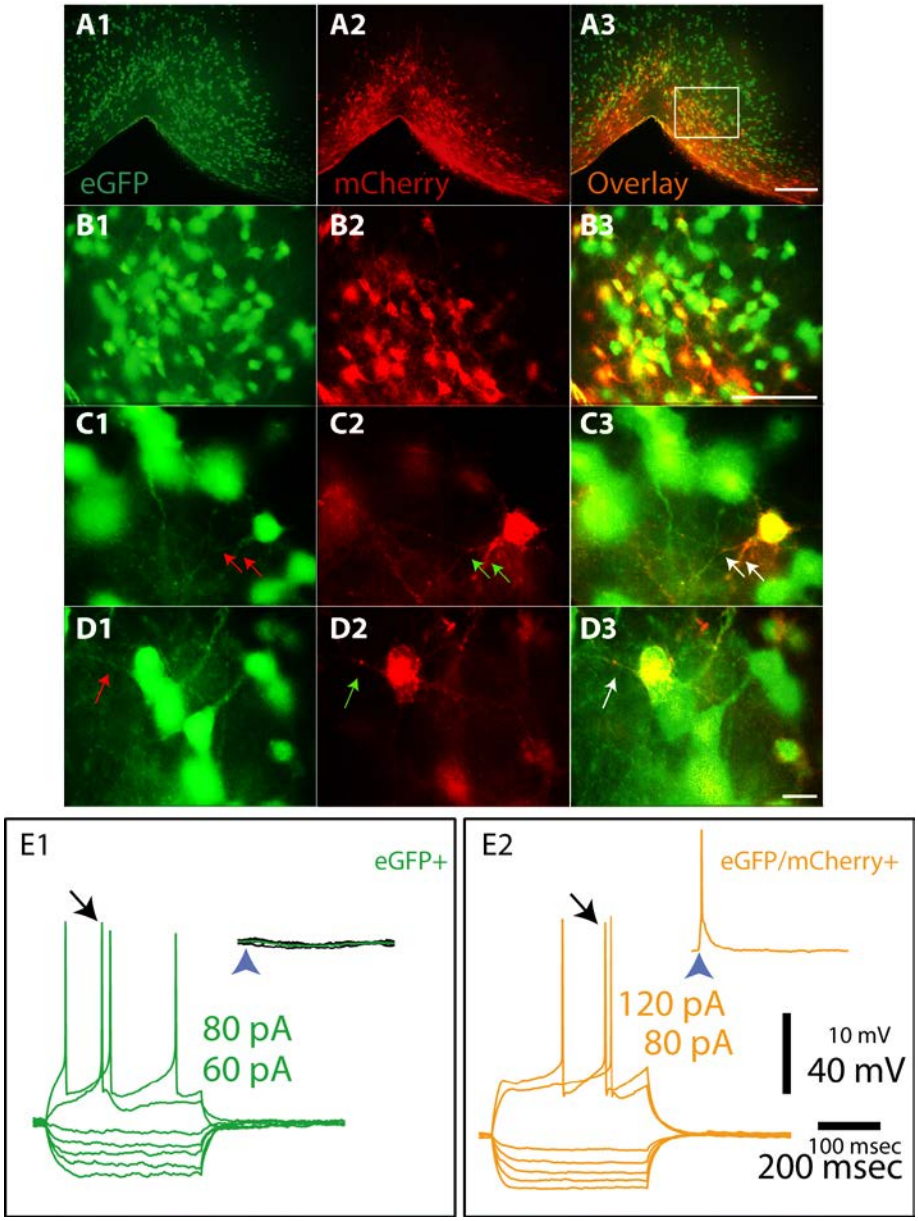

Figure 4.4. A subpopulation of BFc neurons remain uninfected following AAV injections. A1-D1: eGFP+ neurons (green); **A2-D2**: eGFP+/mCherry+ neurons (red) **A3-D3**: Overlay of eGFP and mCherry signal showing a subpopulation of neurons being uninfected. **A**. Low magnification image showing the overall distribution of neurons in the vDB. **B**. Higher magnification images of neurons. The field corresponds to the box in (**A3**). **C** and **D**. Demonstration of eGFP/mCherry+ neurons at higher magnification. Note the neurites pointed with arrows. The co-localized signal in the neurites negates the possibility of false positives (**E1**): An EF neuron positive only for eGFP signal (first spike shown with the arrow) responding to negative current injections ranging from -100 to -20 pA from a membrane potential of ~-70 mV. Action potentials are elicited with +60 and +80 pA current injections in this particular neuron. The blue arrowhead in the inset shows the presence of the blue light pulse and the traces illustrate the absence of direct optogenetic responses. (**E2**): Same arrangement as in (**E1**). The neuron is a late firing neuron positive both for eGFP and mCherry signal. Consistent with this, the neuron responds with an action potential to blue light (inset). Scale bars in in **E2** is applies to **E1**. Smaller numbers on the scalebars apply to the insets.

During fluorescent imaging, BFc neurons that were judged to be mCherry+ reliably fired action potentials in response to blue light application. The delay for action potentials (as measured from the beginning of the light pulse to the peak of the action potential) in 5 neurons patched in this manner showed little variation (6.0 - 6.3 msec).

In 6 neurons that were initially judged to be mCherry negative, blue light evoked direct depolarizations in the range of 0.5-6 mV (not shown). The responses were insensitive to all the blockers tested (CNQX, AP-5, mecamylamine, atropine). These neurons likely expressed very low levels of ChR2 as evidenced by a lack of blue light induced action potentials and undetectable levels of mCherry expression with fluorescent imaging. Hence, they were not included in the analysis. The potential presence of gap junctions in the latter cases was not tested for and they remain a possibility.

Single pulse stimulation with blue light did not lead to any observable responses in 23 mCherry negative BFc neurons. In three such cases, physostigmine (1 µM), an AChE blocker, was applied. This uncovered a minute muscarinic (< 1 mV) response that was sensitive to atropine (1 µM). Figure 4.5 illustrates an example.

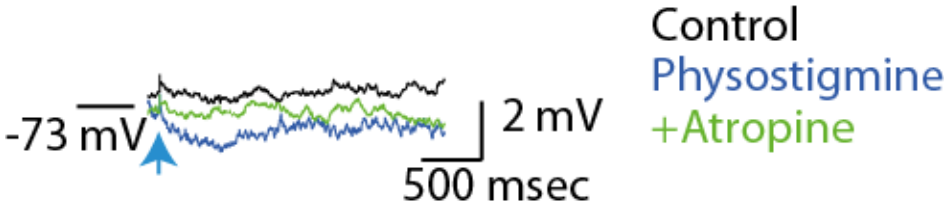

Figure 4.5 Physostigmine uncovers a muscarinic response in some BFc neurons that are otherwise nonresponsive to BFc stimulation. Each trace is the average of 15 traces. The traces are color coded; for pharmacological conditions, see the color text on the right. Note the slight hyperpolarization during physostigmine. Blue arrow points out to the blue light stimulation.

In another set of non-transduced BFc neurons (n = 20), physostigmine was not necessary for observing a hyperpolarizing response during the light activation of transduced BFc neurons. Overall, the amplitude of the responses was in the range of -1.5 to -4.6 mV (-2.74 ± 1.35 mV) from a membrane potential around -70 mV. The IPSPs had a relatively early onset (39 – 55 msec, 52.5 ± 10.3 msec) and long duration (750 – 1766 msec, 1154 ± 321.8 msec) (figure 4.6 A1, C). These IPSPs were significantly blocked by atropine (1 µM, n = 2, not shown) and MTA (1 µM, n = 4) (figure 4.6 A1, B). Based on their additional insensitivity to CGP 55845 (10 µM; a GABA-B receptor blocker, n = 2, not shown), these hyperpolarizations are referred to as muscarinic IPSPs. Single pulse optogenetic stimulation did not alter the firing properties of BFc neurons in an observable manner in most cases nor seemed it to engage/disengage active properties of these neurons when they were artificially subjected to different membrane potentials and firing (not shown). However, in 2 cases, 20 Hz optogenetic stimulation for 10 seconds led to a reduction in intracellular current evoked spikes (see figure 4.6, A2 for an example). Given the small number and the potentially nonphysiological nature of this stimulation paradigm, these data need to be considered cautiously.

For investigating the possible channels underlying these muscarinic IPSPs, iberiotoxin (50 nM, n = 2, a blocker of BK channels) and apamin (100 nM, n = 4 a blocker of SK channels) were tested. While iberiotoxin did not lead to any observable changes in muscarinic IPSPs (not shown), the effects of apamin were interesting and discussed below.

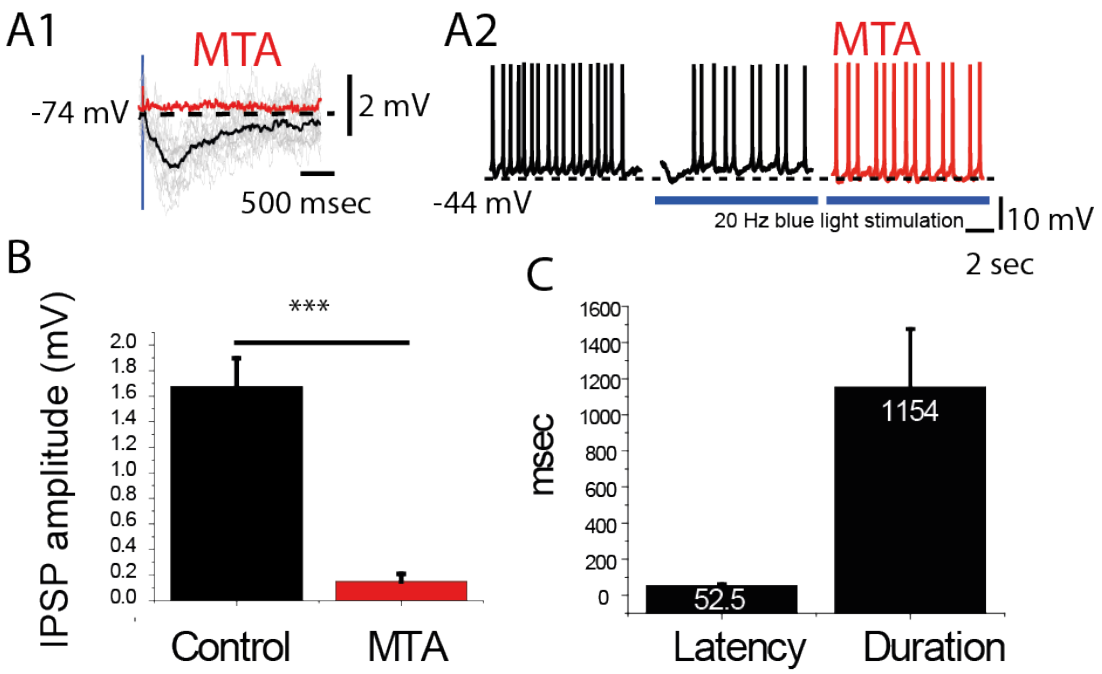

Figure 4.6 Muscarinic IPSPs in BFc neurons. A Averages of 30 muscarinic IPSPs in the absence (black trace) or presence of methoctramine (MTA, 1 µM) (red trace). Light gray traces correspond to the 15 representative traces for the control condition (A1). A2 illustrates reduction in firing rate (black traces on the left and in the middle) as a result of optogenetic BFc stimulation (marked as horizontal blue lines) and the sensitivity of this effect to MTA (red trace). **B** Bar graph showing the average muscarinic IPSP amplitudes under control conditions (black bar) and after MTA application (red bar). **C** Bar graph illustrating the average latency and duration of muscarinic IPSPs. The numbers embedded in bars indicate the average. Error bars indicate S.D. ***P < 0.001.

4.4.4 Apamin effects on muscarinic IPSPs

Under control conditions with sufficient number of traces averaged (n > 20), the muscarinic IPSPs were characterized by an initial voltage deflection that occured ~150 msec after the response onset (see figure 4.7 A, red trace at the top). This voltage deflection was abolished by a 10-15 minutes application of apamin (100 nm), an SK channel blocker, and was associated with a delay in response onset within single BFc neurons tested (n = 4, 39.3 ± 3.51 msec, control vs. 132.3 ± 22.51 msec, apamin

pretreated; $t = 21.90$, $p < 0.01$) (figure 4.7 A, yellow trace on the bottom and top panel in B).

Neurons recorded when apamin was already present in the ACSF (i.e. apamin pre-incubated cases, $n = 3$) displayed a significantly longer IPSP delay as compared to neurons recorded in the absence of apamin (52.5 ± 10.3 msec vs. 113.5 ± 19.1 msec; $t = -6.221$, $p < 0.001$) (figure 4.7, bottom panel in B).

When I compared the onset latencies between neurons that were apamin pre-treated (apamin pre-incubated cases; between cell design) and that were exposed to apamin after whole cell access (within cell design), the differences were not statistically significant (113.5 ± 19.1 msec for apamin pretreated; 132.3 ± 22.51 msec for cases where apamin was applied later; $p = 0.12$) (Figure 4.7 B). Thus, apamin had the same effect regardless of when (before patching and after patching) it was applied. This suggests that whole cell dialysis does not constitute an artifact.

To reveal the voltage changes that underline the abovementioned observations, I subtracted the average traces obtained during apamin from those that were obtained before apamin application to unravel the apamin sensitive component within the muscarinic IPSPs. This strategy unmasked an early onset hyperpolarization with approximately -1 mV amplitude that came to a peak in ~ 100 msec and lasted ~ 300 msec (figure 4.7A, white trace and C). Again, one potential pitfall pertains to the possibility of washout of some channels underlying the muscarinic IPSP. This does not seem to be the case for three reasons, one of which entails the results obtained from apamin pre-treated neurons discussed above. Furthermore, subtracting the initial muscarinic responses

(obtained within the first 5 minutes of a recording) from the final responses (obtained from the last 5 minutes of a 1 hour recording) did not reveal a similar component in a case where apamin was not applied in the bath (Figure 4.7D, black trace). Finally, the apamin sensitive component recorded in different neurons with striking variations in data acquisition durations (~30 minutes vs. ~60 minutes) were not distinguishable on the basis of their temporal properties (Figure 4.7 D).

Overall, these results suggest that BFc neurons inhibit each other largely through M2 receptors. According to the methodologies used so far, this inhibition is of modest size and has little if any effect on the firing properties of BFc neurons. The sensitivity of the responses to muscarinic receptor blockers, the time locked mucarinic IPSPs, and the possible absence of other synaptic events during single pulse stimulation reveals that muscarinic/nicotinic activation of other noncholinergic BF neurons does not play a significant role. This does not exclude the possibility that there are polysynaptic interactions as well but the specific conditions that engage other neurons need to be investigated in future experiments. In addition, the muscarinic IPSP seems to be governed by two different processes: an apamin sensitive, SK-mediated component and a longer component that is insensitive to SK-channel blockade.

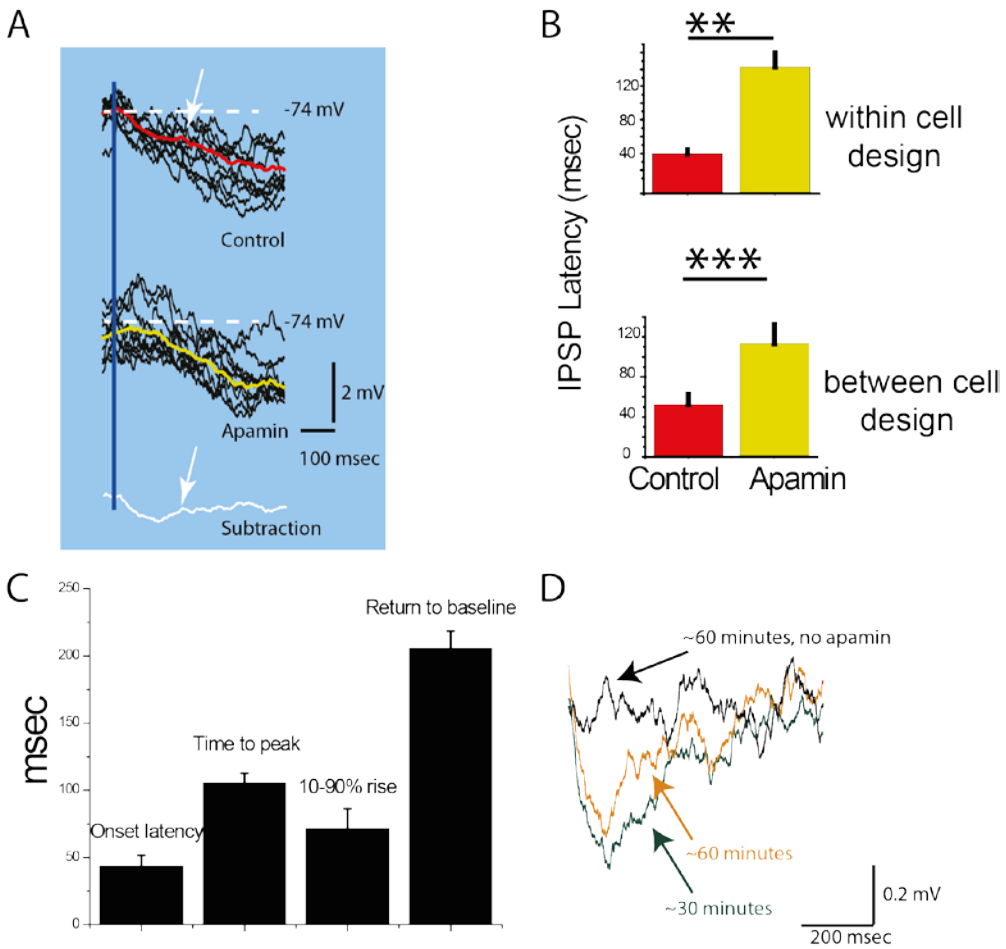

Figure 4.7 An apamin-sensitive component in muscarinic IPSPs. A Muscarinic IPSPs acquired before apamin (red trace, average of 25 traces) and after apamin (yellow trace, average of 25 traces). Ten representative individual traces are shown for each condition. The white trace below shows the SK-channel mediated component acquired by subtracting control from apamin. Note also the delayed onset of muscarinic IPSPs following apamin application. **B** Bar graphs showing apamin mediated delays in muscarinic IPSPs with a within-cell design (bars on the top) and with a between cell design (bars at the bottom). **C** Bar chart summarizing the temporal properties of the apamin-sensitive, SK-mediated component (obtained by subtracting the average response during apamin from the average response of the control period).**D** The apamin sensitive component is not sensitive to recording duration. One case (dark green trace) was acquired by using average control responses and responses during apamin during the first and last ~5 minutes of a ~30 minutes recording. The other case (dark yellow trace) was the same except that responses during apamin were acquired just before the end of a ~60 minutes recording. Note the similarity of the two profiles. The black trace shows a control for washout where the neuron was **not** presented with apamin while the subtraction protocol was done as if apamin was presented. Error bars indicate S.D. **$p < 0.01$; *** $p < 0.001$

4.4.5 Experiments on functional implications

To depict preliminary functional implications of these findings, I did two additional experiments:

The first experiment deals with the meaning of the apamin-sensitive component. As described by others before (e.g. Faber et al., 2005), calcium activated potassium currents in general, and SK (i.e. the channel blocked by apamin) in particular, play crucial roles in shaping incoming inputs apart from their classical roles in determining firing patterns. To illustrate this, I have used ChAT-eGFP mice that received intra-BLA injections of an AAV that promotes ChR2 expression in neurons that express CaMKII (in this case, the glutamatergic BLA projection neurons). Optogenetic BLA stimulation was made in conjunction with carbachol (10 mM) puffs on the dendrites (~50 µm far from the soma) of recorded BFc neurons (these experiments should not be confused with the ones in Chapter VI that investigate transmission in BFc-->BLA direction). The idea behind these experiments was to observe how dendritic CCh puffs modify EPSPs arriving from the BLA and the particular role the muscarinic recepor activated SK channels might play in this process. Some preliminary experiments where I investigated BLA-->BFc transmission with this particular AAV formed the basis of this idea. The specifics about BLA-->BFc interactions are outside the focus of this thesis and will not be described further.

Due to the shortage of animals injected, EPSPs could be recorded only from 2 BFc neurons and dendritic CCh puffs produced an effect in one of them. The effect was obvious and worth mentioning with respect to the possible contribution of within BF cholinergic interactions in shaping inputs impinging onto BFc neurons. In this

experiment, when optogenetic stimulation was coupled to dendritic CCh puffs (same onset with optogenetic stimuli and 100 msec in duration), the EPSPs were observably curtailed. This effect was sensitive to apamin (Figure 4.8). Although these experiments differ profoundly from optogenetic experiments mentioned above, this preliminary finding indicates a potential for the apamin sensitive component of muscarinic IPSPs for modulating incoming inputs.

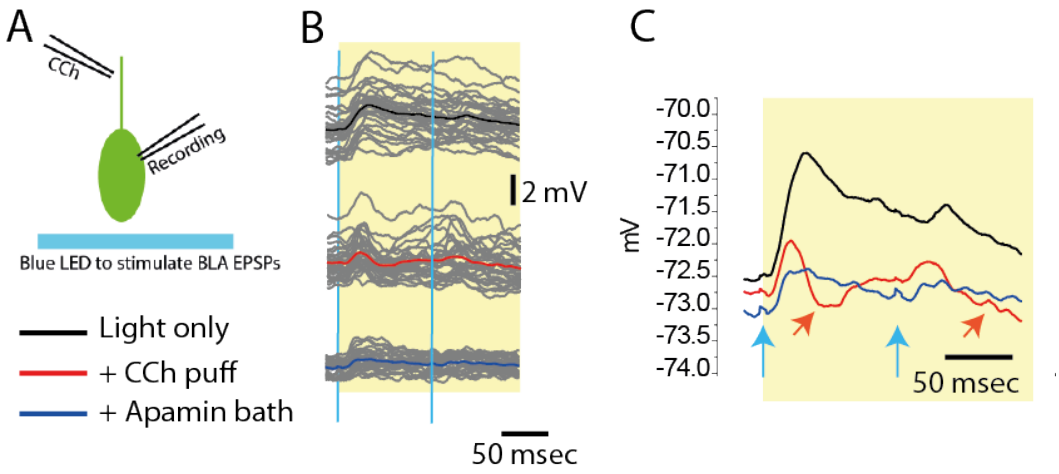

Figure 4.8 Pressure application of carbachol (10 mM) onto the dendrite of a BFc neuron curtails BLA evoked EPSPs. A Experimental configuration. See the lines below for color coding valid for B and C. **B** EPSPs during light stimulation alone (top), during light stimulation coupled to dendritic carbachol application (middle), and during the additional presence of apamin (10 nM) in the bath. Colored traces are average responses **C** Magnified view of the average traces shown in B. Blue lines (in B) and arrows (in C) indicate the onset of the optogenetic pulse. Red arrows in C point out to the curtailed portion of the EPSPs. Transparent yellow boxes in B and C that are superimposed on the traces signify the presence of CCh except for the control trace (black). Picrotoxin (100 µM) was present throughout the recording.

In the second set of experiments, a high potassium solution (see specific methods) was used to cause spontaneous firing in BFc neurons. This spontaneous activity is expected to increase the acetylcholine concentration in the slice. Subsequent to this, atropine (1 µM) was applied to investigate whether local acetylcholine release inhibits BFc neurons. During atropine application, there was approximately a four fold increase in

action potential frequency in BFc neurons, reaching statistical significance ($t = -3.278$, $p < 0.05$). The increased firing frequency was observed within tens of seconds following atropine application (Figure 4.9 A1) except in one case illustrated (Figure 4.9 A2). In the latter case (Figure 4.9 A2), the neuron did not fire action potentials for the entire recording period before atropine. Action potential discharge started following ~100 seconds of atropine application after being preceeded by a slow depolarization possibly reflecting a release from hyperpolarization. Subsequently, the action potential frequency increased constantly until reaching a maximum after ~ 500 seconds. These experiments were carried in the presence of synaptic blockers for ionotropic glutamate and GABA receptors and provide strong evidence for the notion that endogeneous acetylcholine can delimit the firing of BFc neurons through postsynaptic mechanisms.

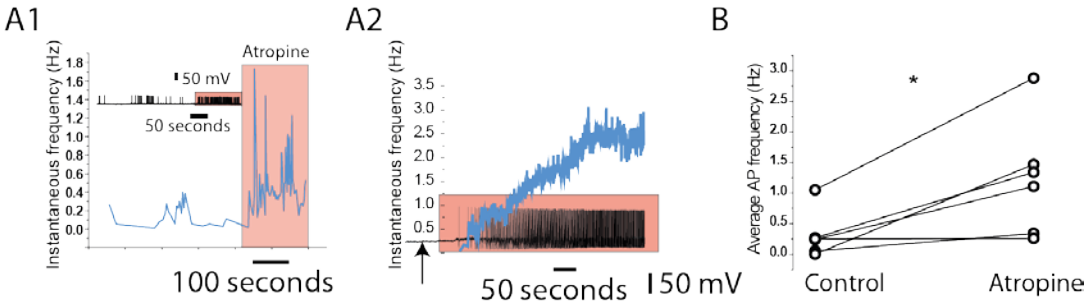

Figure 4.9 Tonic acetylcholine release inhibits spiking in BFc neurons. A A1 Instantaneous frequency plot of a BFc neuron during high potassium solution bath in the absence and presence (red rectangular box) of atropine (1 µM). Inset shows the activity from which the plot was generated. A2 An exception where high potassium solution did not lead to spontaneous spiking. See arrow for baseline and red rectangular box for the activity during atropine. An instantaneous frequency plot is superimposed to illustrate the appearance and accelaration of spiking activity which eventually reached a ceiling. **C** Average firing frequencies of individual BFc neurons before (control) and after atropine application. CNQX (20 µM), AP-5 (100 µM), and picrotoxin (100 µM) were present during the entire recording. *$p < 0.05$.

4.5 Summary of the main findings

a) Axonal varicosities of BFc neurons are preserved in acute slice preparations and can be used for studying local BFc processing.

b) BFc neurons express functional somatodendritic muscarinic receptors and their activation reduces the excitability of these neurons.

c) Paired recordings between BFc neurons can be used for investigating their functional interactions that are inhibitory.

d) Double transgenic strategies where cre and eGFP expression is controlled under the ChAT regulatory elements can be used for studying these functional interactions with optogenetic methodologies.

e) When BFc inputs on BFc neurons are activated via optogenetics, the muscarinic IPSPs are governed by two different processes. The initial short latency and duration component is mediated by SK channel activation while the longer remaining component is insensitive to pharmacological manipulations of SK channels.

f) The SK mediated component might be involved in the curtailing of glutamatergic inputs through the regulation of dendritic excitability.

g) Active slice experiments provide support for the notion that BFc cells can control each other's output.

CHAPTER V (AIM 3): AN OPTOGENETIC INVESTIGATION OF CHOLINERGIC EFFECTS ON REGULAR-SPIKING, BASOLATERAL AMYGDALA NEURONS

5.1 Introduction

Lateral, basolateral, and basomedial amygdala constitute the (BLA), a structure found in the medial temporal lobe. This structure is primarily involved in emotional functions. These include the involvement of this structure in classical fear conditioning (reviewed in Blair et al., 2001) and facilitation of other types of memories which are of emotional relevance (reviewed in McGaugh, 2004). Recent evidence indicates that this structure is not only involved in the processing of noxious stimuli but also plays important roles in appetitive tasks (Popescu et al., 2007; 2009; Tye et al., 2008; Stuber et al., 2011). The BLA achieves these functions through the sensory inputs it receives/integrates from thalamic and cortical regions and its efferents that involve cortical and subcortical structures implicated in cognitive and autonomic control respectively (Pape and Pare, 2010).

In terms of its cellular make-up, the BLA has striking commonalities with other cortical structures. Its principal neurons are spiny glutamatergic neurons that compose ~80% of the total cell population in this area (McDonald, 1992). Moreover, the physiological features of its principal neurons are easily distinguishable from local BLA interneurons. Principal BLA neurons, similar to the majority of hippocampal and cortical principal neurons, exhibit a regular spiking (RS) pattern characterized by wider spikes as compared to interneurons, moderate frequency discharge with adaptation largely determined by calcium activated potassium conductances (Washburn and Moises, 1992; Faber and Sah, 2003). Finally, different kinds of interneurons express identical interneuron markers with their cortical counterparts, exhibit a similar morphological

variability, and possibly are involved in similar functions (McDonald, 1992; Woodruff and Sah, 2007; Bienvenu et al., 2012; Manko et al., 2012).

While it is questionable whether findings from this structure can be translated into other cortical structures, similar problems also exist even when comparing two different neocortical structures. Hence, any such data should be considered cautiously. However, there is an anatomical feature that makes the BLA very suitable for studying cholinergic actions using current optogenetic methodologies. As described by Mesulam (2004), cholinergic innervation tends to be denser in paralimbic areas. This density increase is further evident when moving to core limbic areas such as the hippocampus (described above) and the amygdala (Ben-Ari et al., 1977). In a coronal section processed for ChAT, the abundant immunoreactivity in BLA is indisputable (Figure 5.1).

As in the cortex, M1 receptor expression is specific to principal BLA neurons (McDonald and Mascagni, 2010) while M2 is expressed in a subpopulation of BLA interneurons (McDonald and Mascagni, 2011). Furthermore, BFc neurons indiscriminately innervate both principal and inhibitory interneurons of the BLA (Muller et al., 2011).

A difference entails the absence of p75 receptor expression in BFc neurons projecting to the amygdala (Hecker and Mesulam, 1994; Hecker et al., 1994; Poulin et al., 2006). The extensive innervation of the BLA might stem from the lack of p75 receptors in amygdala projecting BFc neurons. This is based on the findings regarding the role of p75 receptor signaling in axonal pruning in sympathetic axons (Singh et al., 2008).

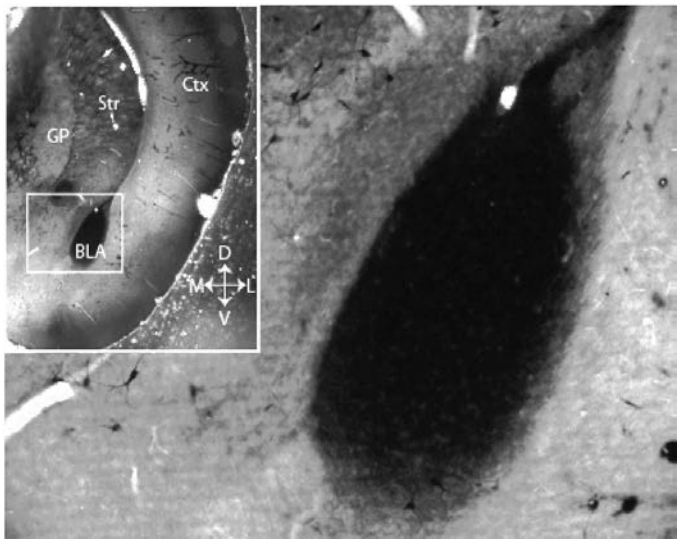

Figure 5.1 ChAT immunocytochemistry reveals the dense innervation of the basolateral amygdala (BLA). A coronal section from rat processed for ChAT immunocytochemistry. The lower magnification image shows the location of the BLA with respect to the striatum (Str), globus pallidus (GP), and the cortext (Ctx) in a slice processed for ChAT immunocytochemistry. Note the immense ChAT immunoreactivity in the BLA which mainly results from the staining of afferent basal forebrain cholinergic fibers.

Despite these differences, acetylcholine actions exhibit similarities with other cholinorecipient cortical structures. These include:

1- Deleterious effects of acetylcholine receptor blockers on BLA dependent tasks (Tinsley et al., 2004).

2- Increased BLA acetylcholine release during learning (Gold, 2003).

3- Depolarizing actions of acetylcholine on principal BLA neurons through the suppression of voltage gated potassium conductances (Womble and Moises, 1993). (As in other regions, exceptions to this exist and will be discussed later).

4- The ability of acetylcholine to activate I(CAN) in principal BLA neurons (Egorov et al., 2006).
5- The ability of acetylcholine to lead to rhythmic IPSPs (Popescu and Pare, 2011).
6- Suppression of intra-BLA neurotransmission through muscarinic receptor activation (Yajeya et al., 2000).

In short, BLA seems to be optimal for studying basic acetylcholine actions using optogenetics. The dense cholinergic innervation is likely to facilitate the presence of fibers amenable to photo-activation following AAV injections and decrease interexperimental variability which might arise when recording from relatively sparsely innervated regions. The presence of classical acetylcholine actions in this structure is a further motivating factor.

5.2 Specific methods

5.2.1 Animals

ChAT-IRES-cre (B6;129S6-ChAT$^{tm1(cre)Lowl}$/J) were used for transducing BFc inputs to BLA.

5.2.2 Injection sites and viruses

Intra-BF injections of 1 µL of AAV5-EF1a-DIO-ChR2-EYFP was made in the following coordinate (in µM with respect to Bregma): AP: -700, LM: 1750, DV: 4260; ~0.33 µL each. This allowed me to specifically stimulate the cholinergic elements via the illumination of the entire slice with the blue LED bulb.

5.2.3 Protocols for electrophysiological data acquisition and analysis

A regular potassium based intracellular solution was used for recording BLA neurons in whole-cell configuration (see general methods). In general, ALEXA 594 (50 µM) was added into the intracellular solution while some recordings were done with .2 % biocytin in the pipette solution. For perforated patch clamp experiments, amphotericin B was dissolved in DMSO in a 60 mg/ml stock solution. A final concentration of 0.24 mg/ml of amphotericin was added into the recording solution. Stocks were prepared daily and final solutions were renewed every ~3 hours.

For perforated patch clamp recordings, the tip of the pipettes was filled with an intracellular solution not containing the antibiotic to facilitate the formation of GΩ seal. Subsequently, large sized neurons were targeted for a tight seal (2-3 GΩ) formation. During this period, a background negative current (-20 pA) was passed through the electrode along with a -100 pA test pulse (at 0.1 Hz and 100 msec in duration) to monitor the access to the cell. At the end of 30-45 minutes, the access resistance was ~25-35 MΩ as measured by the linear portion of the voltage response to -100 pA hyperpolarizing test pulses. Throughout the recording, the integrity of the patch was monitored with fluorescent microscopy in order to visualize the possible dialysis of the cell with ALEXA (Figure 5.7). At the end of successful recordings, the membrane was ruptured and the cell was dialysed for ~5 minutes to visualize the dendrites.

Larger sized BLA neurons were selected for increasing the probability of targeting RS, putative BLA principal neurons. Subsequent to good electrical access, the neurons were immediately presented with depolarizing pulses to characterize their spiking pattern. RS neurons were identified based on the adapting firing pattern as

opposed to a non-adapting pattern (fast spiking BLA neurons) or a late spiking pattern (another set of putative BLA interneurons). In addition, the dendrites filled with ALEXA 594 were inspected for the presence of spines, a distinguishing feature of principal BLA neurons.

5.2.4 Optogenetic experiments

Subsequent to access to neurons, the neurons underwent two kinds of protocols (other protocols were done during pilot experiments but are not included in the thesis):

1- Responses to single optogenetic stimulation achieved through 3-5 msec blue light pulses occuring every 15 – 30 seconds at resting membrane potential.

2- Responses to intracellular current injections (1 second in duration occuring every 2 minutes) in the absence or presence of concurrent 10 Hz optogenetic stimulation of BFc afferents.

   a. Whole-cell recordings. Subsequent to whole cell access, an intracellular current injection (20 – 200 pA) was given along with a 10 Hz optogenetic BFc stimulation (see results for details)

   b. Perforated patch clamp recordings. The intracellular current injections were in most cases standard in the range of 20 – 140 pA in 20 pA increments and/or 50 – 150 pA in 50 pA increments. The order of intracellular stimulation intensities was scrambled.

First (single pulses at rest) and the second (concomitant intracellular depolarization and optogenetic stimulation of BFc afferents) protocols were also scrambled.

5.3 Results

5.3.1 Efficacy of the approach

In every ChAT-cre animal that received intra BF AAV injections into the appropriate coordinates (see methods), YFP fluorescence was evident in the BLA during recordings (Figure 5.2 A). When YFP+ BFc neurons were patched, they responded to blue light pulses with action potentials in a reliable manner, responding to each of the 10 light pulses within a 1 second train (Figure 5.2 B). This is particularly important as it will become evident later, BLA neurons were typically investigated during 10 Hz BFc stimulation. However, it is not clear whether those action potentials have relevant physiological significance (i.e. does release of acetylcholine occur every time the neuron fires?).

To answer this question, I tried to target smaller sized somata with the hope of finding putative interneurons that exhibit fast nicotinic responses. Among the putative interneurons (n = 12), only one late-spiking type exhibited putatively nicotinic, fast cholinergic EPSPs. In this neuron, EPSPs occured at 10 Hz suggesting that stimulating BFc with light pulses at this particular frequency has physiological relevance (Figure 5.2 C). Finally, RS neurons filled with ALEXA during recordings always exhibited spines on their dendrites, in line with the findings that this physiological phenotype is exhibited by spiny projection neurons of the BLA (Figure 5.2 D). This was further verified by biocytin cytochemistry where regular spiking neurons were found to exhibit dendritic spines while non regular spiking neurons did not (Figure 5.3).

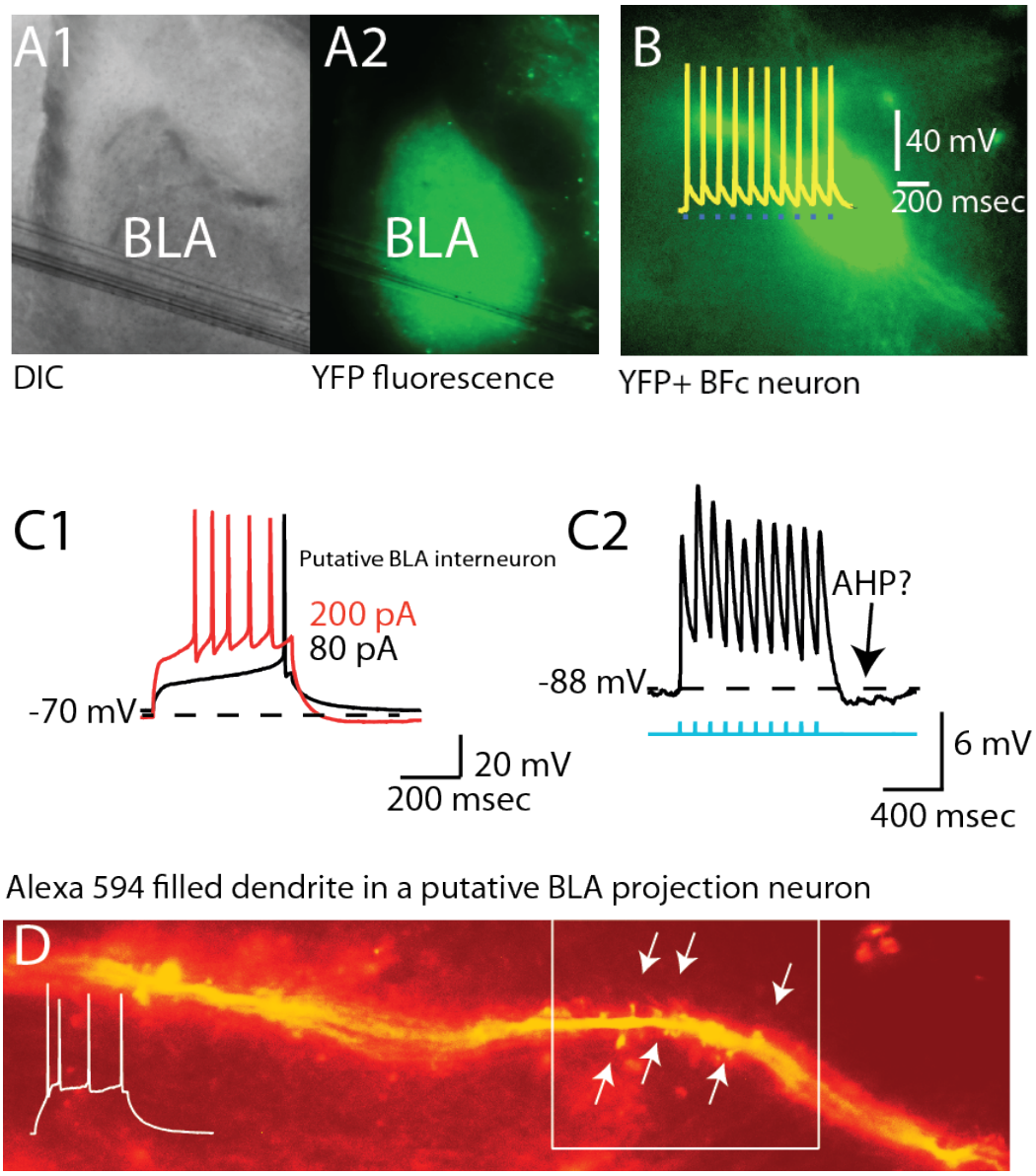

Figure 5.2 Utility of optogenetics in the BLA. A A1 Low magnification DIC image of the BLA during slice recordings. A2 Under fluorescence illumination, YFP+ fibers are seen very densely in the same slice. **B** YFP+ BFc neuron. Inset shows induction of light evoked action potentials at 10 Hz. **C1** A putative BLA interneuron exhibiting a late-spiking phenotype. **C2** This neuron responded with putative nicotinic EPSPs to the 10 Hz optogenetic stimulation of the BFc. **D** A snapshot of the dendrite of a regular spiking BLA neuron filled with ALEXA. Note the spines (arrows) in the focused (white box) area. Inset shows the regular firing in response to intracellular positive current injection. Fluorescent images in A, B, and D were obtained online and later pseudocolored for avoiding confusion between YFP+ elements and neurons recorded and filled with ALEXA 594 in the BLA.

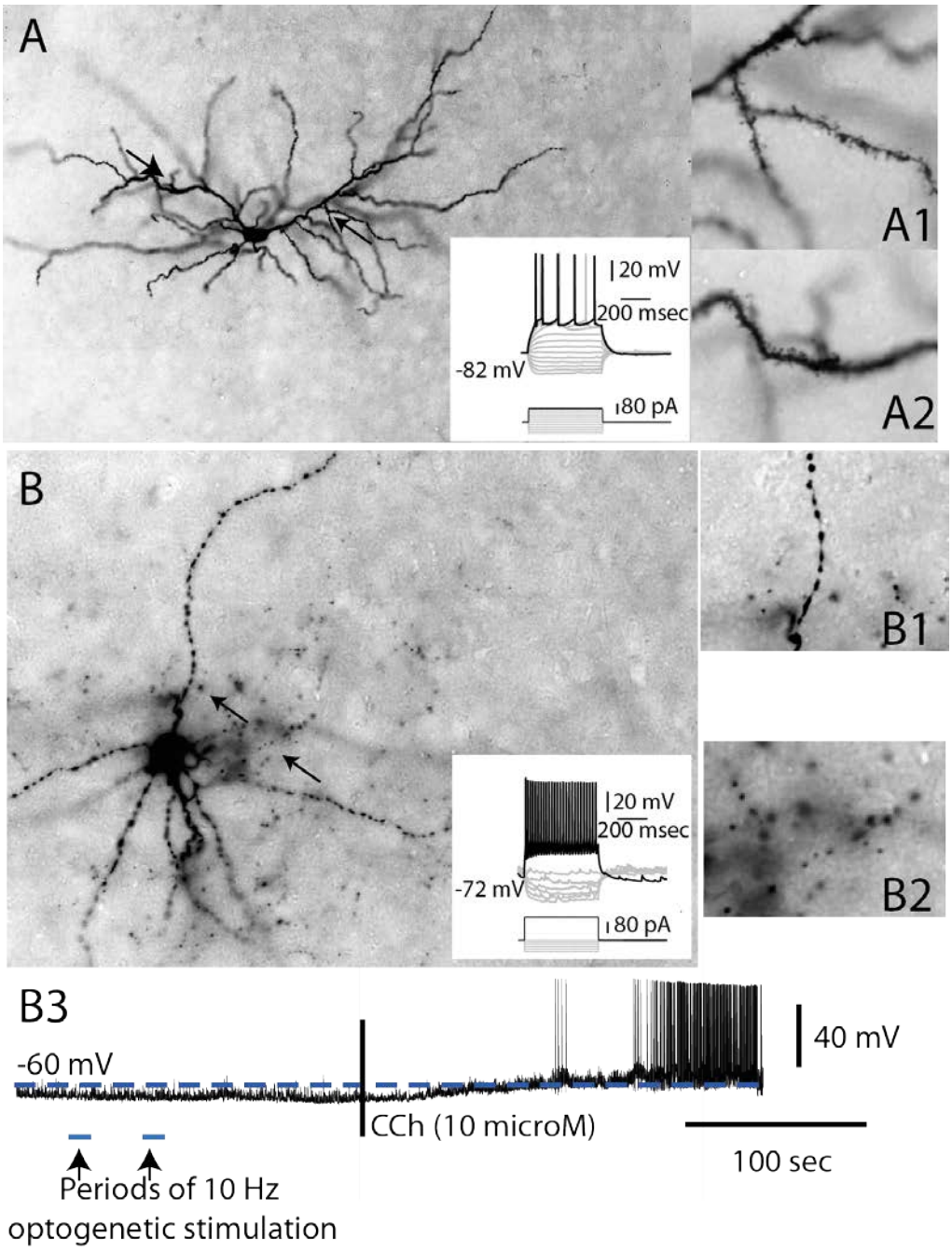

Figure 5.3 Contrasting morphological profiles of RS and FS BLA neurons. A Biocytin filled RS neuron issuing a dense dendritic arbor in an isodendritic fashion. The dendrites are spine rich as evident by the magnified images in A1 and A2 that correspond to areas marked by arrows in A. Inset shows the voltage responses to intracellular current injections. **B** Biocytin filled FS neuron issuing varicose dendrites (see B1 for a magnified image of an area indicated by arrows in A) and putative axonal varicosities around the cell of origin. Magnified view in B2 shows the continuity of these varicosities. Inset shows the voltage responses to intracellular current injections. B3 shows that optogenetic BFc stimulation does not lead to observable alterations on the activity of this neuron. On the other hand, carbachol (10 µM) application led to a slow depolarization followed by spontaneous action potential discharge.

5.3.2 Effects of BFc stimulation on the supratheshold properties of RS BLA neurons

When intracellular current injections were coupled to optogenetic stimulation (10 Hz), afterdepolarizing potentials (ADPs) were observed in RS neurons. This ADP was variable in amplitude and lasted in the range of 7-10 seconds. Irrespective of the intracellularly injected current strength and corresponding action potential discharge, ADPs were not present in the absence of optogenetic BFc stimulation. Initially, my intention was to characterize their amplitude as a function of the frequency of current induced spiking. For this reason, I intended to average three traces for each particular firing frequency (the traces were evoked with 2 minutes intervals). During the course of these experiments, I observed that the ADP amplitude gradually reduced upto ~50% of its initial value independent of the firing frequency during whole cell recordings. On the other hand, perforated patch recordings provided an extremely stable measurement of ADPs, possibly due to its less invasive nature (see Figure 5.4 for examples from each case).

Since it was not very clear exactly when each neuron was patched and how much time elapsed before the acquisition of first ADP measurements, two different approaches were utilized.

Initial recordings were done in the whole cell patch clamp mode for a very limited duration. The cells were simply patched and a current pulse was immediately given along with an optogenetic pulse. The injected current pulse was different (in the range of 20 - 200 pA) for each cell to increase the variability in firing frequency in order to generate a spike frequency vs. ADP amplitude plot (i.e. between cell design). This was done with

the assumption that these initial recordings were minimally affected by the washout of the cellular machinery mediating ADPs.

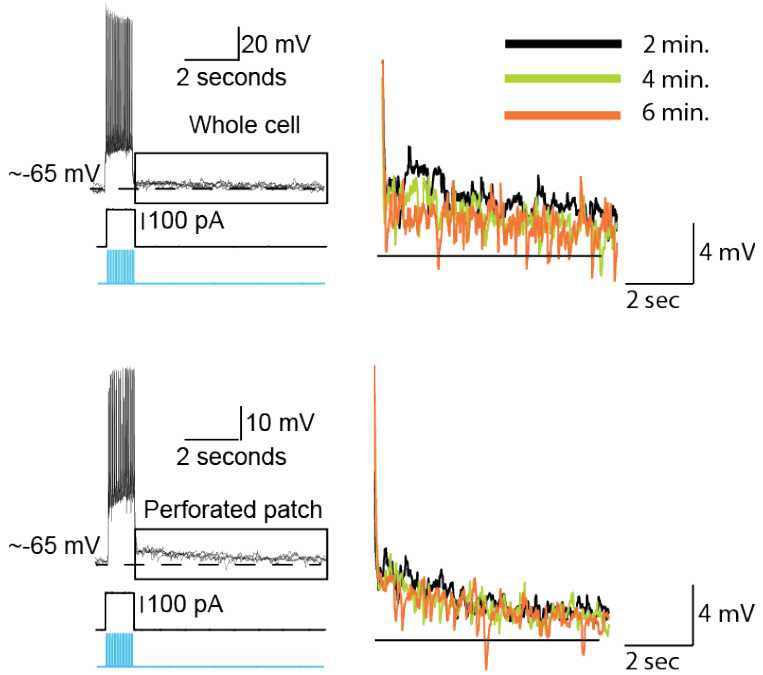

Figure 5.4 Perforated patch clamp is an optimal approach for recording ADPs. Top raw shows a whole cell recording. Bottom raw shows a perforated patch recording. The black and blue traces below the voltage measurements point out to the intracellular current injections and 10 Hz optogenetic pulses respectively. The boxed area is magnified on the images on the right. Each trace is color coded to indicate the approaximate time the measurements were taken following access to the neurons.

As described above, ADPs were not observed in the absence of optogenetic BFc stimulation (not shown). However, they could be reliably evoked when intracellular depolarization was coupled to optogenetic BFc stimulation (Figure 5.5 A, black trace). Finally, they were absent in slices preincubated with atropine (1 µM) (n = 5, figure 5.5 A, red trace) or flufenamic acid (100 µM) (n = 5, not shown) despite the presence of concomitant optogenetic BFc stimulation. The interaction between the number of spikes fired during intracellular current induced depolarization and the subsequent ADP amplitude was a complex one: there was a firing frequency dependent increase in ADP

amplitude until ~20 Hz firing during intracellular current injection. In neurons that fired at higher rates (> 20 Hz) during this period, ADP amplitudes were lower making the overall firing frequency vs. ADP amplitude relationship an inverted U (polynomial fit with 2 terms; p = 0.006) (Figure 5.5). The measured ADP duration did not have a relationship with firing frequency and ranged between 1885 to 13200 msec (6087 ± 3286 msec).

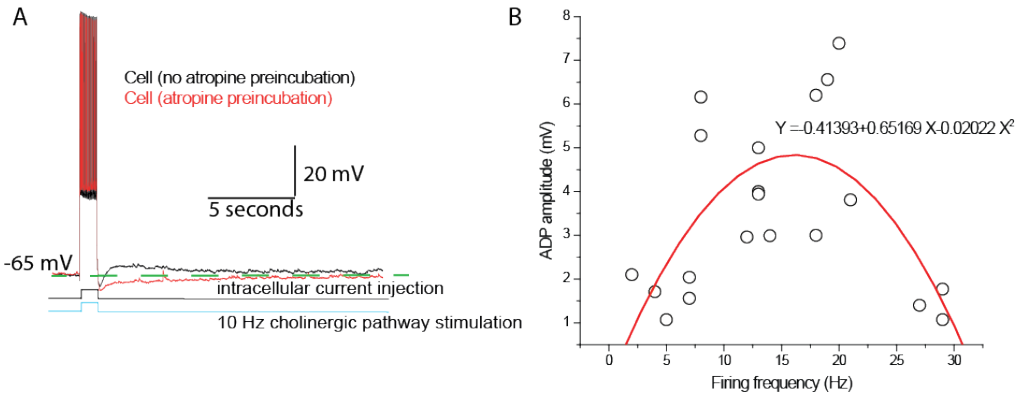

Figure 5.5 Afterdepolarizing potentials (ADPs) recorded during the concomitant presence of intracellular and 10 Hz optogenetic BFc stimulation. A A neuron recorded in the absence of atropine preincubation (black trace) exhibits an ADP while atropine preincubation (red trace) in another neuron possibly masks the ADP. **B** Firing frequency vs. ADP amplitude plot. The red line corresponds to a polynomial fit with two terms (formula included on the plot). Note that each point represents an individual neuron (between-cell design) firing with a different frequency as a function of the intensity of the intracellularly injected current.

Another set of neurons (n = 9) were tested with a lower optogenetic stimulation frequency (4 Hz). These neurons were presented with similar intensities of depolarizing current injections and their overall firing frequency during intracellular current injections did not differ from the neurons presented with a 10 Hz optogenetic stimulation (14.23 ± 7.95 Hz and 13.88 ± 7.50 Hz for neurons presented with 10 and 4 Hz optogenetic pulses respectively, p > 0.05). However, the ADPs occuring during 4 Hz optogenetic pulses

were significantly smaller than the previous group [3.50 ± 1.99 mV for 10 Hz group vs. 1.07 ± 1.34 mV for 4 Hz group, t = 3.308, p > 0.01)] (Figure 5.6). Indeed, during 4 Hz stimulation, 5/9 neurons did not exhibit an observable ADP (not shown).

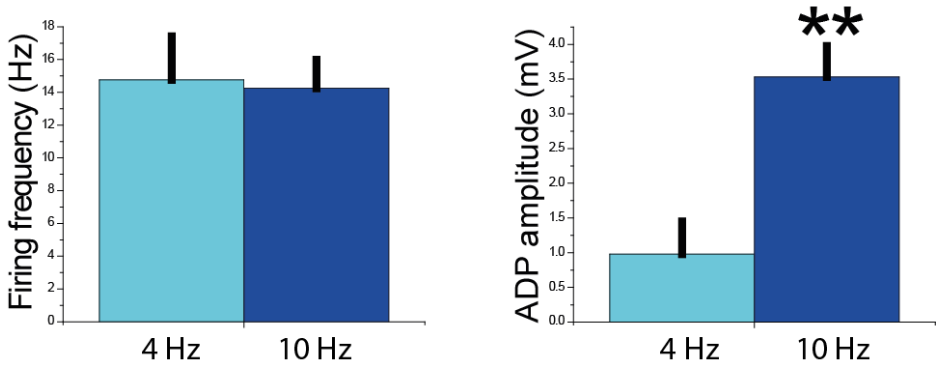

Figure 5.6 Afterdepolarizing potential (ADP) amplitude also depends on the frequency of cholinergic stimulation. Bar graph on the left shows the lack of difference in the firing frequency of 4 and 10 Hz groups. Bar graph on the right side shows the significant difference observed in ADP amplitudes in the two groups. **p < 0.01

The results so far suggest that intracellular depolarization and BFc inputs are necessary to engage a calcium dependent cationic current (I_{CAN}) that leads to an ADP through muscarinic receptor signaling. The amplitude of this ADP is not only determined by the firing frequency of the neuron exhibiting it during cholinergic stimulation but also on the frequency of BFc stimulation itself.

Although every effort was made to keep the recording conditions identical during whole cell recordings, there were inevitably some differences in the timing of protocols. Moreover, the partial washout of the cellular machinery underlying ADPs did not allow reliable within-cell characterization. Following experiments investigating ADPs were done with perforated patch clamp recordings coupled to 10 Hz optogenetic BFc

stimulation. Due to its less invasive nature, perforated patch clamp recording technique provides an ideal way to characterize cellular events that are prone to washout.

The perforated patch recordings were usually associated with higher access resistances. After 30-45 minutes, the access resistance fell to a minimum around ~30 MΩ (±5 MΩ). Although the action potential amplitudes and thresholds were altered, there was no evidence for the attenuation of slower events like synaptic potentials (Figure 5.7).

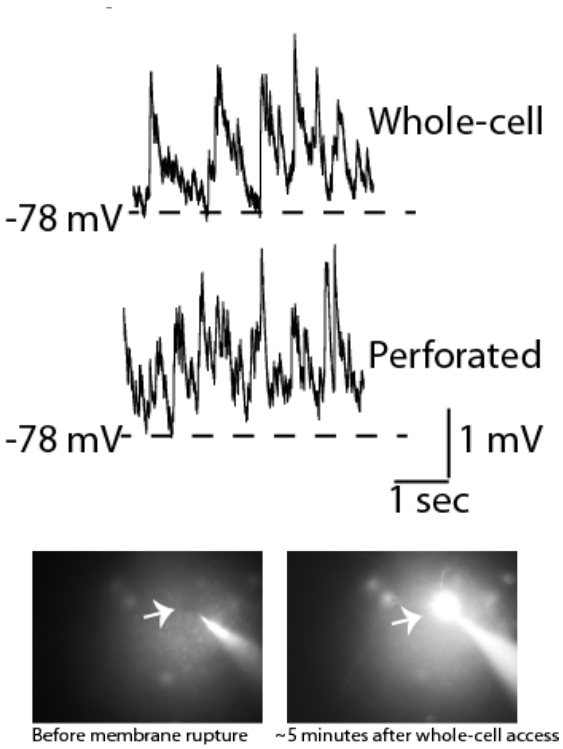

Figure 5.7 Depolarizing postsynaptic potentials (dPSPs) during different recording modes. Top: dPSPs recorded in a BLA neuron in whole cell mode. Bottom: dPSPs recorded in another BLA neuron during perforated patch recording. The bottom left is the fluorescent image of the Alexa filled pipette during recording. On the right side, the neuron is filled with biocytin following slight negative pressure application through the recording pipette.

With this method, the ADPs could be investigated with more control: during a single recording, optogenetic stimulation could be turned on or off during different traces that involve identical amounts of intracellular current injections (Figure 5.8 A) and

pharmacology of ADPs could be done following very stable recordings for tens of minutes (Figure 5.8 B). Shortly, ADPs were not apparent when BFc stimulation was absent (Figure 5.8 A). Moreover, the evoked ADPs (i.e. through concomitant intracellular and BFc stimulation) were blocked by atropine (1 µM, n = 1), pirenzepine (1 µM, n = 2), and flufenamic acid (100 µM, n = 2) (Figure 5.8 B). MTA (1 µM) did not have an effect in the one case tested. In short, ADPs are mediated through the activation of I_{CAN} that occurs through M1 receptor signaling during endogeneous acetylcholine release.

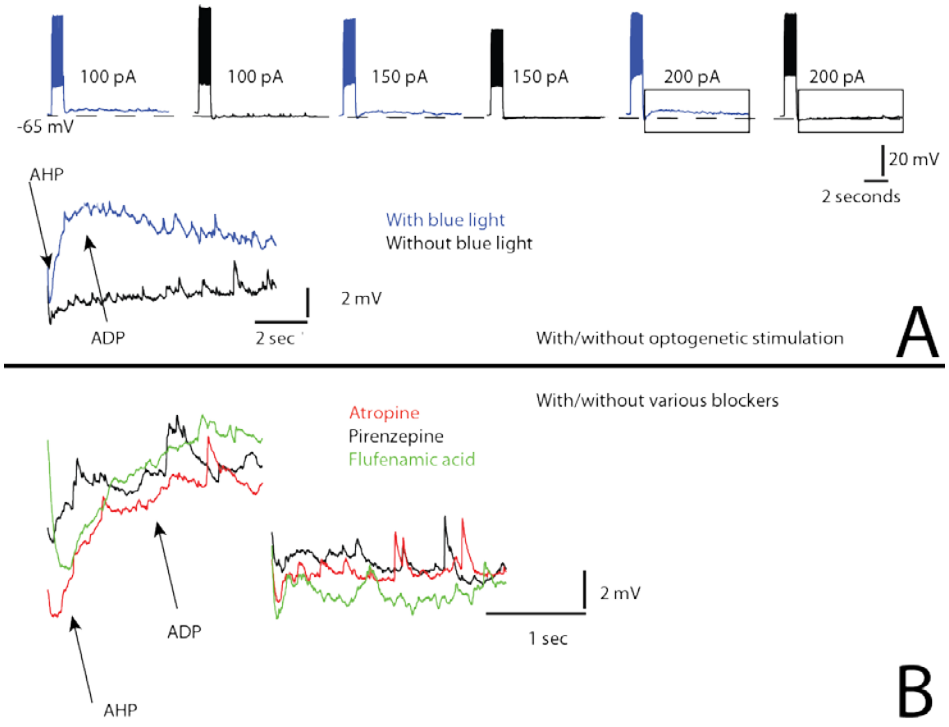

Figure 5.8 Mechanisms of ADP generation. A Concomitant cholinergic input and intracellular depolarization is required for ADP generation. Top: blue traces show responses to current injection during optogenetic BFc stimulation. Black traces show the responses to only intracellular depolarizing pulses. Note that ADPs are not seen in any of the black traces. Numbers next to the traces indicate the intensity of the intracellularly injected current. Below is a magnifiied view of the boxed areas on the top. **B** ADPs depend on the activation of M1 receptors and mediated through I(CAN) as evidenced by the sensitivity to atropine (1 µM) / pirenzepine (1 µM) and pirenzepine (100 µM) respectively. On the left, the beginning portion of the ADPs in different neurons is shown. Right side shows the appearance after pharmacological manipulations which are color coded with the text.

Overall, the ADP amplitudes ranged between 1 to 12 mV (5.12 ± 3.33) while the durations ranged between 2963 to 13169 msec (8289 ± 2967 msec). In particular trials in some neurons, action potentials were observed to ride on the evoked ADPs (2-20 spikes/10 seconds following the offset of the intracellular current pulse). These particular trials were not included in the analysis of ADP amplitudes. Figure 5.9 shows a neuron exhibiting spike discharge during ADPs in all trials varying in intracellular current injection intensity.

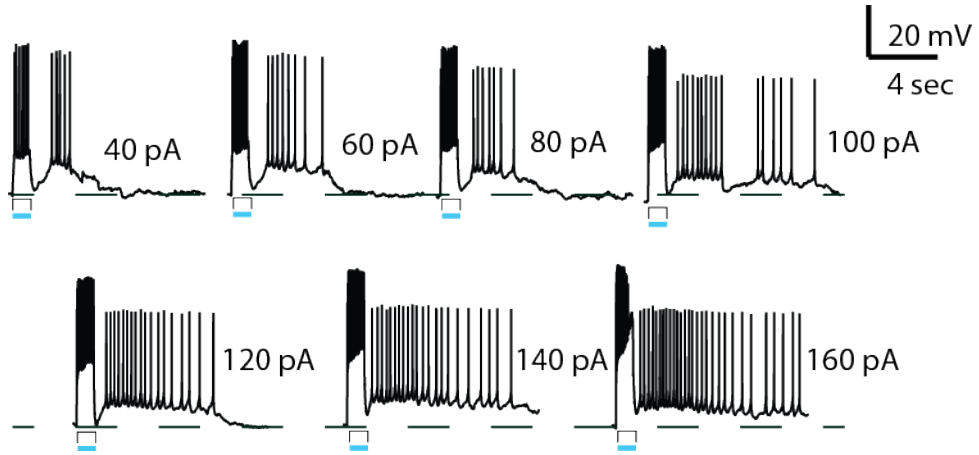

Figure 5.9 ADPs can be associated with proceeding spontaneous activity. Individual traces from a single neuron during responses to concomitant intracellular depolarizing currents and optogenetic BFc stimulation at 10 Hz. The symbols below the traces indicate the onset/offset of intracellular and optogenetic (blue line) stimuli. The numbers on the right of each trace indicate the intensity of injected current. The vertical dashed lines beneath the traces correspond to -65 mV.

The limited number of data points for single neurons did not allow for a stringent investigation of the inverted U-shaped relationship between firing frequency and the ADP amplitude using a within-cell design. Only 3/16 neurons exceeded a firing frequency of 20 Hz (±2) during intracellular stimulation, the frequency that was just before the ADP amplitudes decayed during previous whole cell recordings. In two of

those, the inverted U-shaped relationship existed as evidenced by the fact that the relationship could be explained with a polynomial fit with two terms (p = 0.0092 and p = 0.019) (Figure 5.10). In cases where above 20 Hz firing was not achieved, the relationship was typically linear (not shown), consistent with the results of whole-cell recording experiments. When all the data were brought together as was done for the whole-cell recording experiments, a similar picture was evident (Figure 5.10 B *inset*).

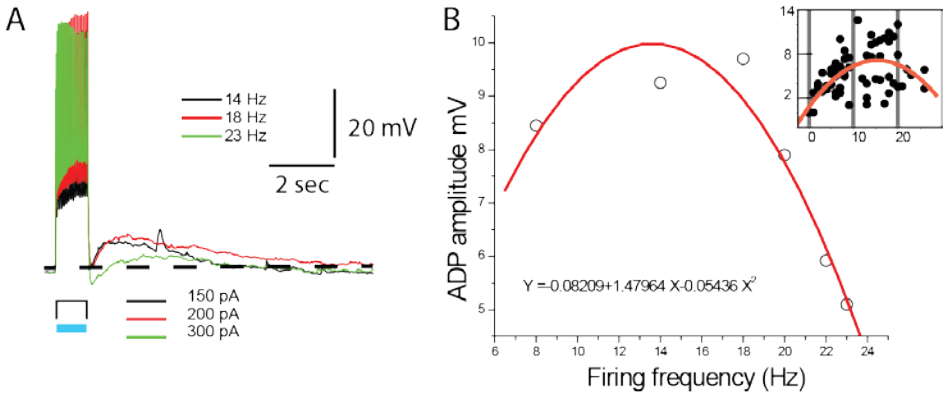

Figure 5.10 A neuron exhibiting an inverted-U shaped relationship between the firing frequency and ADP amplitude. A Three traces from the recording of a single neuron. Different colors correspond to responses to different intensities of intracellular current injections. Injected currents and action potential frequency are color coded. **B** Plot illustrating the relationship between firing frequency (x-axis) and ADP amplitude (y-axis) for the neuron in A. Inset shows the same relationship for the data acquired from all neurons.

So far, I described what happens in artificially activated (i.e. via depolarizing current injections) RS BLA neurons during endogeneous acetylcholine release and focused mostly on the supratheshold effects. Both whole cell and perforated patch clamp recordings show the following regarding acetylcholine actions on RS BLA neurons:

1- ADPs are events that exceed the duration of intracellular stimulation.

2- Intracellular stimulation and BFc afferents are required for the occurence of ADPs.

3- Based on the sensitivity to pharmacological manipulations, I_{CAN} is responsible for ADP generation and its activation is M1 receptor dependent.

4- Current induced firing frequency of the neurons and subsequent ADPs exhibited an inverted U-shaped relationship during the presence of 10 Hz BFc stimulation.

5- Stimulating BFc afferents at a lower frequency (4 Hz) was not associated with a robust ADP suggesting that this phenomenon is also dependent on the amount/pattern of acetylcholine presence.

In the next section, I am considering what happens to these neurons when they are at rest.

5.3.3 Effects of BFc stimulation on subthreshold properties

In response to single 3-5 msec long light pulses at rest, a depolarizing-hyperpolarizing sequence was observed (Figure 5.11 A, black trace). The depolarizing component was ~50 msec long and was followed by a pronounced hyperpolarization, ranging between 400 – 500 msec in different neurons. Atropine (1.5 µM) blocked the hyperpolarizing component and unmasked an additional depolarizing component that prolonged depolarization to ~200 msec (Figure 5.11 A, blue trace). This depolarization reversed ~-60 mV, close to the theoretical Cl^- reversal potential with the recordings solutions (Figure 5.11 A, inset), and in other neurons was blocked by picrotoxin (100 µM) (not shown). This component was also sensitive to mecamylamine (Figure 5.11 A, red trace). These results suggest that cholinergic input from basal forebrain has an

inhibitory influence on BLA pyramidal neurons at rest. The inhibition is underlined by the parallel recruitment of inhibitory interneurons through nicotinic receptors and direct postsynaptic muscarinic hyperpolarization. Even when all muscarinic, nicotinic, and GABA-A receptors were blocked; there remained a small depolarizing component, less than .2 mV. This small depolarization was sensitive to the blockade of ionotropic glutamate receptors with CNQX (20 µM) and AP-5 (100 µM) (not shown). See figure 5.11 for a representative recording.

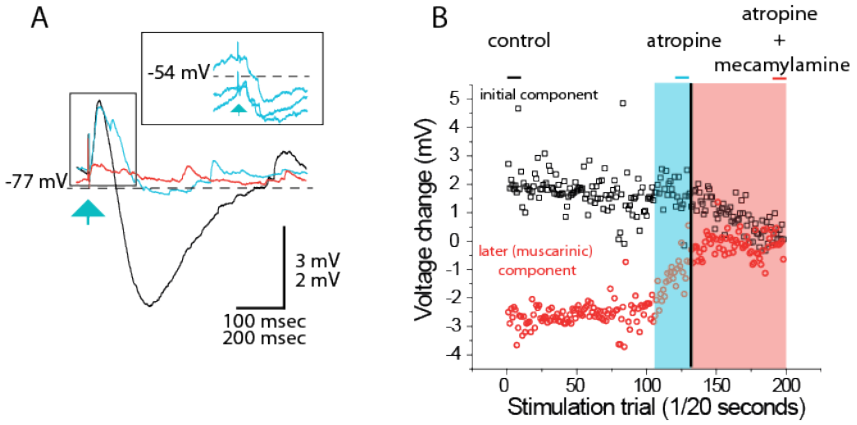

Figure 5.11 Physiological profile of cholinergic responses in RS BLA neurons. **A** Averaged sweeps illustrating the responses to cholinergic stimulation. Control in *black*, atropine in *blue*, and atropine (1 µM) + mecamylamine (10 µM) in *red*. The three individual traces in the *inset* show the reversal of the initial component at -54 mV (during atropine application). Numbers on the top on scale bars correspond to the traces in the inset. Blue arrow represents the optogenetic stimulation (**B**) Quantification of responses for the cell shown on left. Black and red data points represent individual depolarizing and hyperpolarizing responses. The short horizontal lines (*black*, *blue*, and *red*) show the region where the averages in (**A**) were acquired. The transparent boxes represent the times of drug application. Blue light was given every 20 seconds with the exception of just before mecamylamine application where the reversal potential of the depolarizing response was quickly determined within ~1 minute (these data are omitted in the plot).

To characterize the muscarinic component, subsequent recordings of muscarinic IPSPs were done during the blockade of ionotropic glutamate [with CNQX (20 µM) and

AP-5 (100 µM)] and GABA [picrotoxin (100 µM) receptors. Since no washout of this muscarinic IPSP was apparent during whole-cell recordings (Figure 5.11 shows a whole cell recording), data from whole-cell and perforated patch clamp recordings were combined.

Under these circumstances, the following drugs did not have any observable effect on the muscarinic IPSPs (the numbers do not correspond to neurons necessarily; some neurons were exposed to multiple antagonists successively):

CGP 55845 (1-10 µM sequentially applied to each neuron; GABA-B receptor antagonist; n = 5)

MTA (1 µM; M2 receptor antagonist; n = 3)

Apamin (100 nM; SK channel antagonist; n = 5)

Norepinephrine (10 µM to block the slow AHP; n = 1)

These results suggest that the muscarinic IPSPs in RS BLA neurons do not involve: M2 receptor activation, pathways that involve calcium activated potassium channels that mediate medium (apamin sensitive) and long (norepinephrine sensitive) (Faber and Sah, 2002) duration afterhyperpolarizations. The lack of effects of GABA-B antagonist suggests that it is also not mediated through GABA-B receptors.

On the other hand both pirenzepine (1 µM) and barium (400 µM) significantly reduced the amplitude of muscarinic IPSPs (from -2.70 ± 0.34 mV to -0.51 ± 0.38, $t = 7.937$, $p < 0.001$; Figure 5.12 A, red trace and C). The remaining hyperpolarization (in the presence of ionotropic glutamate and GABA receptor blockers) was abolished by

mecamylamine (10 µM, n = 2) (Figure 5.12 A blue trace). In another case, iberiotoxin (50 nM) blocked the hyperpolarization while sparing the minute (> 200-300 µV) depolarization preceeding it (Figure 5.12 B orange trace). These results suggest that the cholinergic IPSPs are mainly mediated through M1 receptor signaling while a small portion is mediated by nicotinic receptors. The identity of the nicotinic receptors involved was not investigated but their activation potentially increase intracellular calcium and recruit iberiotoxin sensitive, calcium activated potassium channels (i.e. BK). Given the higher contribution of muscarinic receptors in these IPSPs (≥ 5 fold bigger amplitude), I will continue to use the term “muscarinic IPSP”. It is important to note that the minute contribution of nicotinic receptors to the hyperpolarization is likely to be negligible under my experimental conditions (see Figure 5.12 D for a sketch of different contributions). However, this does not rule out the possibility that the postsynaptic nicotinic receptor activation plays a cardinal role *in vivo* during continuous synaptic bombardment (see Chapter 6 for discussion). The reader should also remember that nicotinic receptor activation plays a role in activating GABA inputs to RS BLA neurons (Figure 5.11).

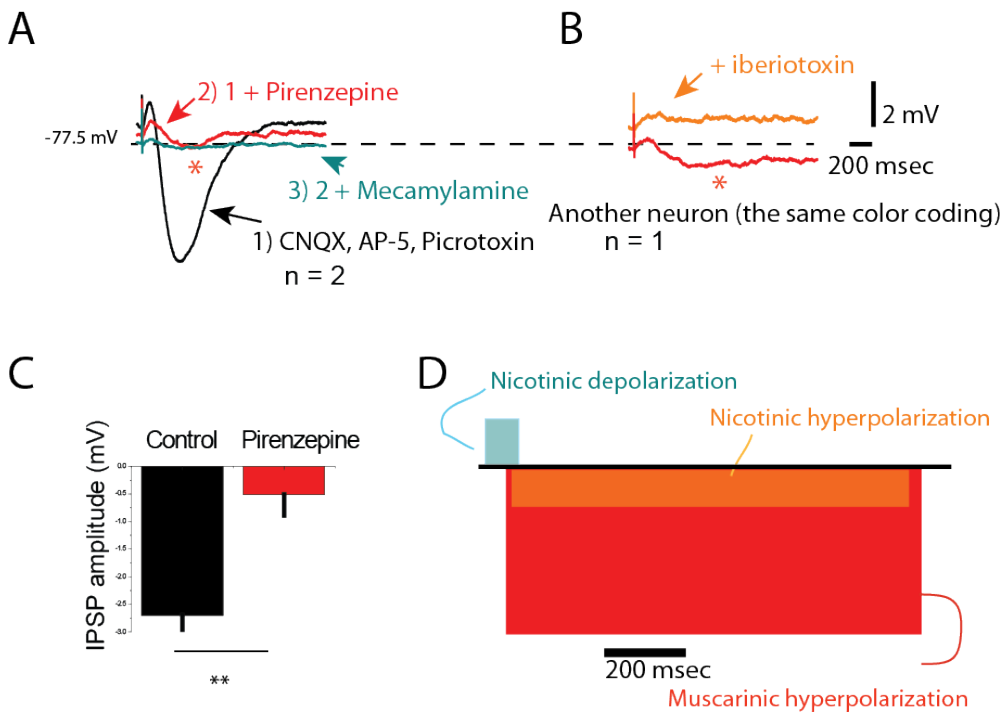

Figure 5.12 Details of acetylcholine mediated hyperpolarization in RS BLA neurons. A A Recording of IPSPs in the presence of CNQX (20 µM), AP-5 (100 µM), and picrotoxin (100 µM) (black trace), additional presence of pirenzepine (1 µM) (red trace), and additional presence of mecamylamine (10 µM) (blue trace). Each trace is the average of 10 individual traces. Note the slight depolarization and the following hyperpolarization (marked with red asterisk) before mecamylamine in the red trace. **B** Another neuron under the same conditions. Orange trace shows the additional iberiotoxin presence (50 nM) which abolishes the slight hyperpolarizing component. **C** Pirenzepine significantly blocks IPSPs. Note also the residual hyperpolarization. **D** A sketch summarizing the different time courses of the contribution by different mechanisms. The nicotinic hyperpolarization corresponds to an iberiotoxin sensitive hyperpolarization. ** $p < 0.01$. n indicates numbers.

5.3.4 Experiments on the possible functional significance

An easy way to have an understanding about the functional significance of a neuromodulatory input is to investigate the effects on input-output (i.e. how much current or synaptic input lead to how many action potentials) relationship of a neuron. In cases where the recorded RS BLA neurons were presented with current injections of high amplitudes (100 to 300 pA), investigating such a relationship proved difficult. In these cases, the artificial depolarization was so strong (especially with current injections of 100

pA and higher where the cells began firing ~10 Hz), the neurons were resistant to any kind of modulation of physiological relevance. For preserving statistical power, only the neurons that were consistently presented with intracellular pulses between 20 to 140 pA (in 20 pA increments) in the presence/absence of 10 Hz optogenetic BFc stimulation were included in this analysis (n = 8 out of 16). These recordings were done in the presence of CNQX (20 µM), AP-5 (100 µM), and picrotoxin (100 µM).

In order to analyze the effective range of BFc stimulation for hyperpolarizing the neurons, 4 measures were taken into account: the threshold current for eliciting action potentials (rheobase current), the threshold current (determined from a range between 20 – 140 pA; see above) for eliciting half-maximal firing, and the action potential frequencies during these current injections. Paired samples t-tests revealed significant effects on the rheobase current ($t = -3.416$, $p < 0.01$, paired samples t-test), the current that elicits half-maximal firing ($t = -2.049$, $p < 0.05$, paired samples t-test) (Figure 5.13 A, B). On the other hand, once the neuron reached firing or half-maximal firing threshold, the discharge frequencies were insensitive to BF stimulation. In other words, BFc stimulation seems to serve a thresholding mechanism while the hyperpolarization-mediated effect disappears at higher firing frequencies (Figure 5.13 C).

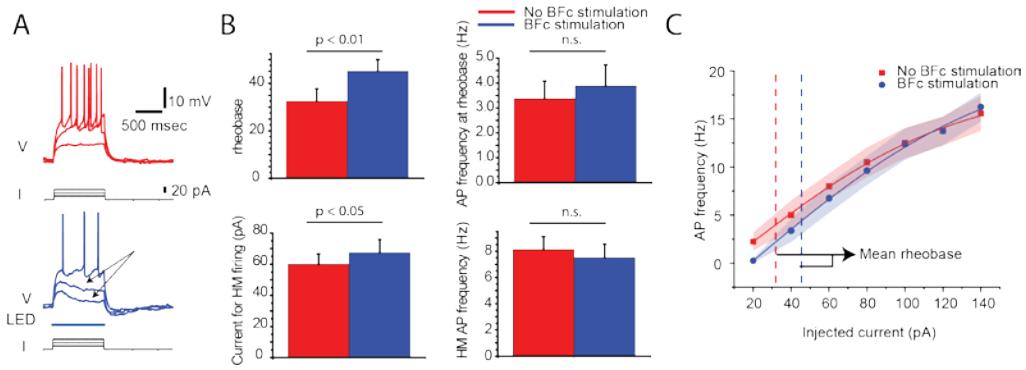

Figure 5.13 BFc stimulation alters the I-O curve in RS BLA neurons. A A representative neuron responding to intracellular current injections in the absence (red traces) and presence (blue traces) of optogenetic BFc stimulation (vertical blue line) at 10 Hz from a baseline of -65 mV. I: Current; V: Voltage. Arrows (bottom) indicate the BFc stimulation induced hyperpolarization **B** Bar graphs illustrating the effectiveness of optogenetic stimulation in heightening the rheobase current (the initial current intensity for evoking an action potential (AP) and the current necessary for inducing half-maximal firing (left raw). The AP frequency during rheobase and half-maximal firing inducing current injections was not altered as a result of BFc stimulation. Error bars indicate standar deviation. **C** AP frequency as a function of injected current for summarizing the effects of BFc stimulation. Mean rheobase values are indicated with color coded, vertical lines.

5.4 Summary of the main findings

a) The BLA constitutes a very convenient system for investigating cholinergic actions in target structures using optogenetics.

b) BFc stimulation produces two different effects on RS BLA neurons in a state dependent manner: when these neurons fire with intracellular depolarization, BFc stimulation leads to ADPs that exceed the duration of stimulation while BFc stimulation is inhibitory at rest and serves a thresholding function.

c) The ADPs are mediated through M1 receptor activation of I_{CAN} currents.

d) The ADP amplitude is graded until ~20 Hz action potential discharge. Its amplitude shows a reduction at firing frequencies higher than 20 Hz.

e) The hyperpolarizing effect at rest is also mediated by M1 receptors and is sensitive to barium suggesting the involvement of an inwardly rectifying potassium channel.

f) A small contribution to the hyperpolarization by nicotinic receptor activation of calcium activated potassium channels, namely BK channels, is likely.

CHAPTER VI: GENERAL DISCUSSION

Using acute slices obtained from different lines of transgenic mice and utilizing optogenetics in some of the experiments, this thesis aimed at answering three questions about the BFc system:

1- The intrinsic physiology of BFc neurons
2- The interactions between BFc neurons
3- The effects of BFc stimulation on RS BLA neurons

6.1 Electrophysiological properties of BFc neurons (Aim 1)

Given the significance of the BFc system in diverse cognitive and physiological functions, characterizing the physiological properties of its constituent neurons is essential for a proper understanding of the mechanisms whereby these neurons exert their effects on cortical processing. Using adult transgenic mice expressing eGFP in cholinergic neurons, sampling from the entire BF and applying systematic physiological criteria, evidence for the existence of two electrophysiologically distinct cholinergic cell populations in the mature BF, characterized by more than 3 fold difference in spike onset latencies and 2 fold difference in spike frequency adaptation rates was obtained; with EF cells exhibiting a more excitable and adapting profile. As evidenced by voltage-clamp analysis, the EF neurons exhibited a higher expression of low voltage activated (LVA) calcium currents compared to the LF neurons. The variability of action potential delay in each group seems to be related to different mechanisms: I_A-like potassium currents, which have been shown to have important roles in determining spike onset latency in diverse systems (Tierney and Harris-Warrick, 1992; Gerber and Jakobsson, 1993; Tell

and Bradley, 1994; Magarinos-Ascone et al., 1999; MacLean et al., 2005), seem to be related to spike delay only in LF neurons. On the other hand, the contribution of I_A is masked by LVA calcium current in EF neurons.

Previous results on the intrinsic physiology of BFc neurons in different BF subregions (e.g. Momiyama and Zaborszky, 2006; Hedrick and Waters, 2010) converge on some basic principles. In short, BFc neurons fire at lower frequencies compared to noncholinergic BF neurons and therefore, they are usually referred to as slow firing BF neurons (Griffith and Matthews, 1986). Moreover, their action potentials are wider and commonly followed by prominent SK channel mediated medium afterhyperpolarizations (mAHPs) (Williams et al., 1997). In addition, anomalous rectification and outward rectification are among the other defining properties of BFc neurons (Bengtson and Osborne, 2000). However, I did not observe “bursting” BFc neurons in any BF subregion. This contrasts with reports of bursting in BFc neurons of the substantia innominata (Khateb et al., 1992; Khateb et al., 1995; Alonso et al., 1996). These discrepancies likely arise from differences in the protocols used to record from these cells. Studies reporting bursting behavior were carried out with ACSF containing a higher Ca^{2+}concentration than the present studies (2.5 mM vs. 2mM). In my experimental conditions, calcium entry might not have been sufficient enough to counteract outward currents and generate bursting, a notion suggested before (Gorelova and Reiner, 1996; Sim and Allen, 1998). Finally, in some experiments I observed eGFP negative neurons firing spike doublets similar to those reported as bursts in BFc neurons (e.g. Khateb et al., 1992) (not shown). Thus, bursting does not seem to be a property of BFc neurons in any BF region and cannot be used as an electrophysiological criterion to identify BFc neurons

in vitro. However, these results do not negate the possibility of burst firing of cholinergic neurons *in vivo* (e.g. Nunez, 1996; Manns et al., 2000a) and *in vitro* under specific experimental conditions (Khateb et al., 1997; Khateb et al., 1998).

In summary, using direct comparison of current and voltage clamp data in the same cells and sampling from the entire BF, this study suggests the existence of two electrophysiologically distinct types of BFc neurons, co-existing in different BF subregions.

6.1.1 Mechanisms underlying the differences between EF and LF neurons (I): Transient potassium currents

Transient potassium currents activate when neurons are depolarized from hyperpolarized potentials (Coetzee et al., 1999; Birnbaum et al., 2004) and have been shown to delay firing and regulate firing frequency (Storm, 1988; Tierney and Harris-Warrick, 1992; Gerber and Jakobsson, 1993; Tell and Bradley, 1994; Del Negro and Chandler, 1997; Kanold and Manis, 1999; Magarinos-Ascone et al., 1999; MacLean et al., 2005). Previous studies have reported the existence of transient potassium currents in BFc neurons recorded in BF cultures without reference to firing delay and other functional properties (Sim and Allen, 1998; Tkatch et al., 2000). The decay time constants of the current I identified resemble the slowly inactivating I_A current which is also referred to as the I_D current. However, in dissociated culture, I_A currents identified in cholinergic neurons had faster inactivation kinetics (Sim and Allen, 1998; Tkatch et al., 2000). A recent study (Garrido-Sanabria et al., 2011) in slices also reported fast inactivating I_A currents in slow firing putative cholinergic neurons in BF slices. The differences in the decay kinetics of this current might reflect differences in preparation

and/or the age of animals used. Indeed, various potassium channels have been shown to be developmentally regulated in different cell types like cortical PV+ neurons (Okaty et al., 2009). Whether such alterations also occur in BFc neurons and their functional implications remain to be tested. Finally, the preponderance of BFc neurons with spike frequency acceleration along with the long decay time constant of the measured currents is suggestive for the presence of a Kv1 mediated I_D current (Miller et al., 2008).

Surprisingly, EF and LF neurons did not differ with respect to the average transient potassium current density or decay time constant. However, I observed a decay time constant to spike onset latency correlation, which can help to explain the spike delay variability of LF neurons, but clearly not that of EF neurons. This led me to consider other possibilities. While the shorter membrane time constant of EF neurons could explain the differences in spike latency to some extent, it is likely not an important factor since the transient potassium current decay time constant's relationship to spike onset latency in both groups remained unchanged after the membrane time constant was subtracted from the spike onset delay. Also, the slight but significant differences in spike thresholds between EF and LF neurons constitute another source for spike onset delay. These differences, although potentially important, are however unlikely to explain differences measured in the order of tens of milliseconds.

6.1.2 Mechanisms underlying the differences between EF and LF neurons (II): Low voltage activated calcium currents

Voltage gated ion channels are expressed in different neurons in different proportions, and the interplay between them has been shown to be critical in determining a neuron's behavior. Indeed, compensatory actions of different ion channels have been

demonstrated in other systems (Linsdell and Moody, 1994; Pape et al., 1994; Del Negro et al., 2002; MacLean et al., 2003; MacLean et al., 2005; Molineux et al., 2005; Hudson and Prinz, 2010). Given these possibilities, I predicted the presence of an inward current in EF neurons that counteract transient potassium currents. Due to their reliable expression profile in these neurons, the most plausible candidate in BFc neurons is the LVA Ca^{2+} channels (Allen et al., 1993). Indeed, it has been reported that different BFc neurons can be distinguished based on their LVA Ca^{2+} current density (Han et al., 2005). Moreover, interplay between transient potassium currents and LVA currents has been demonstrated to play an important role in determining spike latency in cerebellar stellate neurons (Molineux et al., 2005). Consistent with these notions, EF neurons exhibited higher LVA Ca^{2+} current densities than LF neurons and blockade of channels mediating LVA currents in BFc neurons with nickel delayed spike onset latency in these neurons. Thus, it appears that the differences in firing delay between EF and LF neurons are probably due to interplay between membrane currents with different polarities. These findings might also explain the lower spike thresholds observed in EF neurons. Unfortunately, accurately measuring Ca^{2+} and K^{+} currents in the same neurons to determine their possible functional interactions is not possible given the combinations of blocking agents required and thus, establishing a definitive relationship between these currents remains a challenge.

Various types of voltage gated ion channels can have different functions depending on their cellular localization (Brew and Forsythe, 1995; Hoffman et al., 1997; Magee, 1998 ; Migliore et al., 1999; Johnston et al., 2000; Gu et al., 2005; Burkhalter et al., 2006; Kollo et al., 2006; Kollo et al., 2008). Our study is limited to the somatic

current measurements due to problems associated with patching dendrites in adult animals and therefore does not address the degree of involvement of these currents in the electrotonically distal portions of the neurons.

6.1.3 Mechanisms underlying the differences between EF and LF neurons (III): Possible underpinnings of firing properties

SK channel mediated AHPs have been shown to enhance the uniformity of the inter-spike interval in BFc (Gorelova and Reiner, 1996) and in other systems, such as the noncholinergic neurons of the globus pallidus (Deister et al., 2009). Current data are in line with this suggestion where LF neurons are shown to have higher AHP amplitudes and minimal spike frequency adaptation. Thus, SK channel mediated AHPs may be important in recruiting Na^+ channels (via de-inactivation) for action potential generation and contribute to the determination of the electrophysiological properties that distinguish BFc neuron cell types. This is further bolstered by the finding that action potentials can be regenerated in EF neurons when small hyperpolarizing pulses are nested within prolonged depolarizing current injections which possibly de-inactivate sodium channels for action potential generation. Finally, the I_A current is also known to facilitate Na^+ channel recovery from inactivation (Hess and El Manira, 2001). Therefore, in LF neurons mAHP and I_A may in concert help sustain the repetitive firing.

The calcium channel that provides the calcium source for the activation of medium duration AHPs following single spikes show neuronal type-specific differences in many systems. In BFc neurons, calcium entry through the LVA channels has been shown to determine AHP amplitude (Williams *et al.*, 1997). Curiously, the data show a higher LVA density in EF neurons, which I have shown to exhibit lower AHP

amplitudes. It is possible that EF neurons have lower levels of SK channel expression and/or different localization of these channels compared to LF neurons where they might serve other functions such as synaptic integration (Gu et al., 2005).

6.1.4 Pitfalls/strengths

Classifying different kinds of neurons (both principal and interneurons) is perhaps one of the most problematic aspects of neuroscience. No matter the data available (e.g. electrophysiology, PCR, anatomy) and the type of analysis (e.g. cluster analysis), it is ultimately the researchers biases that shape the decision. Years of debate seem to have settled down the issue just recently: for principal and interneurons, a combination of electrophysiological properties and axonal targets seem to generate the most consistent and functionally meaningful data (Ascoli et al., 2008; Dembrow et al., 2010). My morphological data (see appendix) are vastly limited due to the small numbers and the way the tissue was processed. Thus, current results do not capture all the necessary details for a close to definitive conclusion.

Moreover, arbitrarily dividing the neurons into different classes along a limited set of physiological dimensions will certainly lead to significant differences in other electrophysiological properties among these arbitrarily defined sets of neurons for different reasons that include: mere experimental artifacts or expected correlations between different sets of physiological properties. While my method is definitely not immune to these artefacts, I took several measures against it. The physiological dimension (action potential delay) used to differentiate the neurons into different classes has a statistical basis. In addition, the other differing dimensions subsequent to initial characterization did not correlate with action potential delay. Another precaution

included the recording of neurons from pre-determined membrane potentials. As noted by Sosulina et al. (2010), classifying a set of neurons from different membrane potentials entails a problem even for the most widely accepted schemes for classifying neurons. Finally, physiological data were not analyzed before 10 minutes following whole cell access. This measure was taken to dialyse all the cells to the same degree with the intracellular solution. While this approach is not as good as perforated patch clamp recordings, it certainly is useful for avoiding unreliable data due to differential washout of different neurons that might arise from minor differences in pipette tip diameter and soma size. In short, my interpretations remain open for criticisms but the experimental approach and data analysis are consistent and easy to replicate.

6.1.5 Conclusions, functional implications and potential further studies

This study provides evidence for the existence of two subtypes of BFc neurons based on spike onset latency in adult mice. EF neurons with their initial high frequency discharge followed by pronounced spike frequency adaptation could lead to a different acetylcholine release profile than that of LF neurons, which show little spike frequency adaptation when depolarized. Recent amperometric studies suggest that acetylcholine release can be tonic (measured in minutes) or phasic (measured in seconds) depending on attentional demands (Parikh et al., 2007; Parikh and Sarter, 2008; Hasselmo and Sarter, 2011), an observation that may relate to the existence of two functionally distinct BFc neuron populations described in the current thesis. Moreover, the delay to spiking, the main feature distinguishing BFc neurons, may be involved in different aspects of synaptic plasticity given the novel finding regarding the temporal requirements of cholinergic activation for different forms of hippocampal plasticity (Gu and Yakel, 2011).

Another interesting possibility relates to the complex architecture of cholinergic space in the basal forebrain. Statistical analysis of anatomical data based on nearest neighbor density determined that BFc neurons in rats are either found in dense clusters or diffusely located in the background (Nadasdy et al., 2010). Since the projection target of the clusters and the low density locations are different (Zaborszky et al., unpublished observations) it would be functionally important to test in future studies to what extent EF/LF neurons in mice fit into this anatomical scheme.

While preliminary morphological data are promising (see appendix), it is definitely not enough. Ideally, the slices need to be re-sectioned and embedded in resin. This approach would ensure that tissue shrinkage is minimal and analysis will not be hampered by low visibility in thick slices with background staining. I propose that finding possible morphological differences *in vitro* can also aid in identifying different roles these neurons play *in vivo* on the basis of *in vitro* and *in vivo* morphological comparisons. The approach used in these studies can also be combined with retrograde tracer injections to investigate possible differences related to targets innervated by BFc neurons. This is particularly interesting as this approach might start giving valuable details about the distal causes of differences observed in BFc neurons. One interesting possibility is the presence of different neurotrophic factors in different cortical target regions. A similar question was raised in sympathetic neurons and compelling evidence suggests that different neurotrophic factors present in the efferents of sympathetic ganglia neurons shape the electrophysiology of efferent neurons [e.g. Luther and Birren (2009)]. Finally, these differences might not only relate to the particular cortical regions

innervated but also the different layers in these regions, target neurons (e.g. principal or interneuron), or the nature of innervation (synaptic vs. volume transmission).

6.2 Interactions between BFc neurons (Aim II)

The current studies applied different approaches to examine the interactions between BFc neurons. One of the drives for conducting these experiments was their potential relevance to what could occur in the intact brain. Unlike other reports (Bengtson and Osborne, 2000), current experiments show that local BFc fibers can be preserved in acute slices. Hence, the experiments included a diverse array of approaches ranging from pharmacological manipulations/paired recordings to optogenetic experiments. The pharmacological experiments were two-fold. CCh experiments have shown that muscarinic receptor activation reduced the excitability of BFc neurons. On the other hand, active slice experiments where BFc neurons were made spontaneously active revealed that BFc neurons fired at higher frequencies in the presence of atropine, a muscarinic receptor blocker. In other words, atropine likely blocked the effects of endogeneously released local acetylcholine during the spontaneous activity of BFc neurons. Paired recordings, where the potential presynaptic cell was loaded with cesium to increase neurotransmitter release, revealed a connectivity ratio of 3/20 between BFc neurons recorded tens of microns apart. These connections were associated with hyperpolarizing short latency and short duration responses. One pair was successfully recovered for light microscopic investigations and a putative contact site was evident. Optogenetic stimulation led to muscarinic hyperpolarizations as determined by pharmacology. In these optogenetic experiments, SK channel blockade with apamin led

to a delay in the onset of muscarinic IPSPs and subtractions using apamin free period as the control period uncovered the apamin sensitive component of muscarinic IPSPs.

Previous studies investigating local BFc interactions were limited in revealing the physiological relevance of endogeneously released acetylcholine. While Metcalf et al. (1988) revealed acetylcholine release in BF slices, the origin of this was not as clear given the potential contributions of brainstem cholinergic afferents to BF. Moreover, the actions of this increased acetylcholine release was not investigated. In addition to revealing inhibitory actions of muscarine on BFc neurons, Alreja et al. (2000) have found that atropine increased the spontaneous discharge rate of BFc neurons. The antagonist effect certainly reveals the implications of endogeneously released acetylcholine. However, synaptic blockers were not used in this study and acetylcholine actions could not be studied in isolation.

6.2.1 Possible mechanisms of muscarinic IPSPs

The CCh experiments revealed a trend for a drop in input resistance along with hyperpolarization in BFc neurons. These effects were obtained in the presence of blockers for fast glutamatergic/GABAergic neurotransmission at a hyperpolarized potential below the reversal potential for Cl^-. This suggests that the hyperpolarization seen is mediated by the opening of a K^+ conductance. While GABA-A receptor blockade was not present during paired recordings between BFc neurons, the hyperpolarizations seen in these pairs were apparent again at similarly hyperpolarized membrane potentials. In both CCh and paired recording experiments, the muscarinic nature of the response was verified with atropine. However, these data are limited and do not provide sufficient information about the mechanisms of muscarinic IPSPs. In the connected BFc pair

successfully recovered for biocytin cytochemistry, the putative contact site was on the dendrite, a finding consistent with previous ultrastructural studies indicating that cholinergic synapses on BFc neurons are dendritic (Martinez-Murillo et al., 1990; Smiley and Mesulam, 1999).

The optogenetically induced muscarinic IPSPs were apparent at negative voltages suggesting the involvement of K^+ conductances again. However, they were much longer in duration than the ones obtained with paired recordings (750 to 1766 msec for optogenetics vs. 217 – 284 msec for paired recordings). The discrepancies are not accounted for in the current experiments but could be explained by multiple factors like the prolonged presence of acetylcholine in synaptic/perisynaptic areas during optogenetic experiments and/or different number and type of receptors/downstream pathways affected. The contribution of the latter mechanism is bolstered by the findings that optogenetically induced muscarinic IPSPs can be dissociated into two components: one fast onset and short lasting, apamin sensitive component (i.e. SK mediated) and a late onset, longer duration apamin insensitive component. In these experiments, subtracting the average muscarinic IPSPs during apamin application from the ones obtained under control conditions revealed that the temporal properties of the SK-sensitive component are similar to the muscarinic responses obtained during paired recordings. Indeed, the similarity becomes striking when considering the time for the responses to decay into account. More future experiments are necessary to investigate whether the fast onset and short duration muscarinic IPSP component (i.e. SK sensitive component) observed in optogenetic experiments and the responses observed in paired recordings share some mechanisms. Since apamin was not tested during paired recordings, this question remains

unanswered for now. Finally, the muscarinic IPSPs were sensitive to M2 receptor blockade, suggesting that the shorter and longer components of muscarinic IPSPs are governed by the same receptor subtype.

Regardless of the experiments, the onset latencies for muscarinic IPSPs were shorter than what would be expected from metabotropic actions. This comes as no surprise when considering the potential shortcuts muscarinic receptor signaling can take. It has been known that cardiac responses to vagal nerve stimulation can be of short latency (50 - 100 msec) due to the direct activation of Kir 3.X channels by βγ subunits of G-proteins (reviewed in Brown, 2010). As reviewed by Brown (2010) again, similar results were obtained in bullfrog sympathetic neurons (Dodd and Horn, 1983), thalamic reticular neurons (McCormick and Prince, 1986b), and parabrachial motor neurons (Egan and North, 1986). Calabresi et al. (1998) reported a similar time course for muscarinic IPSPs in striatal cholinergic neurons but the underlying channels and pathways were not investigated in this study. While the βγ pathway recruited by M2-receptor activation constitutes a plausible scenario for the current results, additional possibilities exist. One such possibility is the presence of microdomains that organize intracellular signaling molecules to produce fast and efficient signaling. To my knowledge, such microdomains are best characterized in the mammalian nervous system for ionotropic glutamatergic synapses (see Ziff, 1997), but more examples in other systems exist. For instance, phototransduction in the fruitfly *drosophila* takes place through the presence of signaling microdomains that include complexes of scaffolding and effector proteins located in specialized cellular structures referred to as rhabdomeres (reviewed in Delmas et al., 2004). This organizational feature ensures that signaling proteins do not interact with

superfluous signaling molecules and speeds up metabotropic receptor mediated light responses that occur with onset latencies as fast as ~20 msec (reviewed in Delmas et al., 2004). Such an “ultra fast” mechanism in the mammalian brain has not been investigated but Pakhotin and Bracci (2007) have described that muscarinic receptor activation in the striatum can alter glutamate release within onset latencies around 10 – 15 msec. The notions about these nontypical fast responses might be particularly relevant for the SK-sensitive component of the muscarinic IPSP which could occur even slightly faster than the traditional βγ subunit mediated inward rectifier activation (e.g. Dodd and Horn, 1983). While these ideas are very difficult to test, a particular point deserves attention. As reviewed in the background section, most if not all cholinergic synapses in BF targets are symmetric. The cholinergic synapses on noncholinergic BF neurons are symmetric as well (Martinez-Murillo et al., 1990). In this respect, cholinergic synapses on BFc neurons constitute a possible exception as these have been shown to be exclusively asymmetric (Martinez-Murillo et al., 1990). The asymmetric nature might also reflect the presence of specialized postsynaptic proteins that subserve similar functions as in the *drosophila* photoreceptors. As a final point, it has been shown in NL 308 neuroblastoma x fibroblast hybrid cells that M2 and M4 receptor activation can produce spatially localized calcium activated potassium currents through the alpha subunit of the G_i (Noda et al., 1993) and a similar mechanism might have played a role in current experiments.

6.2.2 Pitfalls/strengths

The weaknesses in these experiments are three-fold. First, the sample size for positive responses in some experiments is too small for reaching solid conclusions about the mechanisms and possible functions of muscarinic IPSPs. These experiments include

the paired recordings (n = 3 for connected pairs) and alterations of EPSPs when BLA was stimulated optogenetically along with pressure application of CCh onto the dendrite of a BFc neuron. The latter experiment further suffers from the differences in methodology: Unlike the original experiments which revealed the SK mediated component with optogenetics, the muscarinic receptors in this experiment were activated with dendritic pressure application of CCh. In addition, while I would be happy to conclude whether the atropine sensitive IPSP seen during paired recordings and the SK mediated component in optogenetically induced IPSPs share some mechanisms (or identical), the limited numbers and lack of appropriate pharmacology experiments in paired recordings do not allow me to make such comparisons. Second, the distribution of infected BFc neurons was random, not allowing me to investigate the circuitry mechanisms in detail. Thus, the stimulation protocol just answered whether BFc interactions exist and their polarity (i.e. depolarizing or hyperpolarizing) while leaving functional considerations outside the scope.

Last point pertains to the absence of results regarding the modulation of the release of other neurotransmitters by optogenetic stimulation of BFc elements. Acetylcholine is heavily involved in regulating neurotransmitter release in diverse regions in the central nervous system (e.g. Gray et al., 1996; Maggi et al., 2003). Moreover, recent studies indicated that paired recordings involving a neuron with a neuromodulatory function (e.g. de Rover et al. 2002; Pakhotin and Bracci, 2007; von Engelhardt et al. 2007) or stimulation of cholinergic fibers (Dodd and Horn, 1983; Rogers and Sargent, 2003; Tang et al., 2011) can produce results similar to pharmacological studies but with more physiological relevance. This becomes more of

an issue when considering the pharmacological experiments in the BF showing the strong role played by acetylcholine in regulating the release of other transmitters such as glutamate (Sim and Griffith, 1996). Moreover, a diversity of BF neurons responds to acetylcholine pressure application while those responding to electrical stimulation are extremely rare (Henderson et al., 2005). Based on this, Henderson et al. (2005) suggest that acetylcholine receptors in noncholinergic BF neurons might not be functional at the somatodendritic level and pharmacological responses might reflect receptors to be transported to axon terminals. The experiments in this thesis cannot answer these questions reliably for different reasons; the intracellular solutions and the stimulation protocols used being the most prominent ones. The fact that I did not see potential polysynaptic responses might reflect the distal nature of glutamatergic and GABAergic synapses impinging on BFc neurons. Moreover, the onsets of cholinergic actions on neurotransmitter release typically takes long and require high frequency stimulation [e.g. Dodd and Horn (1983)], making their systematic analysis under most circumstances difficult [but see. Eccles et al. (1954); English et al. (2011); Arroyo et al., 2012].

These weaknesses are poorly dealt with mainly due to the problems in mating colonies (e.g. very rare mating, dead litters, and small litter sizes) for ChAT-eGFP X ChAT-cre mice. In addition, almost half of the mice were used for pilot experiments for allowing sufficient numbers of mCherry negative BFc neurons for recording muscarinic responses in infected areas.

Despite the remaining questions, the findings are of interest. No study in the BF approached the problem of BFc interactions in such detail. The reader is referred to the dicsussion by Duque et al. (2007) regarding our limited knowledge about potential BFc

interactions five years ago. To my knowledge, the paired recordings between BFc neurons and the identification of morphological features in one pair is the first example in the entire literature. In a similar vein, the optogenetic studies are the first ones to evoke postsynaptic metabotropic responses in a particular cell type. Revealing these aspects required a lot of stability in the recordings. Most recordings revealed responses classifiable as small (but see below for the discussion of remaining experiments) but this nonetheless shows that BFc system is endowed with fundemental biological capacities for local interactions. Moreover, the values reported might be an underestimation even for *in vitro* as some proportion of BFc afferents to recorded BFc neurons might not have been infected. The fact that atropine increased spontaneous firing frequency of BFc neurons in active slices support this possibility. In short, the magnitude of these interactions might differ *in vivo* (and even *in* vitro) but there is no good reason to believe that they will change their polarity [see Sim and Griffith (1996)].

6.2.3 Functional implications and potential further studies

The ratio of the connected pairs and weak responses in optogenetic experiments as opposed to the relatively robust effects in active slice experiments suggest that there is a level of specificity in BFc interactions. Further knowledge regarding the specific connection patterns is necessary for reaching solid conclusions about the functions of BFc interactions. As discussed in the background section, neighboring BFc neurons, which possibly constitute functional modules (Nadasdy et al., 2010), exhibit similar dendritic orientations (Zaborszky et al., 2002). In this respect, it is crucial to know whether these neurons, which possibly project to functionally-related cortical areas (Zaborszky et al., unpublished observations), really share common inputs and whether or

not they inhibit each other. I would envision that they indeed receive common inputs but do not inhibit each other. Instead, the inhibition might be specific to interactions between distinct" information processing modules" which relay their information to cortical areas with less connectivity. Ultimately, these interactions might contribute to cortical information processing. Human studies utilizing fMRI revealed two sets of cortical areas exhibiting reciprocal changes in their activation during tasks that gauge attention (Binder et al., 1999; Dosenbach et al., 2007). Recently, a study recording LFPs in homologous regions of cats revealed a similar interaction (Popa et al., 2009). While midline cortical structures exhibited reduced LFP power at all frequencies during heightened attentional demands, there was a reciprocal increase in more laterally found cortical structures (Popa et al., 2009). Though a variety of factors possibly account for these findings, differential afferent regulation by acetylcholine, possibly mediated by BFc interactions, might play a significant role also.

A final point pertains to the view regarding the enhancement of signal to noise ratio by acetylcholine. As reviewed in the background section, acetylcholine reduces the efficacy of cortico-cortical connections. While this strategy might be useful under most circumstances, certain deleterious effects become apparent when considering the functional significance of certain sets of corticocortical connections that are needed for functions like sensorimotor integration [e.g. Mao et al., (2011)]. Thus, for the BFc system to be effective, it has to be able to discriminate between different sets of corticocortical synapses. If this is true, functional interactions between BFc neurons by themselves would constitute the first candidate mechanism. A good experiment could investigate the activation/inactivation of BFc neurons while observing the coherence of LFPs in different

sensorimotor areas/layers during tasks that require sensorimotor integration. An even simpler experiment would investigate intra-BF application of atropine while recording sensorimotor areas.

6.3 Effects of BFc stimulation on RS BLA neurons (Aim III)

Utilizing optogenetics, the current study investigated the effects of selective BFc stimulation on RS BLA neurons. This is an important question as BLA shows many similarities to cortical regions in terms of its cell types. In addition, the BLA is implicated in functions critical for survival (see the Aim III specific introduction). Overall, the effects of acetylcholine seems to be two-fold: A possible increase in the excitability of RS BLA neurons following action potential discharges and a reduced excitability at rest, exerting a thresholding function.

6.3.1 Afterdepolarizations (ADPs) and acetylcholine

The ADPs were characterized as depolarizations exceeding the duration of responses to intracellular current injections and required the concomitant optogenetic stimulation of the BFc afferents. Furthermore, evoked ADPs were blocked by atropine, pirenzepine, and flufenamic acid. These results suggest that ADP generation is dependent on the activation of postsynaptic M1 type receptors recruiting calcium activated cationic conductances (I_{CAN}).

The ADP amplitudes exhibited an inverted U-shaped relationship with firing frequency during intracellular current injections. The amplitudes typically increased until the cell fired ~20 Hz during intracellular depolarizations and showed a reduction following higher than 20 Hz spiking. The frequency with which the BFc was stimulated

also seemed to affect the ADPs: ADPs were not as strong and missing in most cases when the BFc stimulation was carried out at 4 Hz instead of 10 Hz.

These conclusions were based on both whole-cell recordings for which the time of data acquisition was controlled with maximum possible care and perforated patch clamp recordings.

6.3.2Effects on ADP amplitudes in relation to previous findings

While different studies looked at cholinergically mediated ADPs in different cortical areas (see the background section), only two previous studies investigated the involvement of acetylcholine induced I_{CAN} activation in RS BLA neurons. In one of them (Yajeya et al., 1999), CCh application led to a membrane depolarization from rest coupled to a decrease in input resistance in a flufenamic (I_{CAN} blocker) acid dependent manner. In another study (Egorov et al., 2006), CCh application led to ADPs and persistent spiking, reaching upto 40 Hz for minutes, when coupled to intracellular depolarizations. In the latter study (Egorov et al., 2006), the ADPs were graded: their amplitude and the frequency of ADP associated action potentials (referred as persistent firing by these authors) increased as a function of intracellular current induced spiking (at even higher frequencies than 20 Hz reported in current studies). In both these studies, the receptor (i.e. M1 type) and the final mechanism (I_{CAN}) involved was the same as in this study.

Obviously, the effect reported by Egorov et al. (2006) is much stronger than the one reported in current studies. However, the BLA neurons fire at very low frequencies *in vivo* even during emotional arousal (Pare and Collins, 2000), contrasting the findings

by Egorov et al. (2006) who report firing frequencies as high as 40 Hz. Their findings were either obtained with pharmacological manipulations or during electrical BFc stimulations in the presence of acetylcholinesterase blockers. While electrical BFc stimulation by Egorov et al. (2006) was carried out during the presence of drugs that block ionotropic glutamate and ionotropic/metabotropic GABA transmission, the recruitment of other systems during electrical stimulations were not tested for. Thus, the optogenetic stimulation paradigm used in this thesis likely represents a more realistic experimental approach.

For the moment, even if we neglect the fact that ADPs reported by Egorov et al. (2006) were much stronger, inconsistencies persist. Another difference entails the relationship between ADP amplitudes and prior spiking. The ADP amplitudes in current studies do not seem to increase in a graded fashion as reported in Egorov et al. (2006) in the amygdala [or in the entorhinal cortex (Fransen et al. (2006)]. According to the point attractor model of Fransen et al. (2006), the I_{CAN} currents are governed by dynamic interactions between two opposing metabolic processes mediated by intracellular Ca^{2+} separating open/closed states of the underlying channel. However, this does not account for the contribution/competition by other channels. Plausible candidates for diminishing ADP amplitudes after higher firing activity involve the calcium activated potassium conductances that are recruited following action potentials and potentiated through muscarinic receptor stimulation (Power and Sah, 2008). Continuous superfusion with cholinergic agonists in pharmacological studies might deplete the Ca^{2+} stores important for AHPs that otherwise have the potential to counteract ADPs. Whether chronic and physiological cholinergic stimulation can produce effects similar to pharmacological

agents is not clear. Unfortunately, optogenetics might not be ideal for carrying out such chronic procedures.

An indirect support for my studies comes from *in vivo* studies. While it has been speculated that persistent spiking during working memory tasks *in vivo* is also mediated by I_{CAN} activation (Gupta et al., 2012), the results pertaining to graded activity in *in vitro* pharmacological experiments pose some concerns. Unlike what would be expected from pharmacological studies in slices, most entorhinal cortex units show a reduction in their delay activity during working memory tasks (Gupta et al., 2012). Although this could be attributable to network mechanisms, the inverted U-shaped relationship described in this thesis could be an additional contributing factor.

6.3.3 Cholinergic IPSPs at rest

Single pulse stimulation of BFc afferents resulted in a complex response consisting of an initial polysynaptic inhibition mediated by a possible nicotinic receptor mediated activation of interneurons which was followed by a later onset and longer lasting muscarinic inhibition. Because of the contamination of most muscarinic IPSP recordings with slight nicotinic depolarizations, the exact onset latencies were difficult to determine but it is clear that the latencies range between 50 – 100 msec and durations were 500 milliseconds. This hyperpolarization was insensitive to blockers of GABA-B neurotransmission, SK channels, and channels that mediate longer duration AHPs than SK (i.e. norepinephrine was used in the latter case). Contrary, muscarinic IPSPs were sensitive to both atropine and pirenzepine suggesting that the response is mainly mediated by M1 receptor activation. A small hyperpolarizing component (~1/5 of the total hyperpolarization) remained when only nicotinic neurotransmission was left

untouched. The mechanisms of this hyperpolarization was tested in a limited set of neurons and seems to be blocked by inhibitors of nicotinic receptors (n = 2, mecamylamine, a general nicotinic antagonist) and iberiotoxin (n = 1, a toxin that selectively blocks BK channels that mediate short duration afterhyperpolarizations). The latter point will be revisited shortly.

While I attempted to do ramp protocols to characterize possible rectification of the pirenzepine sensitive hyperpolarizing response, these experiments failed to yield meaningful results due to voltage clamp errors, escaped spikes and their related currents. Using TTX in conjunction with 4-AP (i.e. for blocking spikes and rescuing optogenetic release) on the other hand would lead to very inconclusive results. I considered using QX-314 to block spiking activity in the recorded neurons only, but this approach could also be meaningless by the potential blockade of some potassium channels with this agent. Correcting the IPSP amplitude for the input resistance at different voltages was attempted but the occurrence of spontaneous firing ~50 mV did not permit for ideal recordings of a possible rectification of the response. Hence, these data are not included in the thesis. As a last resort, I used barium to block inwardly rectifying potassium channels. This agent completely abolished the muscarinic IPSPs to the same extent as pirenzepine suggesting that M1 receptor activation recruits inwardly rectifying potassium channels.

While the selectivity of barium is questionable, the absence of blockade in the presence of other antagonists (e.g. apamin for SK) argues for the M1 receptor mediated activation of inwardly rectifying potassium conductances. To my knowledge, this has not been demonstrated so far and these findings might entail a novel mechanism. I

would like to emphasize certain points about these inconsistencies. Unexplained differences occur even between studies using the same pharmacological approaches. As discussed before, Yajeya et al. (1999) found that RS BLA neurons are activated by CCh through I_{CAN}. In contrast, direct depolarizations due to a conductance increase were reported also (Washburn and Moises, 1992; Egorov et al., 2006). BLA is not the only place where such inconsistencies are reported (other inconsistencies are reviewed in the background section). I believe that the results obtained in the current study match the *in vivo* situation the best for couple of reasons. The first is the fact that different voltage gated conductances has different sensitivites to acetylcholine concentration (Madison et al., 1987). Even if two different studies use the same concentration, the duration of the application of pharmacological agents and the recording chamber design do have possible drastic influences on a sensitive process. Optogenetics is definitely free of these problems and possibly lead to realistic neurotransmitter concentrations. My thinking that optogenetic stimulation better mimicks the *in vivo* condition gets reinforced by comparing two recent studies investigating cholinergic modulation in the olfactory bulb. One study by Smith and Araneda (2010) investigated this at a pharmacological level in olfactory bulb slices while the other in the intact brain, using optogenetics for selective stimulation of BFc inputs to the olfactory bulb (Ma and Luo, 2012). In the pharmacological study (Smith and Araneda, 2010), acetylcholine led to an increase in excitability in granule and mitral/tufted neurons mainly through mechanisms involving a slow and long-lasting depolarization mediated by M1 receptor activation. On the other hand, spontaneous firing rates of all these neuron types were drastically reduced (complete silencing throughout BFc stimulation) when BFc system was optogenetically

stimulated *in vivo* (Ma and Luo, 2012). Given that all neuron types exhibited a similar silencing in their activity, the possibility of nicotinic activation of interneurons in this case is not likely (Ma and Luo, 2012).

A small hyperpolarizing component was still there when all muscarinic, glutamatergic, and GABAergic transmission were blocked. This was preceeded by a small depolarization. This small depolarization and the hyperpolarization following it were sensitive to mecamylamine application suggesting that these events were mediated through nicotine receptor stimulation. Blockade of BK channels with iberiotoxin left the depolarizing phase intact while abolishing the later hyperpolarizing phase. Nicotinic responses were previously reported in RS BLA neurons (Klein and Yakel, 2006). Although the exact nicotinic receptor subtype was not investigated in my studies, the results by Klein and Yakel (2006) suggest that these depolarizations are mediated through the activation of α7 containing nicotinic receptors, which are permeable to Ca^{2+}. The calcium entry through nicotinic receptor activation might have led to the activation of BK channels. A similar phenomenon, in which nicotinic receptor activation led to a calcium activated potassium entry, was previously reported by Kong et al. (2008) in mouse cochlear hair cells.

6.3.4 Potential functional implications

Undoubtedly, the overall responses during intracellular stimulations were not only governed by mechanisms supporting ADP but also by others, including the barium and M1 sensitive IPSPs mentioned above. While inhibition of the M-current and modulation of different afterhyperpolarizations are likely to have contributions, these were not obvious. Characterizing the effects on AHPs under these circumstances is particularly

difficult as those effects are likely to be masked by parallel mechanisms that govern ADP activation.

However, the injected current intensity vs. the action potential discharge during current injections relationship gives valuable insights about functional implications. In particular, BFc stimulation suppressed action potentials until ~10 Hz while this suppression was overcome at later stages and were replaced by robust ADPs. In other words, this might be a strategy through which acetylcholine might increase signal to noise ratio: it will inhibit “weakly activated” neurons while not exerting this inhibition (through a possible rectification of barium sensitive muscarinic IPSPs) on strongly activated ones. In the latter case, the stronger ADPs might even support further action potential generation. A similar notion was provided by recent pharmacological studies in hippocampus and cortex (Gulledge and Stuart, 2005; Gulledge and Kawaguchi, 2007). Moreover, Ma and Luo (2012) have conclusively shown that optogenetic activation of the BFc system sharpens the receptive fields of mitral/tufted olfactory bulb neurons which are otherwise inhibited by BFc stimulation during baseline conditions.

The functions of ADP do not necessarily need to disclose themselves through immediate changes in firing rates. For instance, the unit responses in BLA neurons to conditional stimuli that predict aversive outcomes are transient and the time gap between these responses and onset of aversive events is in the order of 10s of seconds [see Pape and Pare (2010). In other words, the time gap between the responses to conditional stimuli and associated aversive outcomes are too long to account for phenomena like long-term potentiation (LTP). Conversely, LTP is easily observed *ex vivo* following fear conditioning paradigms (McKernan and Shinnick-Gallagher, 1997; Tsvetkov et al.,

2002). In this respect, I_{CAN} mediated ADPs might have a crucial permissive role in the induction of synaptic plasticity during amygdala mediated fear conditioning. In line with this thinking, transgenic mice lacking the transient receptor potential channel 5 (TRPC5), the channel type abundantly expressed in the BLA, are impaired in fear learning (Riccio et al., 2009).

A previous study has reported functional compartmentalization in BLA dendrites with respect to differential calcium signaling in thalamo- and cortico-recipient dendritic spines (Humeau et al., 2005). Determining the location of BK channels with respect to different kinds of dendritic spines (thalamo-, BLA-, and cortico-recipient) and their functional interactions with nicotinic receptors will in the long run help in understanding whether the current findings regarding nicotinic BK activation fit into this comparmentalized scheme. I find it plausible that nicotine receptor activated BK channels are in close proximity to the intrinsic BLA inputs and this might be an additional mechanism whereby acetylcholine can increase signal to noise ratio by selectively attenuating recurrent inputs while possibly not influencing thalamic inputs. While the latter speculation seems to be “far-fetched”, one should keep in mind that most cholinergic synapses in the CNS are found on the dendrites where they are expected to function as regulators of different synaptic inputs.

6.4 Concluding remarks

While the important role of the BFc system in cognition is widely accepted, the specifics of this system are poorly understood. Until now, most studies characterizing BFc neurons were limited to single BF subregions. Apart from this, no functional study directly investigated the connectivty within this nucleus. Finally, most studies on

cholinergic actions were limited to pharmacological approaches. In short, even the very basic questions about BFc organization and acetylcholine actions were unanswered.

The experiments in this thesis asked some of the most basic questions about: the physiological properties of its constituent neurons, the interactions among them, and how they influence target structures. To this end, slice electrophysiology was coupled with transgenic strategies to allow targeted recordings/stimulations of BFc neurons. The results revealed the presence of two BFc neurons subtypes based on electrophysiological criteria. In the second part, inhibitory interactions between BFc neurons were revealed. Experiments on cholinergic interactions in a target structure (BLA) revealed that cholinergic actions depend on the state of putative principal neurons.

The importance of electrophysiologically distinct subtypes can probably be best investigated using *in vivo* recordings. The morphological data presented in the appendix section is promising: there seems to be morphological differences between the two electrophysiological subtypes. If the morphological differences hold true with an increased sample size, an idea about the "*in vitro* identity" of BFc neurons recorded/filled during *in vivo* experiments can be formed. Current optogenetic strategies will certainly facilitate the targeted recordings of BFc neurons *in vivo*. Currently, it can only be speculated that the two populations might be involved in different modes of acetylcholine release as can be deduced from their different firing patterns.

The connectivity between BFc neurons is certainly a harbinger for the presence of some organizational principles. Previously, these principles were largely deduced by pure anatomical studies and this thesis for the first time brings it to the realm of physiology.

Future experiments utilizing more complex strategies will provide more definitive answers about the BFc organization.

The complexity of acetylcholine actions in target structures was revealed in final experiments, taking the putative principal neurons of the BLA as a “model system”. In short, the actions dependent on the short term history of the cholinorecipient neurons: they were excitatory when the cells had recently fired and inhibitory when they were at rest. The inhibition was a bigger contributing factor also during below ~8 Hz firing (Figure 5.13 C). These mechanisms resemble the concept of signal to noise ratio enhancement. Future studies will definitely test the generalizability of these results to other cortical structures.

The experiments in this thesis are not immune to problems associated with scientific investigation. *In vitro* slices definitely provide an oversimplification of overall connectivity and function. When interpreting current results, it is cardinal to keep in mind that BFc system interacts with other neuromodulatory systems [e.g. Akasu et al. (1988) and noncholinergic BF neurons and the circuits (short- and long-range) modified by acetylcholine are far more complicated than that could be envisioned with slice experiments.

CHAPTER VII: APPENDIX

7.1 Morphological features of BFc neurons

In this analysis, data from durcupan embedded sections were considered. Due to the thickness of the slices (250 µM) and the tissue processing protocols, high magnification oil-immersion lenses could not be used (60 X and 100 X). Instead, the neurons were reconstructed using a 40 X lens using the neurolucida software. The less than desired magnification and the darkness of the sections as compared to unembedded slices, did not allow the tracing of axons. Therefore, only the dendritic arbors and soma could be reconstructed from a limited set of neurons (numbers: EF = 4; LF = 6). In future experiments, prior tissue re-sectioning along with durcupan embedding need to be used (Antal et al., 2006).

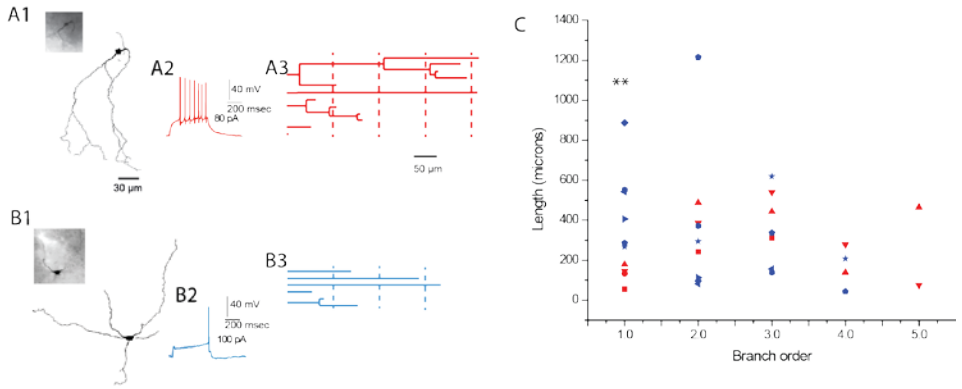

Figure 7.1 The dendritic organization of reconstructed EF and LF BFc neurons exhibit differences. A A1 3-D reconstruction of an EF neuron. Inset shows the photomicrograph from a single level. A2 The response of this neuron to a rheobase current injection from -70 mV. A3 Dendogram of the dendrites. **B** The same arrangement as in A. **C** Total dendritic lengths of individual neurons by branch order.

Figure 7.1 illustrates the significant differences in the length of primary dendrites in these two neuronal populations. The data show that the primary dendrites of LF neurons take a longer distance to bifurcate. Statistical analysis demonstrated significant

differences along two other dimensions such as the tortuosity of primary dendrites and different numbers of dendritic intersections at different radii. Given the differences in the length of the primary dendrites, these results were expected and are not further discussed.

Somatic measurements did not reveal significant differences (not shown).

CHAPTER VIII: BIBLIOGRAPHY

Akasu T, Ariyoshi M, Tokimasa T (1988) Postsynaptic modulation of cholinergic transmission by endogenous substances. Comp Biochem Physiol C 91:241-246.

Albuquerque EX, Pereira EFR, Alkondon M, Rogers S (2009) Mammalian nicotinic acetylcholine receptors: from structure to function. Physiol Rev 89:73-120.

Alkondon M, Albuquerque EX (1993) Diversity of nicotinic acetylcholine receptors in rat hippocampal neurons. I. Pharmacological and functional evidence for distinct structural subtypes. J Pharmacol Exp Ther 265:14555-14573.

Alkondon M, Pereira EF, Barbosa CT, Albuquerque EX (1997) Neuronal nicotinic acetylcholine receptor activation modulates gamma-aminobutyric acid release from CA1 neurons of rat hippocampal slices. J Pharmacol Exp Ther 283:1396-1411.

Allen TGJ, Sim JA, Brown DA (1993) The whole-cell calcium current in acutely dissociated magnocellular basal forebrain neurones of the rat. J Physiol 460:91-116.

Allen TGJ, Brown DA (1996) Detection and modulation of acetylcholine release from neurites of rat-cultured basal forebrain cells. J Physiol 492:453-466.

Alonso A, Khateb A, Fort P, Jones BE, Muhlethaler M (1996) Differential oscillatory properties of cholinergic and noncholinergic nucleus basalis neurons in guinea pig brain slice. Eur J Neurosci 8:169-182.

Alreja M, Wu M, Liu W, Atkins JB, Leranth C, Shanabrough M (2000) Muscarinic tone sustains impulse flow in the septohippocampal GABA but not cholinergic pathway: implications for learning and memory. J Neurosci, 20:8103-8110.

Amaral DG, Kurz J (1985) An analysis of the origins of the cholinergic and noncholinergic septal projections to the hippocampal formation of the rat. J Comp Neurol 240:37-59.

Antal M, Eyre M, Finklea B, Nusser Z (2006) External tufted cells in the main olfactory bulb form two distinct subpopulations. Eur J Neurosci 24:1124-1136.

Arendt T, Bigl V, Tennstedt A, Arendt A (1985) Neuronal loss in different parts of the nucleus basalis is related to neuritic plaque formation in cortical target areas in Alzheimer's disease. Neuroscience 14:1-14.

Arroyo S, Bennett C, Aziz D, Brown SP, Hestrin S. (2012) Prolonged disynaptic inhibition in the cortex mediated by slow, non-α7 nicotinic excitation of a specific subset of cortical interneurons. J Neurosci. 32: 3859-3864.

Asanuma C, Porter LL (1990) Light and electron microscopic evidence for a GABAergic projection from the caudal basal forebrain to the thalamic reticular nucleus in rats. J Comp Neurol 302:159-172.

Aznavour N, Mechawar N, Descarries L (2002) Comparative analysis of cholinergic innervation in the dorsal hippocampus of adult mouse and rat: a quantitative immunocytochemical study. Hippocampus 12:206-217.

Bartos M, Vida I, Jonas P (2007) Synaptic mechanisms of synchronized gamma oscillations in inhibitory interneuron networks. Nat Rev Neurosci 8:45-56.

Baskerville KA, Schweitzer JB, Herron P (1997) Effects of cholinergic depletion on experience-dependent plasticity in the cortex of the rat. Neuroscience 80:1159-1169

Baskerville KA, Chang HT, Herron P. (1993) Topography of cholinergic afferents from the nucleus basalis of Meynert to representational areas of sensorimotor cortices in the rat. J Comp Neurol 335:552-562.

Ben-Ari Y, Zigmond RE, Shute CC, Lewis PR (1977) Regional distribution of choline acetyltransferase and acetylcholinesterase within the amygdaloid complex and stria terminalis system. Brain Res 120:435-444.

Bengtson CP, Osborne PB (2000) Electrophysiological properties of cholinergic and noncholinergic neurons in the ventral pallidal region of the nucleus basalis in rat brain slices. J Neurophysiol 83:2649-2660.

Benson JA (1988) Bicuculline blocks the response to acetylcholine and nicotine but not to muscarine or GABA inisolated insect neuronal somata. Brain Res 458:65-71.

Bienvenu TC, Busti D, Magill PJ, Ferraguti F, Capogna M (2012) Cell-type-specific recruitment of amygdala interneurons to hippocampal theta rhythm and noxious stimuli in vivo. Neuron 74:1059-1074.

Bina KG, Guzman P, Broide RS, Leslie FM, Smith MA, O'Dowd DK (1995) Localization of α7 nicotinic receptor subunit mRNA and α-bungaratoxin binding sites in developing mouse somatosensory thalamocortical system. J Comp Neurol 363:321-332.

Binder JR, Frost JA, Hammeke TA, Bellgowan PS, Rao SM, Cox RW (1999) Conceptual processing during the conscious resting state. A functional MRI study. J Cogn Neurosci. 11:80-95.

Birnbaum SG, Varga AW, Yuan LL, Anderson AE, Sweatt JD, Schrader LA (2004) Structure and function of Kv4-family transient potassium channels. Physiol Rev 84:803-833.

Blair HT, Schafe GE, Bauer EP, Rodrigues SM, LeDoux JE (2001) Synaptic plasticity in the lateral amygdala: a cellular hypothesis of fear conditioning. Learn Mem 8:229-242.

Brandon EP, Mellott T, Pizza DP, Coufal N, D'Amour KA, Gobeske K, Lortie M, Lopez-Coviella I, Berse B, Thal LJ, Cage FH, Blusztajin JK (2004) Choline

transporter 1 maintains cholinergic functions in choline acetyltransferase haploinsufficiency. J Neurosci 24:5459-5466.

Brashear HR, Zaborszky L, Heimer L (1986) Distribution of GABAergic and cholinergic neurons in the rat diagonal band. Neuroscience 17:439-451.

Brew HM, Forsythe ID (1995) Two voltage-dependent K+ conductances with complementary functions in postsynaptic integration at a central auditory synapse. J Neurosci 15:8011-8022.

Brocher S, Artola A, Singer W (1992) Agonists of cholinergic and noradrenergic receptors facilitate synergistically the induction of long-term potentiation in slices of rat visual cortex. Brain Res 573:27-36.

Brown DA (2010) Muscarinic acetylcholine receptors (mAChRs) in the nervous system: some functions and mechanisms. J Mol Neurosci 41:340-346.

Bruno RM, Sakmann B (2006) Cortex is driven by weak but synchronously active thalamocortical synapses. Science 312:1622-1627.

Buckley NJ, Bonner TI, Brann MR (1988) Localization of a family of muscarinic receptor mRNAs in rat brain. J Neurosci 8:4646-4652.

Burkhalter A, Gonchar Y, Mellor RL, Nerbonne JM (2006) Differential expression of I(A) channel subunits Kv4.2 and Kv4.3 in mouse visual cortical neurons and synapses. J Neurosci 26:12274-12282.

Buzsaki G (2006) Rhythms of the Brain. Oxford University Press New York.

Buzsaki G, Bickford RG, Ponomareff G, Thal LJ, Mandel R, Gage FH (1988) Nucleus basalis and thalamic control of neocortical activity in the freely moving rat. J Neurosci 8:4007-4026.

Buzsaki G, Anastassiou CA, Koch C (2012) The origin of extracellular fields and currents--EEG, ECoG, LFP and spikes. Nat Rev Neurosci 13:407-420.

Buzsaki G, Bickford RG, Ponomareff G, Thal LJ, Mandel R, Gage FH (1988) Nucleus basalis and thalamic control of neocortical activity in the freely moving rat. J Neurosci 8:4007-4026.

Calabresi P, Centonze D, Pisani A, Sancesario G, North RA, Bernardi G (1998) Muscarinic IPSPs in rat striatal cholinergic interneurones. J Physiol 510:421-4277.

Callaghan B, Koh SD, Keef KD (2004) Muscarinic M2 receptor stimulation of Cav1.2b requires phosphatidylinositol 3-kinase, protein kinase C, and c-Src. Circ Res 94:625-633.

Cantrell AR, Ma JY, Scheuer T, Catterall WA (1996) Muscarinic modulation of sodium current by activation of protein kinase C in rat hippocampal neurons. Neuron 16:1019-1026.

Cape EG, Jones BE (2000) Effects of glutamate agonist versus procaine microinjections into the basal forebrain cholinergic cell area upon gamma and theta EEG activity and sleep-wake state. Eur J Neurosci 12:2166-2184.

Carlsen J, Zaborszky L, Heimer L (1985) Cholinergic projections from the basal forebrain to the basolateral amygdaloid complex: a combined retrograde fluorescent and immunohistochemical study. J Comp Neurol 234:155-167.

Carrillo-Reid L, Tecuapetla F, Vautrelle N, Hernández A, Vergara R, Galarraga E, Bargas J. (2009) Muscarinic enhancement of persistent sodium current synchronizes striatal medium spiny neurons. J Neurophysiol 102:682-690.

Castro NG, Albuquerque EX (1995) The α-bungarotoxin-sensitive hippocampal nicotinic acetylcholine receptor channel has a high calcium permeability. Biophys J 68:516-524.

Cea-del Rio CA, Lawrence JJ, Tricoire L, Erdelyi F, Szabo G, McBain CJ (2010) M3 muscarinic acetylcholine receptor expression confers differential cholinergic modulation to neurochemically distinct hippocampal basket cell subtypes. J Neurosci 30:6011-6024.

Chang HT, Kuo H (1991) Calcium-binding protein (Calbindin D-28K) immunoreactive neurons in the basal forebrain of the monkey and the rat: Relationship with the cholinergic neurons. Adv Exp Med Biol 295:119-142.

Chaudhuri JD, Hiltunen M, Nykänen M, Ylä-Herttuala S, Soininen H, Miettinen R. (2005) Localization of M2 muscarinic receptor protein in parvalbumin and calretinin containing cells of the adult rat entorhinal cortex using two complementary methods. Neuroscience 131:557-566.

Chen Y, Cantrell AR, Messing RO, Scheuer T, Catterall WA (2005) Specific modulation of Na+ channels in hippocampal neurons by protein kinase C epsilon. J Neurosci 25:507-513.

Coetzee WA, Amarillo Y, Chiu J, Chow A, Lau D, McCormack T, Moreno H, Nadal MS, Ozaita A, Pountney D, Saganich M, Vega-Saenz de Miera E, Rudy B. (1999) Molecular diversity of K+ channels. Ann N Y Acad Sci 868:233-285.

Cole AE, Nicoll RA (1984) Characterization of a slow cholinergic postsynaptic potential recorded in vitro from rat hippocampal pyramidal cells. J Physiol (London) 352:173-188.

Colino A, Halliwell JV (1993) Carbachol potentiates Q current and activates a calcium-dependent non-specific conductance in rat hippocampus in vitro. Eur J Neurosci 5:1198-1209.

Collier B, Mitchell JF. (1967) The central release of acetylcholine during consciousness and after brain lesions. J Physiol 188:83-98.

Conner JM, Culberson A, Packowski C, Chiba AA, Tuszynski MH (2003) Lesions of the Basal forebrain cholinergic system impair task acquisition and abolish cortical plasticity associated with motor skill learning. Neuron 38:819-829.

Constanti A, Sim JA (1987) Muscarinic receptors mediating suppression of the M-current in guinea-pig olfactory cortex neurones may be of the M2-subtype. Br J Pharmacol 90:3-5.

Cruikshank SJ, Urabe H, Nurmikko AV, Connors BW (2010) Pathway-specific feedforward circuits between thalamus and neocortex revealed by selective optical stimulation of axons. Neuron 65:230-245.

Cullinan WE, Zaborszky L (1991) Organization of ascending hypothalamic projections to the rostral forebrain with special reference to the innervation of cholinergic projection neurons. J Comp Neurol 306:631-667.

Dasari S, Gulledge AT (2011) M1 and M4 receptors modulate hippocampal pyramidal neurons. J Neurophysiol. 105:779-792.

De Rover M, Lodder JC, Kits KS, Schoffelmeer AN, Brussaard AB (2002) Cholinergic modulation of nucleus accumbens medium spiny neurons. Eur J Neurosci 16:2279-2290.

Deister CA, Chan CS, Surmeier DJ, Wilson CJ (2009) Calcium-activated SK channels influence voltage-gated ion channels to determine the precision of firing in globus pallidus neurons. J Neurosci 29:8452-8461.

Del Negro, CA, Chandler, SH (1997) Physiological and theoretical analysis of K+ currents controlling discharge in neonatal rat mesencephalic trigeminal neurons. J Neurophysiol 77:537-553.

Delmas P, Crest M, Brown DA (2004) Functional organization of PLC signaling microdomains in neurons. Trends Neurosci 27:41-47.

Dembrow NC, Chitwood RA, Johnston D (2010) Projection-specific neuromodulation of medial prefrontal cortex neurons. J Neurosci 30:16922-16937.

Descarries L, Mechawar N, Aznavour N, Watkins KC (2004) Structural determinants of the roles of acetylcholine in cerebral cortex. Progr Brain Res 145:45-59.

Destexhe A, Paré D (1999) Impact of network activity on the integrative properties of neocortical pyramidal neurons in vivo. J Neurophysiol 81:1531-1547.

Detari L (2000) Tonic and phasic influence of basal forebrain unit activity on the cortical EEG. Behav Brain Res 115:159-170.

Detari L, Juhasz G, Kukorelli T (1987) Neuronal firing in the pallidal region: firing patterns during sleep-wakefulness cycle in cats. Electroencephalogr Clin Neurophysiol 67:159-66.

Detari L, Rasmusson DD, Semba K (1997) Phasic relationship between the activity of basal forebrain neurons and cortical EEG in urethane-anesthetized rat. Brain Res 759:112-121.

Dinopoulos A, Parnavelas JG, Eckenstein F (1986) Morphological characterization of cholinergic neurons in the horizontal limb of the diagonal band of Broca in the basal forebrain of the rat. J Neurocytol 15:619-628.

Dodd J, Horn JP (1983) Muscarinic inhibition of sympathetic C neurones in the bullfrog. J Physiol 334:271-291.

Dosenbach NU, Fair DA, Miezin FM, Cohen AL, Wenger KK, Dosenbach RA, Fox MD, Snyder AZ, Vincent JL, Raichle ME, Schlaggar BL, Petersen SE (2007) Distinct brain networks for adaptive and stable task control in humans. Proc Natl Acad Sci U S A 104:11073-11088.

Dougherty KD, Milner TA (1999) Cholinergic septal afferent terminals preferentially contact neuropeptide Y-containing interneurons compared to parvalbumin-containing interneurons in the rat dentate gyrus. J Neurosci 19:10140-10152.

Douglas R, Markram H, Martin K (2004) Neocortex. The Synaptic Organization of the Brain. Edited by Shepherd GM. pp. 499-558. Oxford University Press New York.

Dudar JD, Szerb JC (1969) The effect of topically applied atropine on resting and evoked cortical acetylcholine release. J Physiol 203:741-762.

Duque A, Balatoni B, Detari L, Zaborszky L (2000) EEG correlation of the discharge properties of identified neurons in the basal forebrain. J Neurophysiol 84:1627-1685.

Duque A, Tepper JM, Detari L, Ascoli GA, Zaborszky L (2007) Morphological characterization of electrophysiologically and immunohistochemically identified basal forebrain cholinergic and neuropeptide Y-containing neurons. Brain Struct Funct 212:55-73.

Durstewitz D, Seamans JK, Sejnowski TJ (2000) Neurocomputational models of working memory. Nature Neurosci 3:1184-1191.

Dykes, R.W., 1997. Mechanisms controlling neuronal plasticity in somatosensory cortex. J. Physiol. Pharmacol 75: 535-545.

Eccles JC, Fatt P, Koketsu K (1954) Cholinergic and inhibitory synapses in a pathway from motor-axon collaterals to motoneurones. J Physiol 126:524-562.

Eckenstein F, Sofroniew MV (1983) Identification of central cholinergic nerons containing both choline acetytransferase and acetylcholinesterase and of central neurons containing only acetylcholinesterase. 3:2286-2291.

Egan TM, North RA (1986) Acetylcholine hyperpolarizes central neurones by acting on an M2 muscarinic receptor. Nature 319:405–407.

Eggermann E, Feldmeyer D (2009) Cholinergic filtering in the recurrent excitatory microcircuit of cortical layer 4. Proc Natl Acad Sci USA 106:11753-11758.

Eggermann E, Serafin M, Bayer L, Machard D, Saint-Mleux B, Jones BE (2001) Orexins/hypocretins excite basal forebrain cholinergic neurons. Neuroscience 108:177-181.

Egorov AV, Unsicker K, von Bohlen und Halbach O. (2006) Muscarinic control of graded persistent activity in lateral amygdala neurons. Eur J Neurosci 24: 3183-3194.

English DF, Ibanez-Sandoval O, Stark E, Tecuapetla F, Buzsáki G, Deisseroth K, Tepper JM, Koos T (2011) GABAergic circuits mediate the reinforcement-related signals of striatal cholinergic interneurons. Nat Neurosci 15:123-130.

Faber ES, Delaney AJ, Sah P (2005) SK channels regulate excitatory synaptic transmission and plasticity in the lateral amygdala. Nat Neurosci 8:635-641.

Faber ES, Sah P (2003) Calcium-activated potassium channels: multiple contributions to neuronal function. Neuroscientist 9:181-194.

Faber ES, Sah P (2002) Physiological role of calcium-activated potassium currents in the rat lateral amygdala. J Neurosci 22:1618-1628.

Fanselow EE, Richardson KA, Connors BW (2008) Selective, state-dependent activation of somatostatin-expressing inhibitory interneurons in mouse neocortex. J Neurophysiol 100:2640-2652.

Feldmeyer D, Lubke J, Sakmann B (2006) Efficacy and connectivity of intracolumnar pairs of layer 2/3 pyramidal cells in the barrel cortex of juvenile rats. J Physiol 575:583-602.

Ferguson SM, Savchenko V, Apparsundaram S, Zwick M, Wright J, Heilman CJ, Yi H, Levey AI, Blakely RD (2003) Vesicular localization and activity-dependent trafficking of presynaptic choline transporter. J Neurosci 23:9697-9709.

Fleig A, Penner R (2004) The TRPM ion channel subfamily: molecular, biophysical and functional features. Trends Pharmacol Sci 25:633-639.

Forloni G, Grzanna R, Blakely RD, Coyle JT (1987) Co-localization of N-acetyl-aspartyl-glutamate in central cholinergic, noradrenergic, and serotonergic neurons. Synapse 1:455-460.

Fournier GN, Semba K, Rasmusson DD (2004a) Modality- and region-specific acetylcholine in the rat neocortex. Neuroscience 126:257-262.

Fournier GN, Materi LM, Semba K, Rasmusson DD (2004b) Cortical acetylcholine release and electroencephalogram activation evoked by ionotropic glutamate receptor agonists in the rat basal forebrain. Neuroscience 123:785-792.

Franceschetti S, Taverna S, Sancini G, Panzica F, Lombardi R, Avanzini G (2000) Protein kinase C-dependent modulation of Na+ currents increases the excitability of rat neocortical pyramidal neurones. J Physiol 528:291-304.

Fransen E, Tahvildari B, Egorov AV, Hasselmo ME, Alonso AA (2006) Mechanism of graded persistent cellular activity of entorhinal cortex layer V neurons. Neuron 49:735-746.

Fraser DD, MacVicar BA (1991) Low-threshold transient calcium current in rat hippocampal lacunosum-moleculare interneurons: kinetics and modulation by neurotransmitters. J Neurosci 11:2812-2820.

Fraser DD, MacVicar BA (1996) Cholinergic-dependent plateau potential in hippocampal CA1 pyramidal neurons. J Neurosci 16:4113-4128.

Frazier CJ, Buhler AV, Weiner JL, Dunwiddie TV (1998) Synaptic potentials mediated via alpha-bungarotoxin-sensitive nicotinic acetylcholine receptors in rat hippocampal interneurons. J Neurosci 18:8228-8235.

Freund TF, Katona I (2007) Perisomatic inhibition. Neuron 56:33-42.

Freund TF, Meskenaite V (1992) Gamma-aminobutyric acid-containing basal forebrain neurons innervate inhibitory interneurons in the neocortex. Proc Natl Acad Sci USA 89:738-742.

Garrido-Sanabria ER, Perez MG, Banuelos C, Reyna T, Hernandez S, Castaneda MT, Colom LV (2007) Electrophysiological and morphological heterogeneity of slow firing neurons in medial septal/diagonal band complex as revealed by cluster analysis. Neuroscience 146:931-945.

Garrido-Sanabria ER, Perez-Cordova MG, Colom LV (2011) Differential expression of voltage-gated K+ currents in medial septum/diagonal band complex neurons exhibiting distinct firing phenotypes. Neurosci Res 70:361-369.

Gasbarri A, Sulli A, Pacitti C, McGaugh JL (1999) Serotonergic input to cholinergic neurons in the substantia innominata and nucleus basalis magnocellularis in the rat. Neuroscience 91:1129-1142.

Gaykema R, Zaborszky L (1996) Direct catecholaminergic-cholinergic interactions in the basal forebrain. II. Substantia nigra-ventral tegmental area projections to cholinergic neurons. J. Comp. Neurol 374: 555-577.

Gaykema RP, Zaborszky L (1997) Parvalbumin-containing neurons in the basal forebrain receive direct input from the substantia nigra-ventral tegmental area. Brain Res 747:173-179.

Gerber B, Jakobsson E (1993) Functional significance of the A-current. Biol Cybern 70:109-114.

Gioanni Y, Rougeot C, Clarke PB, Lepouse C, Thierry AM, Vidal C (1999) Nicotinic receptors in the rat prefrontal cortex: increase in glutamate release and facilitation of mediodorsal thalamo-cortical transmission. Eur J Neurosci 11:18-30.

Giocomo LM, Hasselmo ME (2007) Neuromodulation by glutamate and acetylcholine can change circuit dynamics by regulating the relative influence of afferent input and excitatory feedback. Mol Neurobiol 36:184-200.

Glickfeld LL, Scanziani M (2006) Distinct timing in the activity of cannabinoid-sensitive and cannabinoid-insensitive basket cells. Nat Neurosci 9:807-815.

Goard M, Dan Y (2009) Basal forebrain activation enhances cortical coding of natural scenes. Nature Neurosci 12:1444-1451

Gold PE (2003) Acetylcholine modulation of neural systems involved in learning and memory. Neurobiol Learn Mem 80:194-210.

Golmayo L, Nunez A, Zaborszky L. (2003) Electrophysiological evidence for the existence of a posterior cortical-prefrontal-basal forebrain circuitry in modulating sensory responses in visual and somatosensory rat cortical areas. Neuroscience 119: 597-609.

Gorelova N, Reiner PB (1996) Role of the afterhyperpolarization in control of discharge properties of septal cholinergic neurons in vitro. J Neurophysiol 75:695-706.

Gray R, Rajan AS, Radcliffe KA, Yakehiro M, Dani JA (1996) Hippocampal synaptic transmission enhanced by low concentrations of nicotine. Nature 383:713-716.

Griffith WH (1988) Membrane properties of cell types within guinea pig basal forebrain nuclei in vitro. J Neurophysiol 59:1590-612.

Griffith WH, Matthews RT (1986) Electrophysiology of AChE-positive neurons in basal forebrain slices. Neurosci Lett 71:169-174.

Griffith WH, Sim JA (1990) Comparison of 4-aminopyridine and tetrahydroaminoacridine on basal forebrain neurons. J Pharmacol Exp Ther 255:986-993.

Griffith WH, Sim JA, Matthews RT (1991) Electrophysiologic characteristics of basal forebrain neurons In Vitro. The Basal Forebrain Anatomy to Function. Edited by Napier TC, Kalivas PW, Hanin I. pp. 143-157. Plenum Press New York and London.

Gritti I, Mainville L, Mancia M, Jones BE (1997) GABAergic and other noncholinergic basal forebrain neurons, together with cholinergic neurons project to the mesocortex and isocortex in the rat. J Comp Neurol 383:163-177

Grove EA (1988) Neural associations of the substantia innominata in the rat: afferent connections. J Comp Neurol 277:315-346.

Gu N, Vervaeke K, Hu H, Storm, JF (2005) Kv7/KCNQ/M and HCN/h, but not KCa2/SK channels, contribute to the somatic medium after-hyperpolarization and excitability control in CA1 hippocampal pyramidal cells. J Physiol 566:689-715.

Gu Z, Yakel JL (2011) Timing-dependent septal cholinergic induction of dynamic hippocampal synaptic plasticity. Neuron 71:155-165.

Gulledge AT, Kawaguchi Y (2007) Phasic cholinergic signaling in the hippocampus: functional homology with the neocortex? Hippocampus 17:327-332.

Gupta K, Keller LA, Hasselmo ME (2012) Reduced spiking in entorhinal cortex during the delay period of a cued spatial response task. Learn Mem 19:219-230.

Gyengesi E, Paxinos, G, Zaborszky L (2011) Distribution of the secretagogin containing neurons in the basal forebrain. Vol. 45.6, Soc for Neurosci Mtg. City.

Haenny PE, Schiller PH (1988) State dependent activity in monkey visual cortex. I. Single cell activity in V1 and V4 on visual tasks. Exp Brain Res 69:225-244.

Hajos N, Papp EC, Acsády L, Levey AI, Freund TF (1998) Distinct interneuron types express m2 muscarinic receptor immunoreactivity on their dendrites or axon terminals in the hippocampus. Neuroscience 82:355-376.

Hajszan T, Zaborszky L (2000). Serotoninergic innervation of basal forebrain neurons in the rat. Serotonin: From the molecule to the clinic. A Serotonin Club/Brain Research Bulletin Conference, Elsevier Science, Abstract, p. 97.

Hajszan T, Zaborszky L (2002) Direct catecholaminergic-cholinergic interactions in the basal forebrain. III. Adrenergic innervation of choline acetyltransferase-containing neurons in the rat. J Comp Neurol 449:141-157.

Hallanger AE, Wainer BH (1988) Ascending projections from pedunculopontine tegmental nucleus and the adjacent mesopontine tegmentum in rat. J Com Neurol 274:483-515.

Halliwell JV, Adams PR (1982) Voltage-clamp analysis of muscarinic excitation in hippocampal neurons. Brain Res 250:71-92.

Han SH, McCool BA, Murchison D, Nahm SS, Parrish AR, Griffith WH (2002) Single-cell RT-PCR detects shifts in mRNA expression profiles of basal forebrain neurons during aging. Brain Res Mol Brain Res 98:67-80.

Han SH, Murchison D, Griffith WH (2005) Low voltage-activated calcium and fast tetrodotoxin-resistant sodium currents define subtypes of cholinergic and noncholinergic neurons in rat basal forebrain. Brain Res Mol Brain Res 134:226-238.

Harata N, Tateishi N, Akaike N (1991) Acetylcholine receptors in dissociated nucleus basalis of Meynert neurons of the rat. Neurosci Lett 130:153-6.

Harris KD, Thiele A (2011) Cortical state and attention. Nat Rev Neurosci 12:509-523.

Hassani OK, Lee MG, Henny P, Jones BE (2009) Discharge profiles of identified GABAergic in comparison to cholinergic and putative glutamatergic basal forebrain neurons across the sleep-wake cycle. J Neurosci 29:11828-11840.

Hasselmo ME, Cekic M (1996) Suppression of synaptic transmission may allow combination of associative feedback and self-organizing feedforward connections in the neocortex. Behav Brain Res 79:153-161.

Hasselmo ME, Sarter M (2011) Modes and models of forebrain cholinergic neuromodulation of cognition. Neuropsychopharmacology 36:52-73.

Hecker S, Mesulam MM (1994) Two types of cholinergic projections to the rat amygdala. Neuroscience 60:383-397.

Hecker S, Ohtake T, Wiley RG, Lappi DA, Geula C, Mesulam MM (1994) Complete and selective cholinergic denervation of rat neocortex and hippocampus but not amygdala by an immunotoxin against the p75 NGF receptor. J Neurosci 14:1271-1289.

Hedrick T, Waters J (2010) Physiological properties of cholinergic and non-cholinergic magnocellular neurons in acute slices from adult mouse nucleus basalis. PLoS One 10:1-9.

Heimer L, Alheid GF (1991) Piecing together the puzzle of basal forebrain anatomy. The Basal Forebrain Anatomy to Function. Edited by Napier TC, Kalivas PW, Hanin I. pp. 253-267. Plenum Press New York and London.

Henderson Z (1987) A small proportion of cholinergic neurons in the nucleus basalis magnocellularis of ferret appear to stain positively for tyrosine hydroxylase. Brain Res 412:363-369.

Henderson Z, Boros A, Janzso G, Westwood AJ, Monyer H, Halasy K (2005) Somato-dendritic nicotinic receptor responses recorded in vitro from the medial septal diagonal band complex of the rodent. J Physiol 562:165-182.

Henderson Z, Morris NP, Grimwood P, Fiddler G, Yang HW, Appenteng K (2001) Morphology of local axon collaterals of electrophysiologically characterised neurons in the rat medial septal/ diagonal band complex. Comp Neurol 430:410-432.

Henny P, Jones BE (2006) Innervation of orexin/hypocretin neurons by GABAergic, glutamatergic, or cholinergic basal forebrain terminals evidenced by immunostaining for presynaptic vesicular transporter and postsynaptic scaffolding proteins. J Comp Neurol 499:645-661.

Henny P, Jones BE (2008) Projections from basal forebrain to prefrontal cortex comprise cholinergic, GABAergic and glutamatergic inputs to pyramidal cells or interneurons. Eur J Neurosci 27:654-670.

Hess D, El Manira A (2001) Characterization of a high-voltage-activated IA current with a role in spike timing and locomotor pattern generation. Proc Natl Acad Sci USA 98:5276-5281.

Heys JG, Hasselmo ME (2012) Neuromodulation of I(h) in layer II medial entorhinal cortex stellate cells: a voltage-clamp study. J Neurosci 32:9066-9072.

Hille B (2001) Ion channels of excitable membranes. 3rd edition (Sinauer Associates).

Hoffman DA, Magee JC, Colbert CM, Johnston D (1997) K+ channel regulation of signal propagation in dendrites of hippocampal pyramidal neurons. Nature 387:869-875.

Horikawa J, Hosokawa Y, Kubota M, Nasu M, Taniguchi I. (1996) Optical imaging of spatiotemporal patterns of glutamatergic excitation and GABAergic inhibition in the guinea-pig auditory cortex in vivo. J Physiol 497:629-638.

Hsieh CY, Cruikshank SJ, Metherate R (2000) Differential modulation of auditory thalamocortical and intracortical synaptic transmission by cholinergic agonist. Brain Res 880:51-64.

Hudson AE, Prinz, AA (2010) Conductance ratios and cellular identity. PLoS Comput Biol, 6, e1000838.

Humeau Y, Herry C, Kemp N, Shaban H, Fourcaudot E, Bissiere S, Lüthi A (2005) Dendritic spine heterogeneity determines afferent-specific Hebbian plasticity in the amygdala. Neuron 45:119-131.

Jasper HH, Tessier J (1971) Acetylcholine liberation from cerebral cortex during paradoxical (REM) sleep. Science 172:601-602.

Johnston D, Hoffman DA, Magee JC, Poolos NP, Watanabe S, Colbert CM, Migliore M (2000) Dendritic potassium channels in hippocampal pyramidal neurons. J Physiol 525:75-81.

Jones S, Yakel JL (1997) Functional nicotinic ACh receptors on interneurons in the rat hippocampus. J Physiol 504:603-610.

Juliano SL, Ma W, Bear MF, Eslin D (1990). Cholinergic manipulation alters stimulus-evoked metabolic activity in cat somatosensory cortex. J Comp Neurol 297: 106-120.

Kalmbach A, Hedrick T, Waters J (2012) Selective optogenetic stimulation of cholinergic axons in neocortex. J Neurophysiol 107: 2008-2019.

Kanai T, Szerb JC (1965) Mesencephalic reticular activating system and cortical acetylcholine output. Nature 205:80-82.

Kanold PO, Manis PB (1999) Transient potassium currents regulate the dischargepatterns of dorsal cochlear nucleus pyramidal cells. J Neurosci 19:2195-2208.

Kassam SM, Herman PM, Goodfellow NM, Alves NC, Lambe EK (2008) Developmental excitation of corticothalamic neurons by nicotinic acetylcholine receptors. J Neurosci28:8756-8764.

Katz B, Miledi R (1966) The release of acetylcholine from nerve endings by graded electrical pulses. Proc Roy Soc 167:23-38.

Kawaguchi Y (1997) Selective cholinergic modulation of cortical GABAergic cell subtypes. J Neurophysiol 78:1743-1747.

Khateb A, Fort P, Pegna A, Jones BE, Mühlethaler M (1995) Cholinergic nucleus basalis neurons are excited by histamine in vitro. Neuroscience 69:495-506.

Khateb A, Fort P, Williams S, Serafin M, Jones BE, Mühlethaler M (1997) Modulation of cholinergic nucleus basalis neurons by acetylcholine and N-methyl-D-aspartate. Neuroscience 81:47-55.

Khateb A, Fort P, Williams S, Serafin M, Mühlethaler M, Jones BE (1998) GABAergic input to cholinergic nucleus basalis neurons. Neuroscience 86:937-947.

Khateb A, Muhlethaler M, Alonso A, Serafin M, Mainville L, Jones BE (1992) Cholinergic nucleus basalis neurons display the capacity for rhythmic bursting activity mediated by low-threshold calcium spikes. Neuroscience 51:489-494.

Kilgard MP, Merzenich MM (1998) Cortical map reorganization enabled by nucleus basalis activity. Science 279: 1714-1718.

Kimura F, Fukuda M, Tsumoto T (1999) Acetylcholine suppresses the spread of excitation in the visual cortex revealed by optical recording: possible differential effect depending on the source of input. Eur J Neurosci 11:3597-3609.

Klein RC, Yakel JL (2006) Functional somato-dendritic alpha7-containing nicotinic acetylcholine receptors in the rat basolateral amygdala complex. J Physiol 576:865-872.

Klink R, Alonso A (1997) Ionic mechanisms of muscarinic depolarization in entorhinal cortex layer II neurons. J Neurophysiol 77:1829-1843.

Koliatsos VE, Martin LJ, Walker LC, Richardson RT, DeLong MR, Price DL (1988) Topographic, non-collateralized basal forebrain projections to amygdala, hippocampus, and anterior cingulate cortex in the rhesus monkey. Brain Res 463:133-139.

Kollo M, Holderith N, Antal M, Nusser Z (2008) Unique clustering of A-type potassium channels on different cell types of the main olfactory bulb. Eur J Neurosci 27:1686-1699.

Kollo M, Holderith NB, Nusser Z (2006) Novel subcellular distribution pattern of A-type K+ channels on neuronal surface. J Neurosci 26:2684-2691.

Kong JH, Adelman JP, Fuchs PA (2008) Expression of the SK2 calcium-activated potassium channel is required for cholinergic function in mouse cochlear hair cells. J Physiol 586:5471-5485.

Kosaka T, Tauchi M, Dahl JL (1988) Cholinergic neurons containing GABA-like and/or glutamic acid decarboxylase-like immunoreactivities in various brain regions of the rat. Exp Brain Res 70:605-617.

Krnjević K (2004) Synaptic mechanisms modulated by acetylcholine in cerebral cortex. Prog Brain Res145:81-93.

Krnjevic K, Phillis, JW (1963) Actions of certain amines on cerebral cortical neurones. Br J Pharmacol Chemother 20:471-490.

Krook-Magnuson E, Varga C, Lee SH, Soltesz I (2012) New dimensions of interneuronal specialization unmasked by principal cell heterogeneity. Trends Neurosci 35:175-184.

Lavine N, Reuben M, Clarke PBS (1997) A population of nicotinic receptors is associated with thalamocortical afferents in the adult rat: laminal and areal analysis. J Comp Neurol 380:175-190.

Lawrence JJ (2008) Cholinergic control of GABA release: emerging parallels between neocortex and hippocampus. Trends Neurosci 31:317-327.

Leranth C, Vertes RP (1999) Median raphe serotonergic innervation of medial septum/diagonal band of broca (MSDB) parvalbumin-containing neurons: possible involvement of the MSDB in the desynchronization of the hippocampal EEG. J Comp Neurol 410:586-598.

Levey AI, Edmunds SM, Hersch SM, Wiley RG, Heilman CJ (1995a) Light and electron microscopic study of m2 muscarinic acetylcholine receptor in the basal forebrain of the rat. J Comp Neurol 351:339-356.

Levey AI, Edmunds SM, Kollatsos V, Wiley RG, Heilman CJ (1995b) Expression of m1-m4 muscarinic acetylcholine receptor proteins in rat hippocampus and regulation by cholinergic innervation. J Neurosci 15:4077-4092.

Levey AI, Kitt CA, Simonds WF, Price DL, Brann MR (1991) Identification and localization of muscarinic acetylcholine receptor proteins in brain with subtype-specific antibodies. J Neurosci 11:3218-3226.

Linsdell P, Moody WJ (1994) Na+ channel mis-expression accelerates K+ channel development in embryonic Xenopus laevis skeletal muscle. J Physiol 480:405-410.

Livingstone MS, Hubel DH (1981) Effects of sleep and arousal on the processing of visual information in the cat. Nature 291:554-561.

Lovett-Barron M, Turi GF, Kaifosh P, Lee PH, Bolze F, Sun XH, Nicoud JF, Zemelman BV, Sternson SM, Losonczy A (2012) Regulation of neuronal input transformations by tunable dendritic inhibition. Nat Neurosci 15:423-430.

Luskin MB, Price JL (1982) The distribution of axon collaterals from the olfactory bulb and the nucleus of the horizontal limb of the diagonal band to the olfactory cortex, demonstrated by double retrograde labeling technique. J Comp Neurol 209:249-263.

Luther JA, Birren SJ (2009) p75 and TrkA signaling regulates sympathetic neuronal firing patterns via differential modulation of voltage-gated currents. J Neurosci 29:5411-5424.

Ma M, Luo M (2012) Optogenetic activation of basal forebrain cholinergic neurons modulates neuronal excitability and sensory responses in the main olfactory bulb. J Neurosci 32:10105-10116.

MacLean JN, Zhang Y, Goeritz ML, Casey R, Oliva R, Guckenheimer J, Harris-Warrick RM (2005) Activity-independent coregulation of IA and Ih in rhythmically active neurons. J Neurophysiol. 94:3601-3617.

Madison DV, Lancaster B, Nicoll RA (1987) Voltage clamp analysis of cholinergic action in the hippocampus. J Neurosci 7:733-741.

Magarinos-Ascone C, Núñez A, Delgado-García JM (1999)Different discharge properties of rat facial nucleus motoneurons. Neuroscience 94:879-886.

Magee JC (1998) Dendritic hyperpolarization-activated currents modify the integrative properties of hippocampal CA1 pyramidal neurons. J Neurosci 18:7613-7624.

Maggi L, Magueresse C, Changeux JP, Cherubini E (2003) Nicotine activates immature "silent" connections in the developing hippocampus. Proc Natl Acad Sci USA 100:2059-2064.

Manko M, Bienvenu TC, Dalezios Y, Capogna M (2012) Neurogliaform cells of amygdala: a source of slow phasic inhibition in the basolateral complex. J Physiol, 2012Oct 8. [Epub ahead of print]

Manns ID, Alonso A, Jones BE (2000a) Discharge properties of juxtacellularly labeled and immunohistochemically identified cholinergic basal forebrain neurons recorded in association with the electroencephalogram in anesthetized rats. J Neurosci 20:1505-1518.

Manns ID, Alonso A, Jones BE (2000) Discharge profiles of juxtacellularly labeled and immunohistochemically identified GABAergic basal forebrain neurons recorded in association with the electroencephalogram in anesthetized rats. J Neurosci 20:9252-9263.

Mao T, Kufefoglu D, Hooks BM, Huber D, Petreanu L, Svoboda K (2011) Long-range neuronal circuits underlying the interaction between sensory and motor cortex. Neuron 72:111-123.

Markram H, Segal M (1990) Electrophysiological characteristics of cholinergic and non-cholinergic neurons in the rat medial septum-diagonal band complex. Brain Res 513:171-174.

Martinez-Murillo R, Villalba RM, Rodrigo J (1990) Immunocytochemical localization of cholinergic terminals in the region of the nucleus basalis magnocellularis of the rat: a correlated light and electron microscopic study. Neuroscience 36:361-376.

McCormick DA, Prince DA (1985) Two types of muscarinic response to acetylcholine in mammalian cortical neurons. Proc Natl Acad Sci USA 82:6344-6348.

McCormick DA, Prince DA (1986a) Mechanisms of action of acetylcholine in the guinea-pig cerebral cortex in vitro. J Physiol 375:169-194.

McCormick DA, Prince DA (1986b) Acetylcholine induces burst firing in thalamic reticular neurones by activating a potassium conductance. Nature 319:402–405.

McDonald AJ (1991) Organization of amygdaloid projections to the prefrontal cortex and associated striatum in the rat. Neuroscience 44:1-14.

McDonald AJ (1992) Projection neurons of the basolateral amygdala: a correlative Golgi and retrograde tract tracing study. Brain Res Bull 28:179-185.

McDonald AJ, Mascagni F (2011) Neuronal localization of M2 muscarinic receptor immunoreactivity in the rat amygdala. Neuroscience 196:49-65.

McDonald AJ, Mascagni F. (2010) Neuronal localization of m1 muscarinic receptor immunoreactivity in the rat basolateral amygdala. Brain Struct Funct 215:37-48.

McGaugh JL (2004) The amygdala modulates the consolidation of memories of emotionally arousing experiences. Annu Rev Neurosci 27:1-28.

McGaughy J, Kaiser T, Sarter M (1996) Behavioral vigilance following infusions of 192 IgG-saporin into the basal forebrain: selectivity of the behavioral impairment and relation to cortical AChE-positive fiber density. Behav Neurosci 110:247-265.

McKernan MG, Shinnick-Gallagher P (1997) Fear conditioning induces a lasting potentiation of synaptic currents in vitro. Nature 390:607-611.

Mechawar N, Cozzari C, Descarries L (2000) Cholinergic innervation in adult rat cerebral cortex: a quantitative immunocytochemical description. J Comp Neurol 428:305-318.

Melander T, Staines WA (1986) A galanin-like peptide coexists in putative cholinergic somata of the septum-basal forebrain complex and in acetylcholinesterase-containing fibers and varicosities within the hippocampus in the owl monkey (Aotus trivirgatus). Neurosci Lett 68:17-22.

Mesulam ,M-M, Van Hoesen GW (1976) Acetylcholinesterase-rich projections from the basal forebrain of the rhesus monkey to neocortex. Brain Research 109:152-157.

Mesulam MM (2004) The cholinergic innervation of the human cerebral cortex. Prog Brain Res 145:67-78.

Mesulam MM, Mufson EJ (1984) Neural inputs into the nucleus basalis of the substantia innominata (Ch4) in the rhesus monkey. Brain 107:253-274.

Metcalf RH, Boegman RJ (1989) Release of acetylcholine from tissue slices of the rat nucleus basalis magnocellularis. J Neurochem 52:1143-1148.

Metcalf RH, Boegman RJ, Riopelle RJ, Ludwin SK (1988) The release of endogenous acetylcholine from the medial septum/diagonal band of rat brain. Neurosci Lett 93:85-90.

Metherate R, Ashe JH (1993) Ionic flux contributions to neocortical slow waves and nucleus basalis-mediated activation: whole-cell recordings in vivo. J Neurosci 13:5312-5323.

Metherate R, Ashe JH. (1991) Basal forebrain stimulation modifies auditory cortex responsiveness by an action at muscarinic receptors. Brain Res 559: 163-167.

Metherate R, Cox CL, Ashe JH (1992) Cellular bases of neocortical activation: modulation of neural oscillations by the nucleus basalis and endogenous acetylcholine. J Neurosci 12:4701-4711.

Metherate R, Intskirveli I, Kawai HD (2012) Nicotinic filtering of sensory processing in auditory cortex. *Front. Behav. Neurosci*. 6:44. doi: 10.3389/fnbeh.2012.00044

Migliore M, Hoffman DA, Magee JC, Johnston D (1999) Role of an A-type K+ conductance in the back-propagation of action potentials in the dendrites of hippocampal pyramidal neurons. J Comput Neurosci 7:5-15.

Mike A, Castro NG, Albuquerque EX (2000) Choline and acetylcholine have similar kinetic properties of activation and desensitization on the alpha7 nicotinic receptors in rat hippocampal neurons. Brain Res 882:155-168.

Miller LM, Escabi MA, Read HL, Schreiner CE (2001) Functional convergence of response properties in the auditory thalamocortical system. Neuron 32:151-160.

Miller MN, Okaty BW, Nelson SB (2008) Region-specific spike-frequency acceleration in layer 5 pyramidal neurons mediated by Kv1 subunits. J Neurosci 28:13716-13726.

Mittmann T, Alzheimer C (1998) Muscarinic inhibition of persistent Na+ current in rat neocortical pyramidal neurons. J Neurophysiol 79:1579-1582.

Molineux ML, Fernandez FR, Mehaffey WH, Turner RW (2005) A-type and T-type currents interact to produce a novel spike latency-voltage relationship in cerebellar stellate cells. J Neurosci 25:10863-10873.

Momiyama T, Zaborszky L (2006) Somatostatin presynaptically inhibits both GABA and glutamate release onto rat basal forebrain cholinergic neurons. J Neurophysiol 96:686-694.

Morris NP, Harris SJ, Henderson Z (1999) Parvalbumin-immunoreactive, fast-spiking neurons in the medial septum/diagonal band complex of the rat: intracellular recordings in vitro. Neuroscience 92:589-600.

Moruzzi G, Magoun HW (1949) Brain stem reticular formation and activation of the EEG. Electroencephalogr Clin Neurophysiol 1:455-473.

Mrzljak L, Levey AI, Belcher S, Goldman-Rakic PS (1998) Localization of the m2 muscarinic acetylcholine receptor protein and mRNA in cortical neurons of the normal and cholinergically deafferented rhesus monkey. J Comp Neurol 390:112-132.

Mrzljak L, Levey AI, Goldman-Rakic PS (1993) Association of m1 and m2 muscarinic receptor proteins with asymmetric synapses in the primate cerebral cortex: morphological evidence for cholinergic modulation of excitatory neurotransmission. Proc Natl Acad Sci USA 90:5194-5198.

Mrzljak L, Pappy M, Leranth C, Goldman-Rakic PS (1995) Cholinergic synaptic circuitry in the macaque prefrontal cortex. J Comp Neurol 357:603-661.

Muller JF, Mascagni F, McDonald AJ. (2011) Cholinergic innervation of pyramidal cells and parvalbumin-immunoreactive interneurons in the rat basolateral amygdala. J Comp Neurol 519:790-805.

Muller W, Misgeld U (1986) Slow cholinergic excitation of guinea pig hippocampal neurons is mediated by two muscarinic receptor subtypes. Neurosci Lett 67:107-112.

Nadasdy Z, Varsanyi P, Zaborszky L (2010) Clustering of large cell populations: method and application to the basal forebrain cholinergic system. J Neurosci Methods 194:46-55.

Nagel G, Ollig D, Fuhrmann M, Kateriya S, Musti AM, Bamberg E, Hegemann P (2002) Channelrhodopsin-1: a light-gated proton channel in green algae. Science (5577):2395-2398.

Nagode DA, Tang AH, Karson MA, Klugmann M, Alger BE (2011) Optogenetic release of ACh induces rhythmic bursts of perisomatic IPSCs in hippocampus. PLoS One 6(11):e27691.

Nakajima Y, Nakajima S, Leonard RJ, Yamaguchi K (1986) Acetylcholine raises excitability by inhibiting the fast transient potassium current in cultured hippocampal neurons. Proc Natl Acad Sci U S A 83:3022-3026.

Nishimura LM, Boegman RJ (1990) N-methyl-D-aspartate-evoked release of acetylcholine from the medial septum/diagonal band of rat brain. Neurosci Lett 115:259-264.

Noda M, Katayama M, Brown DA, Robbins J, Marsh SJ, Ishizaka N, Fukuda K, Hoshi N, Yokoyama S, Higashida H (1993) Coupling of m2 and m4 muscarinic

acetylcholine receptor subtypes to Ca(2+)-dependent K+ channels in transformed NL308 neuroblastoma x fibroblast hybrid cells. Proc Biol Sci 251:215-224.

Nunez A (1996) Unit activity of rat basal forebrain neurons: relationship to cortical activity. Neuroscience 72:757-766.

Okaty BW, Miller MN, Sugino K, Hempel CM, Nelson SB (2009) Transcriptional and electrophysiological maturation of neocortical fast-spiking GABAergic interneurons. J Neurosci 29:7040-7052.

Pakhotin P, Bracci E (2007) Cholinergic interneurons control the excitatory input to the striatum. J Neurosci 27:391-400.

Palhalmi J, Paulsen O, Freund TF, Hajos N (2004) Distinct properties of carbachol- and DHPG-induced network oscillations in hippocampal slices. Neuropharmacology 47:381-389.

Pape HC, Budde T, Mager R, Kisvarday ZF (1994) Prevention of Ca(2+)-mediated action potentials in GABAergic local circuit neurones of rat thalamus by a transient K+ current. J Physiol 478:403-422.

Pape HC, Driesang RB (1998) Ionic mechanisms of intrinsic oscillations in neurons of the basolateral amygdaloid complex. J Neurophysiol 79:217-226.

Pape HC, Pare D (2010) Plastic synaptic networks of the amygdala for the acquisition, expression, and extinction of conditioned fear. Physiol Rev 90:419-463.

Paré D, Collins DR (2000) Neuronal correlates of fear in the lateral amygdala: multiple extracellular recordings in conscious cats. J Neurosci 20:2701-2710.

Parent A, Pare D, Smith Y, Steriade M (1988) Basal forebrain cholinergic and noncholinergic projections to the thalamus and brainstem in cats and monkeys. J Comp Neurol 277:281-301.

Parikh V, Kozak R, Martinez V, Sarter M (2007) Prefrontal acetylcholine release controls cue detection on multiple timescales. Neuron 56:141-154.

Parikh V, Sarter M (2008) Cholinergic mediation of attention: contributions of phasic and tonic increases in prefrontal cholinergic activity. Ann N Y Acad Sci 1129:225-235.

Penetar DM, McDonough JH (1983) Effects of cholinergic drugs on delayed match to sample performance of rhesus monkeys. Pharmacol Biochem Behav 19:963-967.

Petilla Interneuron Nomenclature Group, Ascoli GA, Alonso-Nanclares L, Anderson SA, Barrionuevo G, Benavides-Piccione R, Burkhalter A, Buzsáki G, Cauli B,Defelipe J, Fairén A, Feldmeyer D, Fishell G, Fregnac Y, Freund TF, Gardner D, Gardner EP, Goldberg JH, Helmstaedter M, Hestrin S, Karube F, Kisvárday ZF,Lambolez B, Lewis DA, Marin O, Markram H, Muñoz A, Packer A, Petersen CC, Rockland KS, Rossier J, Rudy B, Somogyi P, Staiger JF, Tamas G, Thomson AM, Toledo-Rodriguez M, Wang Y, West DC, Yuste R (2008) Petilla terminology:

nomenclature of features of GABAergic interneurons of the cerebral cortex. Nat Rev Neurosci 9:557-568.

Petrovich GD, Risold PY, Swanson LW (1996) Organization of projections from the basomedial nucleus of the amygdala: a PHAL study in the rat. J Comp Neurol 374:387-420.

Pinault D (1996) A novel single-cell staining procedure performed in vivo under electrophysiological control: morpho-functional features of juxtacellularly labeled thalamic cells and other central neurons with biocytin or neurobiotin. J Neurosci Methods 65:113-136.

Pirch J, Rigdon G, Rucker H, Turco K (1991) Basal forebrain modulation of cortical cell activity during conditioning. The Basal Forebrain Anatomy to Function. Edited by Napier TC, Kalivas PW, and Hanin I. pp. 253-267. Plenum Press New York and London.

Popa D, Popescu AT, Paré D. (2009) Contrasting activity profile of two distributed cortical networks as a function of attentional demands. J Neurosci 29:1191-1201.

Popescu AT, Pare D (2011) Synaptic interactions underlying synchronized inhibition in the basal amygdale: evidence for existence of two types of projection cells. J Neurophysiol 105:687-696.

Popescu AT, Popa D, Pare D (2009) Coherent gamma oscillations couple the amygdala and striatum during learning. Nat Neurosci 12:801-807.

Popescu AT, Saghyan AA, Pare D (2007) NMDA-dependent facilitation of corticostriatal plasticity by the amygdala. Proc Natl Acad Sci USA 104:341-346.

Porter JT, Cauli B, Tsuzuku K, Lambolez B, Rossier J, Audinat E (1999) Selective excitation of subtypes of neocortical interneurons by nicotinic receptors. J Neurosci 19:5228-5235.

Poulin JF, Chevalier B, Laforest S, Drolet G (2006) Enkephalinergic afferents of the centromedial amygdala in the rat. J Comp Neurol 496:859-876.

Power JM, Sah P.(2008) Competition between calcium-activated K+ channels determines cholinergic action on firing properties of basolateral amygdala projection neurons. J Neurosci 28:3209-3220.

Price JL, Stern R (1983) Individual cells in the nucleus basalis—diagonal band complex have restricted axonal projections to the cerebral cortex in the rat. Brain Res 269:352-356.

Quinn LK, Nitz DA, Chiba AA (2010) Learning-dependent dynamics of beta-frequency oscillations in the basal forebrain of rats. Eur J Neurosci 32:1507-1515.

Rahman J, Berger T. (2011) Persistent activity in layer 5 pyramidal neurons following cholinergic activation of mouse primary cortices. Eur J Neurosci 341:22-30.

Ramon-Moliner E, Nauta WJ (1966) The isodendritic core of the brain stem. J Comp Neurol 126:311-335.

Rasmusson DD, Smith SA, Semba K (2007) Inactivation of prefrontal cortex abolishes cortical acetylcholine release evoked by sensory or sensory pathway stimulation in the rat. Neuroscience 149:232-241.

Rasmusson DD (2000) The role of acetylcholine in cortical synaptic plasticity. Behav Brain Res 115:205-218.

Rasmusson DD, Clow K, Szerb JC (1994) Modification of neocortical acetylcholine release and electroencephalogram desynchronization due to brainstem stimulation by drugs applied to the basal forebrain. Neuroscience 60:665-677.

Riccio A, Li Y, Moon J, Kim KS, Smith KS, Rudolph U, Gapon S, Yao GL, Tsvetkov E, Rodig SJ, Van't Veer A, Meloni EG, Carlezon WA Jr, Bolshakov VY, Clapham DE (2009) Essential role for TRPC5 in amygdala function and fear-related behavior. Cell 137:761-772.

Richardson RT, DeLong MR (1990) Context-dependent responses of primate nucleus basalis neurons in a go/no-go task. J Neurosci 10:2528-2540.

Richardson RT, DeLong MR (1991) Electrophysiological studies of the functions of the nucleus basalis in primates. Adv Exp Med Biol 295:233-252.

Rigdon GC, Pirch JH (1986) Nucleus basalis involvement in conditioned neuronal responses in the rat frontal cortex. J Neurosci 6:2535-2542.

Roerig B, Nelson DA, Katz LC (1997) Fast synaptic signaling by nicotinic acetylcholine and serotonin 5-HT3 receptors in developing visual cortex. J Neurosci 17:8353-8362.

Rogers M, Sargent PB (2003) Rapid activation of nicotinic acetylcholine receptors by nerve-released transmitter. Eur J Neurosci 18:2946-2956.

Rouse ST, Edmunds SM, Yi H, Gilmor ML, Levey AI. (2000) Localization of M(2) muscarinic acetylcholine receptor protein in cholinergic and non-cholinergic terminals in rat hippocampus. Neurosci Lett 284:182-186.

Rubin RP (2007) A brief history of great discoveries in pharmacology: in celebration of the centennial anniversary of the founding of the American Society of Pharmacology and Experimental Therapeutics. Pharmacol Rev 59:289-359.

Sahin M, Bowen WD, Donoghue JP (1992) Location of nicotinic and muscarinic cholinergic and mu-opiate receptors in rat cerebral cortex: evidence from thalamic and cortical lesions. Brain Res 579:135-147.

Salgado H, Bellay T, Nichols JA, Bose M, Martinolich L, Perrotti L, Atzori M (2007) Muscarinic M2 and M1 receptors reduce GABA release by Ca2+ channel modulation through activation of PI3K/Ca2+ -independent and PLC/Ca2+ -dependent PKC. J Neurophysiol 98:952-965.

Sarter M, Hasselmo ME, Bruno JP, Givens B (2005) Unraveling the attentional functions of cortical cholinergic inputs: interactions between signal-driven and cognitive modulation of signal detection. Brain Res Brain Res Rev 48:98-111.

Semba K (2004) Phylogenetic and ontogenetic aspects of the basal forebrain cholinergic neurons and their innervations of the cerebral cortex. Prog Brain Res 145, 3-36.

Silberberg G, Markram H (2007) Disynaptic inhibition between neocortical pyramidal cells mediated by Martinotti cells. Neuron 53:735-746.

Silva LR, Amitai Y, Connors BW (1991) Intrinsic oscillations of neocortex generated by layer 5 pyramidal neurons. Science 251:432-435.

Sim JA, Allen TG (1998) Morphological and membrane properties of rat magnocellular basal forebrain neurons maintained in culture. J Neurophysiol 80:1653-1569.

Sim JA, Griffith WH (1996) Muscarinic inhibition of glutamatergic transmissions onto rat magnocellular basal forebrain neurons in a thin-slice preparation. Eur J Neurosci 8:880-891.

Singh KK, Park KJ, Hong EJ, Kramer BM, Greenberg ME, Kaplan DR, Miller FD (2008) Developmental axon pruning mediated by BDNF-p75NTR-dependent axon degeneration. Nat Neurosci 11:649-658.

Smiley JF, Mesulam M-M (1999) Cholinergic neurons of the nucleus basalis of Meynert (Ch4) receive cholinergic, catecholaminergic, and GABAergic synapses: an electron microscopic investigation in the monkey. Neuroscience 88:241-255.

Smiley JF, Morrell F, Mesulam MM (1997) Cholinergic synapses in human cerebral cortex: an ultrastructural study in serial sections. Exp Neurol 144:361-368.

Smith RS, Araneda RC (2010) Cholinergic modulation of neuronal excitability in the accessory olfactory bulb. J Neurophysiol 104:2963-2974.

Soreq H, Seidman S (2001) Acetylcholinesterase—new roles for an old actor. Nat Rev Neurosci 2:294-302.

Sosulina L, Graebenitz S, Pape HC (2010) GABAergic interneurons in the mouse lateral amygdala: a classification study. J Neurophysiol 104:617-626.

Sotty F, Danik M, Manseau F, Laplanta F, Quirion R, Williams S (2003) Distinct electrophysiological properties of glutamatergic cholinergic and GABAergic rat septohippocampal neurons: novel implications for hippocampal rhythmicity. J Physiol 551:927-943.

Steriade M (2004) Acetylcholine systems and rhythmic activities during the waking—sleep cycle. Prog Brain Res 145:179-196.

Steriade M, Timofeev I, Grenier F (2001) Natural waking and sleep states: a view from inside neocortical neurons. J Neurophysiol 85:1969-1985.

Stewart DJ, MacFabe DF, Vanderwolf CH (1984) Cholinergic activation of the electrocorticogram: role of the substantia innominata and effects of atropine and quinuclidinyl benzilate. Brain Res 322:219-232.

Stiefel KM, Gutkin BS, Sejnowski TJ (2009)The effects of cholinergic neuromodulation on neuronal phase-response curves of modeled cortical neurons. J Comput Neurosci 26:289-301.

Storm JF (1988)Temporal integration by a slowly inactivating K+ current in hippocampal neurons. Nature, 336:379-381.

Stuber GD, Sparta DR, Stamatakis AM, van Leeuwen WA, Hardjoprajitno JE, Cho S, Tye KM, Kempadoo KA, Zhang F, Deisseroth K, Bonci A (2011) Excitatory transmission fromthe amygdala to nucleus accumbens facilitates reward seeking. Nature 475:377-380.

Szabo GG, Holderith N, Gulyás AI, Freund TF, Hájos N (2010) Distinct synaptic properties of perisomatic inhibitory cell types and their different modulation by cholinergic receptor activation in the CA3 region of the mouse hippocampus. Eur J Neurosci 31:2234-2246.

Tang AH, Karson MA, Nagode DA, McIntosh JM, Uebele VN, Renger JJ, Klugmann M, Milner TA, Alger BE (2011) Nerve terminal nicotinic acetylcholine receptors initiate quantal GABA release from perisomatic interneurons by activating axonal T-Type (Ca_v3) Ca^{2+} channels and Ca^{2+} release from stores. J Neurosci 31:13546-13561.

Tell F, Bradley RM (1994) Whole-cell analysis of ionic currents underlying the firing pattern of neurons in the gustatory zone of the nucleus tractus solitarii. J Neurophysiol 71:479-492.

Tierney AJ, Harris-Warrick RM (1992) Physiological role of the transient potassium current in the pyloric circuit of the lobster stomatogastric ganglion. J Neurophysiol 67:599-609.

Tinsley MR, Quinn JJ, Fanselow MS (2004) The role of muscarinic and nicotinic cholinergic neurotransmission in aversive conditioning: comparing pavlovian fear conditioning and inhibitory avoidance. Learn Mem 11:35-42.

Tkatch T, Baranauskas G, Surmeier DJ (2000) Kv4.2 mRNA abundance and A-type K(+) current amplitude are linearly related in basal ganglia and basal forebrain neurons. J Neurosci 20:579-588.

Toselli M, Lux HD (1989) Opposing effects of acetylcholine on the two classes of voltage-dependent calcium channels in hippocampal neurons. EXS 57:97-103.

Tsvetkov E, Carlezon WA, Benes FM, Kandel ER, Bolshakov VY (2002) Fear conditioning occludes LTP-induced presynaptic enhancement of synaptic transmission in the cortical pathway to the lateral amygdala. Neuron 34:289-300.

Turi GF, Fekete C, Hrabovszky E, Liposits Z, Zaborszky L (2004). Histaminergic

innervation of cholinergic neurons in the basal forebrain of the rat. Soc. Neurosci. Abst. 33.

Turrini P, Casu MA, Wong TP, Koninck Y, Ribeiro-da-Silva A, Cuello AC (2001) Cholinergic nerve terminals establish classical synapses in the rat cerebral cortex: synaptic pattern and age-related atrophy. Neuroscience 105:277-285.

Tye KM, Stuber GD, de Ridder B, Bonci A, Janak PH (2008) Rapid strengthening of thalamo-amygdala synapses mediates cue-reward learning. Nature 453:1253-1257.

Umbriaco D, Watkins, KC., Descarries L, Cozzari C, Hartman BK (1994) Ultrastructural and morphometric features of the acetylcholine innervations in adult rat parietal cortex: An electron microscopic study in serial sections. J Comp Neurol 348:351-373.

Unal CT, Golowasch JP, Zaborszky L (2012) Adult mouse basal forebrain harbors two distinct cholinergic populations defined by their electrophysiology. *Front. Behav. Neurosci*. 6:21. doi: 10.3389/fnbeh.2012.00021

Vidal C, Changeux JP (1993) Nicotinic and muscarinic modulations of excitatory synaptic transmission in the rat prefrontal cortex in vitro. Neuroscience 56:23-32.

Von Engelhardt J, Eliava M, Meyer AH, Rozov A, Monyer H (2007) Functional characterization of intrinsic cholinergic interneurons in the cortex. J Neurosci 27:5633-5642.

Wada E, McKinnon D, Heinemann S, Patrick J, Swanson LW (1990) The distribution of mRNA encoded by a new member of the neuronal nicotinic acetylcholine receptor gene family (α5) in the rat central nervous system. Brain Res 526:45-53.

Wada E, Wada K, Boulter J, Deneris E, Heinemann S, Patrick J, Swanson LW (1989) Distribution of alpha2, alpha3, alpha4, and beta2 neuronal nicotinic receptor subunit mRNAs in the central nervous system: A hybridization histochemical study in the rat. J Comp Neurol 284:314-335.

Wallace MN, Kitzes LM, Jones EG (1991) Intrinsic inter- and intralaminar connections and their relationship to the tonotopic map in cat primary auditory cortex. Exp Brain Res 86:527-544.

Wang Y, Toledo-Rodriguez M, Gupta A, Wu C, Silberberg G, Luo J, Markram H (2004) Anatomical, physiological and molecular properties of Martinotti cells in the somatosensory cortex of the juvenile rat. J Physiol 561:65-90.

Wang YX, Dhulipala PD, Li L, Benovic JL, Kotlikoff MI (1999)Coupling of M2 muscarinic receptors to membrane ion channels via phosphoinositide 3-kinase gamma and atypical protein kinase C. J Biol Chem 274:13859-13864.

Wang YX, Fleischmann BK, Kotlikoff MI (1997) M2 receptor activation of nonselective cation channels in smooth muscle cells: calcium and Gi/G(o) requirements. Am J Physiol 273:500-508.

Washburn MS, Moises HC (1992) Electrophysiological and morphological properties of rat basolateral amygdaloid neurons in vitro. J Neurosci 12:4066-4079.

Weight FF, Votava J (1970) Slow synaptic excitation in sympathetic ganglion cells: evidence for synaptic inactivation of potassium conductance. Science 170:755-758.

Williams S, Serafin M, Muhlethaler M, Bernheim L (1997) Distinct contributions of high- and low-voltage-activated calcium currents to afterhyperpolarizations in cholinergic nucleus basalis neurons of the guinea pig. J Neurosci 17:7307-7315.

Wilson FAW (1991) The relationship between learning, memory, and neuronal responses in the primate basal forebrain. The Basal Forebrain Anatomy to Function. Edited by Napier TC, Kalivas PW, Hanin I. pp. 253-267. Plenum Press New York and London.

Womble MD, Moises HC (1993) Muscarinic modulation of conductances underlying the afterhyperpolarization in neurons of the rat basolateral amygdala. Brain Res 621:87-96.

Woodruff AR, Sah P (2007) Inhibition and synchronization of basal amygdala principal neuron spiking by parvalbumin-positive interneurons. J Neurophysiol 98:2956-2961.

Woolf NJ (1996) Global and serial neurons form A hierarchically arranged interface proposed to underlie memory and cognition. Neuroscience 74:625-651.

Wu M, Hajszan T, Xu C, Leranth C, Alreja M (2004) Group I metabotropic glutamate receptor activation produces a direct excitation of identified septohippocampal cholinergic neurons. J Neurophysiol 2:1216-1225.

Wu M, Shanabrough M, Leranth C, Alreja M (2000) Cholinergic excitation of septohippocampal GABA but not cholinergic neurons: implications for learning and memory. J Neurosci 20:3900-3908.

Yajeya J, De La Fuente A, Criado JM, Bajo V, Sánchez-Riolobos A, Heredia M (2000) Muscarinic agonist carbachol depresses excitatory synaptic transmission in the rat basolateral amygdala in vitro. Synapse 38:151-160.

Yajeya J, de la Fuente Juan A, Bajo VM, Riolobos AS, Heredia M, Criado JM (1999) Muscarinic activation of a non-selective cationic conductance in pyramidal neurons in rat basolateral amygdala. Neuroscience 88:159-167.

Yamasaki M, Matsui M, Watanabe M. (2010) Preferential localization of muscarinic M1 receptor on dendritic shaft and spine of cortical pyramidal cells and its anatomical evidence for volume transmission. J Neurosci 30:4408-4418

Yuste R (2005) Origin and classification of neocortical interneurons. Neuron 48:524-527.

Zaborszky L, Buhl DL, Pobalashingham S, Bjaalie JG, Nadasdy Z (2005) Three-dimensional chemoarchitecture of the basal forebrain: spatially specific association of cholinergic and calcium binding protein-containing neurons. Neuroscience 136:697-713.

Zaborszky L, Csordas A, Buhl DL, Duque A, Somogyi J, Nadasdy Z (2002) Computational anatomical analysis of the basal forebrain corticopetal system. Edited by Ascoli GA. pp. 171-197. Humana Press Inc Totowa, NJ.

Zaborszky L, Cullinan WE (1989) Hypothalamic axons terminate on forebrain cholinergic neurons: an ultrastructural double-labeling study using PHA-L tracing and ChAT immunocytochemistry. Brain Res 479:177-184.

Zaborszky L, Cullinan WE (1992) Projections from the nucleus accumbens to cholinergic neurons of the ventral pallidum: a correlated light and electron microscopic double-immunolabeling study in rat. Brain Res 570:92-101.

Zaborszky L, Cullinan WE (1996) Direct catecholaminergic-cholinergic interactions in the basal forebrain. I. Dopamine-beta-hydroxylase- and tyrosine hydroxylase input to cholinergic neurons. J Comp Neurol 374:535-554.

Zaborszky L, Cullinan WE, Luine VN. (1993) Catecholaminergic-cholinergic interaction in the basal forebrain. Prog Brain Res 98:31-49.

Zaborszky L, Duque A (2000) Local synaptic connections of basal forebrain neurons. Behav Brain Res 115:143-158.

Zaborszky L, Duque A (2003) Sleep-wake mechanisms and basal forebrain circuitry. Front Biosci 8:1146-1169.

Zaborszky L, Duque A, Alreja M, Dumalska I, Ovsepian SV (2009) Effect of NPY in the cholinergic basal forebrain in rat: a double-immunolabeling electron microscopy and in vitro electrophysiological studies. Neuropeptides: 19th Neuropharmacology Conference Satellite to the 2009 Meeting of the Society for Neuroscience. Abstract, P2.1.04.

Zaborszky L, Duque A. (2000) Local synaptic connections of basal forebrain neurons. Behav Brain Res 15: 143-158.

Zaborszky L, Gaykema RP, Swanson DJ, Cullinan WE (1997). Cortical input to the basal forebrain. Neuroscience 79:1051-1078.

Zaborszky L, Leranth C, Heimer L (1984) Ultrastructural evidence of amygdalofugal axons terminating on cholinergic cells of the rostral forebrain. Neurosci Lett 52:219-225.

Zaborszky L, Pang, K, Somogyi J, Nadasdy Z, Kallo I (1999) The basal forebrain corticopetal system revisited. In Advancing from the Ventral Striatum to the Extended Amygdala: Implications for Neuropsychiatry and Drug Abuse Ann NY Acad Sci 877:339-367.

Zaborszky L, van den Pol A, Gyengesi E (2011) The basal forebrain cholinergic projection system in mice. In: The Mouse Nervous System, Ch Watson et al.,Elsevier, London, pp. 684-718.

Zhang F, Aravanis AM, Adamantidis A, de Lecea L, Deisseroth K (2007) Circuit-breakers: optical techniques for probing neural signals and systems. Nat Rev Neurosci 8:577-581.

Zhang L, Weiner JL, Carlen PL (1992) Muscarinic potentiation of IK in hippocampal neurons: electrophysiological characterization of the signal transduction pathway. J Neurosci 12:4510-4520.

Zhang W, Basile AS, Gomeza J, Volpicelli LA, Levey AI, Wess J (2002) Characterization of central inhibitory muscarinic autoreceptors by the use of muscarinic acetylcholine receptor knock-out mice. J Neurosci 22:1709-1717.

Ziff EB (1997) Enlightening the postsynaptic density. Neuron 19:1163-1174.

Zmarowski A, Sarter M, Bruno JP (2005) NMDA and dopamine interactions in the nucleus accumbens modulate cortical acetylcholine release. Eur J Neurosci 22:1731-1740.

Zmarowski A, Sarter M, Bruno JP (2007) Glutamate receptors in nucleus accumbens mediate regionally selective increases in cortical acetylcholine release. Synapse 61:115-123.

Curriculum vitae

ÇAĞRI TEMUÇİN ÜNAL

1982	Born December 14th in İstanbul, Turkey
2001 - 2006	Bachelor of Arts, Department of Psychology, Boğaziçi University, İstanbul, Turkey
2009	Unal CT, Beverley JA, Willuhn I, Steiner H. Long-lasting dysregulation of gene expression in corticostriatal circuits after repeated cocaine treatment in adult rats: effects on zif 268 and home 1a. European Journal of Neuroscience, 29:1615-1626.
2010	Amano T, Unal CT, Pare D. Synaptic correlates of fear extinction in the amygdala. Nature Neuroscience, 13:489:494.
2012	Unal CT, Golowasch JP, Zaborszky L. Adult mouse basal forebrain harbors two distinct cholinergic populations defined by their electrophysiology. *Front. Behav. Neurosci*. 6:21. doi: 10.3389/fnbeh.2012.00021
2007 - 2013	Doctor of Philosophy, Graduate Program in Behavioral and Neural Science, Rutgers, The State University of New Jersey, Newark, New Jersey, USA